Modelling the freshwater cycle of the Arctic Ocean and North Atlantic during the Holocene

Davies, Frazer John

2021

document version
Publisher's PDF, also known as Version of record

VRIJE UNIVERSITEIT AMSTERDAM

MODELLING THE FRESHWATER CYCLE OF THE ARCTIC OCEAN AND THE NORTH ATLANTIC DURING THE HOLOCENE

ACADEMISCH PROEFSCHRIFT

ter verkrijging van de graad Doctor of Philosophy aan
de Vrije Universiteit Amsterdam,
op gezag van de rector magnificus
prof.dr. V. Subramaniam,
in het openbaar van de promotiecommissie
van de Faculteit der Bètawetenschappen
op woensdag 3 februari 2021 om 9.45 uur
in de online bijeenkomst van de universiteit,
De Boelelaan 1105

door

Frazer John Davies

geboren te Coventry, Verenigd Koninkrijk

promotor: prof.dr. H. Renssen

copromotor: prof.dr. D.M.V.A.P. Roche

Reading committee:

1. prof.dr. Han Dolman - VU-Earth Sciences
2. prof.dr. Michel Crucifix - UCL Louvain la Neuve
3. dr. Katrine Husum - Norwegian Polar Institute
4. dr. Gerard van der Schrier - KNMI
5. dr. Paolo Scussolini - VU-IVM

This research was carried out at:
Vrije Universiteit Amsterdam
Faculty of Science
Department of Earth Sciences
De Boelelaan 1085
1081 HV Amsterdam
The Netherlands

This research was funded by the 'European Communities 7th Framework Programme FP7/2013, Marie Curie Actions, under Grant Agreement No. 238111: CASEITN'

Modelling the freshwater cycle of the Arctic Ocean and the North Atlantic during the Holocene

Modelleren van de zoetwater cyclus van de Arctische en Noord Atlantische Oceaan tijdens het Holoceen

Author: Frazer John Davies
Printed by: Ipskamp Printing, The Netherlands
ISBN: 978-94-6421-199-3

Table of Contents

"Difficulties are just things to overcome, after all"

Ernest Shackleton

Acknowledgements

The journey that I have been on whilst completing this PhD has been a rollercoaster of emotions and life events. From the highs of getting married to the extreme lows of losing the closest of loved ones, the past 10 years has had it all. It has also seen me move from the Netherlands to Switzerland, working fulltime whilst trying to complete this thesis, and raising a family. So, to finally see the end is one hell of a relief and a moment I have dreamt about in the past years and numerous dark moments.

If it were not for the continued patience, assistance, guidance, understanding, support and input from my supervisor Hans, this thesis would never have come to fruition. I would like to thank him greatly for enduring numerous meetings, missed deadlines, my annoyance, and often hot-headed reactions to reviews of our papers. Also, I would like to thank him for making my stay in the Netherlands a pleasurable one.

In addition, I should thank my office companions Pepijn and Michael. I would like to thank them both for interesting discussions on work, life and any topic that came up. Especially Pepijn for the early morning chats and Michael for his company on the numerous trips we made as part of our project, in particular the trip to the Arctic onboard the Helmer Hansen. I would also like to thank my fellow CASE PhD students. I think we would all agree we were a mixed bunch, but somehow, we all managed to get along through the numerous meetings, trips and adventures we shared. From the first nervous meeting in the Bistro in Bordeaux, where the initial impressions of everyone remained throughout the project. For instance, Sara being one of the last to arrive!! But we must also remember Michaels dancing on the table in the bar in Bordeaux, to the drinking games in Svalbard until 2am, before we got on the boat at 5am, and the numerous casualties of that!!! We must also remember the bonfire on the beach in Trondheim, and the 2 weeks on the cruise. These are just a few of the many memories I have from the CASE project.

I would also like to thank the leader of the CASE project, Jacques. Without him this opportunity would not have happened. In fact, if his original project proposal had been accepted first time, there would have been no modelling involved, so I should really thank the EU committee for realising climate modelling is the way forward!!!

I would also like to thank my colleagues at the VU, who include, Wouter for sharing my sense of humour, Brett for sharing a beer or two with me, Martin for attending the Ajax games together, and Kristina and Paolo for engaging in conversations about running with me.

I would also like to thank my family. My Dad has been a source of inspiration and motivation throughout my life and without him I would never achieved half of what I have done. Since I was young, he has always pushed me to give 100% in everything I do, be it sport, music, work, but most importantly education. He placed a great emphasis on education above all other things when I was growing up and completing my PhD is my way of showing him that I thank him for that. He instilled within me the need to attain knowledge and for that I am thankful and will continue to do so for the rest of my life. I would also like to thank Sandra, who along with my Dad has been extremely supportive of me through my years. She deserves a medal in that she took on the unenviable task of

raising me, an energetic, enthusiastic, and quick-lipped child. So, thank you for sticking it out!!! Also, I would like to than my brother and sisters. I hope I can be a source of motivation for them. I would also like to thank my late mother, who was taken from us far too early. She showed such courage and determination throughout her life, but especially so in her final days. I sorely miss her, but at least she is no longer suffering. She epitomises the strength and determination I aspire to have.

The final thanks are reserved for my beautiful wife, Rie. I was most fortunate to meet Rie when I was living in Osaka, Japan. Since that day she has continually been there supporting me in all I do, even though we spent several years living on different continents. Eventually, on 19th December 2013 we got married and without her in my life, encouraging me to follow my dreams and aspirations back in 2009, achieving a PhD would never have happened. We have been through an awful lot in the past few years. We lost our first son, Yuma John, after only 2 months to a terrible disease, Spinal Muscular Atrophy (SMA), but we have since been blessed with another son, Soma John, and a daughter, Yuna Elizabeth. They bring us immense joy every day and we feel very lucky to have them. In addition, whenever I return to Japan it is with great pleasure as Rie's family have welcomed me into their lives with open arms and I thank them for their continued support and for letting me take their beautiful daughter overseas. I promise one day we shall return.

Summary

The Arctic is at the forefront of climate change, given that it is warming at a rate faster than elsewhere on the planet and because the impacts of this warming extend much further than the Arctic region itself. Thus, the Arctic region has rightfully attracted a great deal of research interest that is geared towards understanding what has happened, what is happening and what is going to happen in the Arctic region and further afield in the 21st century and beyond.

However, one issue researchers face is trying to understand the context of the current changes we are observing. For example, is an observed freshening of the Arctic Ocean due to melting glaciers and sea-ice, thawing permafrost, increased rainfall, a result of anthropogenic climate change we are observing, or is it part of a natural low-frequency cycle and how much can be accredited to anthropogenic forcings and how much is due to natural forcings. These are questions that I have grappled with within this thesis and I have presented here before you.

To be able to do so I have employed the use of a climate model, called LOVECLIM. A climate model is a mathematical representation of the Earth's atmosphere, oceans, land and vegetation. While such models do have their limitations, they are an essential part of climate studies when investigating mechanisms of the climate for which we have either limited observed data or reconstructed, proxy, data.

The following thesis is split into 4 main chapters that are the focus of the research, which are bookended by a general Introduction (**Chapter 1**) and a concluding Synthesis, Conclusions and Recommendations section (**Chapter 6**).

Chapter 2 "The Arctic Freshwater Hydrological Cycle during a naturally and an anthropogenically induced warm climate" focuses on comparing the climate simulations of two periods, the mid-Holocene (approximately 6ka BP) and one in the future, the 21st century, and the response of the Arctic Freshwater Hydrological Cycle. These two periods were chosen because the projected temperature increase in the Arctic during the 21st century is similar to what was observed during the mid-Holocene. As a result, the mid-Holocene is often taken as an analogy for the future. But is this correct? This is what I wanted to investigate.

The climate of these two periods, while showing similar temperature profiles, evolved due to different sets of forcings. While both these periods were preceded by increasing levels of atmospheric CO_2 and this is the primary driver of temperature increases in the 21st century, this was not the case for the mid-Holocene. The warming during the mid-Holocene was a result of higher levels of summer insolation and as a result an overall warmer annual mean climate. Given that the forcings for this period are different, could the response of the Arctic hydrological freshwater cycle also be different?

Our results, showed that within the 21st century simulation, up until the year 2010, the average annual surface temperature in the Arctic region is within the bounds of natural variability observed during the mid-Holocene simulation, however it is closer to the warmer, more extreme end of the confidence range. Following 2010, we see that the mean annual surface temperatures continue to increase, close to those of an extreme mid-

Holocene warm climate, making it no longer comparable to the mid-Holocene and thus we can say only the first decade of the 21st century is analogous to the mid-Holocene.

One interesting result we observed during our research in this chapter was a distinct, multi-centennial pattern of Arctic Ocean freshwater content variability. This was observed within a transient simulation with annually varying forcings, thus making it difficult to understand the mechanisms driving this observation. This discovery led us to **Chapter 3** "The driving mechanisms of multicentennial variability of the Arctic Ocean freshwater content with the LOVECLIM climate model". Taking this observation from Chapter 2, we performed a 10,000-year long preindustrial control simulation.

This simulation revealed a peak periodicity at 165-years, with 95% significance, of the Arctic Ocean Freshwater content. Further analysis revealed that this intrinsic variability is driven by the low-frequency modulation of the heat and saline fluxes entering the Arctic Ocean, predominantly via the Barents and Kara Seas, via the North Atlantic Current. Our observations complement other work that has identified low-frequency modes of variability in the Arctic region. The main takeaway from this chapter is that further work is required on these low-frequency modes of natural variability, so that present day observations can be placed within the correct context and the correct attribution of the driving mechanisms, behind modern day observations, can be made.

The study performed in Chapter 3 allowed us to isolate and understand the driving mechanisms of the intrinsic mode of multicentennial variability within the Arctic Ocean freshwater cycle. The next step was to see if this mechanism held up in a more realistic transient simulation. Therefore, the next chapter, **Chapter 4** "Simulating the Multicentennial variability of the Arctic Ocean freshwater content over the Holocene with the LOVECLIM climate model" was geared towards that task. In this chapter we performed a Holocene run, from 8ka to 0ka with the relevant orbital parameters and greenhouse gas concentrations.

The transient simulation revealed a peak periodicity of 220-years, with 95% significance. The mechanisms driving this periodicity were the same as in Chapter 3 and when statistically analysed the robustness of the results from Chapter 3 were verified. In Chapter 3, one result that was difficult to interpret was the fact that sea-ice transport to the North Atlantic via the Fram Strait was not significant in the control simulation, which we did not expected to be the case. However, in the transient simulation this was not the case and the sea-ice transport to the North Atlantic via the Fram Strait was deemed to be a significant mechanism controlling the Arctic Ocean freshwater content.

Overall, the results of both Chapter 3 and 4 showed that the Arctic Ocean possess an intrinsic low-frequency mode of variability and they both highlight the need for low-frequency mechanisms within the Artic Ocean, and from elsewhere, to be incorporated into discussions on the causes of the climate variability we are currently observing.

Chapter 5 "The impact of Sahara desertification on Arctic cooling during the Holocene" does not directly follow on from the previous chapters, however it expands on the point I make in the previous paragraph, which calls for alternative mechanisms to be included within the causes of the current climate debate. There have been numerous

research papers looking into the driving mechanism behind the mid-Holocene desertification of the Sahara region, going form a grassland to the desert we all know today. However, we could find no research that looked at the impact the desertification had on the climate, which is what we investigated. Our results showed that through a long-range land-atmosphere teleconnection, the desertification of the Sahara in the mid-Holocene accounts for anywhere between 17 and 40% of the observed Arctic cooling between 9k and 0ka.

Samenvatting

Het noordpoolgebied staat in het brandpunt van de belangstelling als het gaat om klimaatverandering, aangezien de opwarming hier sneller gaat dan elders op onze planeet en omdat de gevolgen van deze opwarming veel verder reiken dan de Arctische regio zelf. Het noordpoolgebied heeft dus terecht veel interesse van onderzoekers getrokken, welke erop gericht is te begrijpen wat er in het verleden is gebeurd, wat er nu gebeurt en wat er gaat gebeuren in de Arctische regio en daarbuiten in de 21e eeuw en daarna.

Onderzoekers proberen nu de context te begrijpen van de veranderingen die we waarnemen. Is bijvoorbeeld de waargenomen verzoeting van de Noordelijke IJszee – als gevolg van het smelten van gletsjers en zeeijs, dooiende permafrost en toegenomen regenval – deel van een natuurlijke laagfrequente cyclus, of wordt het veroorzaakt door de opwarming die we waarnemen? En als dit laatste het geval is, hoeveel van deze verandering kunnen we toeschrijven aan menselijke invloed, en welk deel is het gevolg van natuurlijke processen? Dit zijn vragen waarmee ik in dit proefschrift heb geworsteld en die ik hier voor u heb gepresenteerd.

Om dit te kunnen doen heb ik gebruik gemaakt van een klimaatmodel, genaamd LOVECLIM. Een klimaatmodel is een wiskundige weergave van de atmosfeer, oceanen, land en vegetatie op aarde. Hoewel dergelijke modellen beperkingen hebben, zijn ze een essentieel onderdeel van klimaatonderzoek, bij het analyseren van klimaatmechanismen waarvan we beperkte waarnemingen en gereconstrueerde gegevens ('proxy data') hebben.

Dit proefschrift is opgedeeld in vier kernhoofdstukken die de focus van het onderzoek vormen, welke aangevuld worden door een algemene inleiding (**Hoofdstuk 1**) en een afsluitende sectie met een synthese, conclusies en aanbevelingen (**Hoofdstuk 6**).

Hoofdstuk 2 "*The Arctic Freshwater Hydrological Cycle during a naturally and an anthropogenically induced warm climate*" richt zich op de vergelijking van klimaatsimulaties van twee perioden, het midden-Holoceen (ongeveer 6 duizend jaar geleden of ka BP), en de toekomst, in de 21e eeuw, en met name op de respons van de zoetwaterbalans in het noordpoolgebied. Deze twee periodes werden gekozen omdat de geprojecteerde temperatuurtoename in het noordpoolgebied gedurende de 21^{e} eeuw vergelijkbaar is met de waargenomen toename in het midden-Holoceen. Vanwege deze overeenkomst wordt het midden-Holoceen vaak als analogie voor de toekomst genomen. Maar klopt dit? Dit is wat ik wilde onderzoeken.

Alhoewel de temperatuurprofielen van beide perioden op elkaar lijken, werden de klimaten aangedreven door verschillende forceringen. Beide perioden werden weliswaar voorafgegaan door stijgende CO_2 concentraties in de atmosfeer, maar dit is alleen de dominerende sturende factor voor de temperatuurtoename in de 21^{e} eeuw, en niet voor het midden-Holoceen. De opwarming in het midden-Holoceen was het gevolg van hogere waarden van de zonnestraling in de zomer, welke ook zorgden voor een warmer jaargemiddeld klimaat. Gezien het feit dat deze forceringen verschillend waren, zou het kunnen dat de zoetwaterbalans in het noordpoolgebied ook anders reageerde?

Onze resultaten van de simulatie van de 21e eeuw lieten zien dat de jaargemiddelde temperatuur in het noordpoolgebied tot het jaar 2010 binnen de grenzen van de natuurlijke variabiliteit bleef, zoals gesimuleerd voor het midden-Holoceen. Wel was de temperatuur toen al dichtbij het warme extreem van het betrouwbaarheidsbereik. Na 2010 zien we de jaargemiddelde oppervlaktetemperatuur echter verder stijgen, zodat het klimaat niet langer vergelijkbaar is met het midden-Holoceen. We kunnen dus concluderen dat alleen het eerste decennium van de 21e eeuw analoog was met het midden-Holoceen.

Een interessant resultaat dat we tijdens ons onderzoek in dit hoofdstuk hebben waargenomen, was een duidelijk wederkerend patroon in de variabiliteit van het zoetwatergehalte van de Noordelijke IJszee, op een tijdschaal van meerdere eeuwen. Dit werd waargenomen in een tijdsafhankelijke simulatie met jaarlijks veranderde forceringen, waardoor het moeilijk was om de mechanismen achter deze observatie te begrijpen. Deze ontdekking resulteerde in **Hoofdstuk 3** *"The driving mechanisms of multicentennial variability of the Arctic Ocean freshwater content with the LOVECLIM climate model"*. Op basis van de waarneming uit Hoofdstuk 2 hebben we een 10,000 jaar durend controle-experiment uitgevoerd met pre-industriële randvoorwaarden.

Deze simulatie onthulde een periodiciteit met een piek op 165 jaar (met 95% significantie) in het zoetwatergehalte van de Noordelijke IJszee. Verdere analyse toonde aan dat deze intrensieke variabiliteit wordt aangedreven door laagfrequente veranderingen in de warmte- en zoutstromen naar de Noordelijke IJszee, vooral via de Barentsz- en Karazee, en via de Noord-Atlantische Drift. Onze waarnemingen vullen ander werk aan dat laagfrequente variabiliteit heeft vastgesteld in het noordpoolgebied. De belangrijkste boodschap uit dit hoofdstuk is dat verder onderzoek aan laagfrequente modi van natuurlijke variabiliteit noodzakelijk is, zodat recente waarnemingen in de juiste context kunnen worden geplaatst, en de juiste attributie van de drijvende mechanismen achter hedendaagse waarnemingen kan worden gedaan.

De resultaten van het controle-experiment uit Hoofdstuk 3 stelden ons in staat om het mechanisme achter de laagfrequente interne variabiliteit in het zoetwatergehalte van de Noordelijke IJszee vast te stellen en te begrijpen. De volgende stap was om te zien of dit mechanisme ook stand hield in een tijdsafhankelijke simulatie. Het volgende hoofdstuk, **Hoofdstuk 4** *"Simulating the Multicentennial variability of the Arctic Ocean freshwater content over the Holocene with the LOVECLIM climate model"* was daarom gericht op deze taak. Voor dit hoofdstuk voerden we een Holocene simulatie uit voor de periode 8 tot 0 ka BP, aangedreven met de relevante orbitale parameters en broeikasgasconcentraties.

Deze tijdsafhankelijke simulatie liet een periodiciteit met een piek op 220 jaar zien, met een 95% significantie. De mechanismen achter deze periodiciteit waren dezelfde als in Hoofdstuk 3, en na een statistische analyse werd de robuustheid van de resultaten van Hoofdstuk 3 geverifieerd. Een moeilijk interpreteerbaar resultaat uit Hoofdstuk 3 was dat de bijdrage van het zeeijstransport via Framstraat naar de Noord-Atlantische Oceaan niet significant was, wat niet verwacht werd. Echter, in de tijdsafhankelijke simulatie in

Hoofdstuk 4 was dit zeeijstransport prominenter aanwezig en had het een significante invloed op het zoetwatergehalte in de Noordelijke IJszee.

Over het geheel genomen toonden de resultaten van Hoofdstuk 3 en 4 aan dat een laagfrequente intrensieke variabiliteit aanwezig is in de Noordelijke IJszee en beide hoofdstukken benadrukken dat het mechanisme achter deze laagfrequente variabiliteit meegenomen moet worden in de discussies over de oorzaken van klimaatvariabiliteit die we momenteel waarnemen.

Hoofdstuk 5 *"The impact of Sahara desertification on Arctic cooling during the Holocene"* volgt niet direct op de voorgaande hoofdstukken, maar gaat verder op het punt dat ik maakte in de vorige paragraaf, waarin wordt opgeroepen tot het opnemen van alternatieve mechanismen in het huidige klimaatdebat. Er is een aantal wetenschappelijke artikelen verschenen waarin wordt gekeken naar de drijvende kracht achter woestijnvorming in het midden-Holoceen in de Sahara, gaande van grasland naar de bekende woestijn van van nu. We konden echter geen onderzoek vinden waarin werd gekeken naar de invloed van deze woestijnvorming op het klimaat. Deze invloed hebben we vervolgens onderzocht. Onze resultaten lieten zien dat via een land-atmosfeer teleconnectie over een lange afstand de woestijnvorming in de Sahara in het midden-Holoceen een bijdrage van 17 tot 40% had in de waargenomen afkoeling in het noordpoolgebied tussen 9 en 0 ka BP.

"Men wanted for hazardous journey, small wages, bitter cold, long months of complete darkness, constant danger, safe return doubtful, honor and recognition in case of success"

Ernest Shackleton

Chapter 1: General Introduction

1.1 Background and Framework

There is now unequivocal evidence showing climate change has been driven by human activities, with nearly two-thirds of regional climate impacts on natural and human systems related to atmosphere and ocean temperature being directly accredited to anthropogenic forcing (Hansen and Stone, 2016). Indeed, the past three decades have been successively warmer than any of the preceding decades since 1850 (IPCC, 2014). In addition, the northern-hemisphere over the period 1983 to 2012, was likely to have been the warmest 30-year period of the last 1400-years (Stocker *et al.*, 2013).

Given the thermal inertia of the oceans, a certain degree of warming is unavoidable within the near-term future, defined as up to 2035 by the IPCC (Stocker *et al.*, 2013). Across the 4 IPCC Representative Concentration Pathways (RCP) used in the 5th Assessment report, the global mean surface temperature increase for the period 2016 to 2035 will likely range from 0.3 to 0.7°C, relative to the period 1986 to 2005. These results were corroborated by findings of the CMIP5 project which project a global mean surface temperature increase of 0.36°C to 0.79°C over the period 2012 to 2035 (Kirtman *et al.*, 2013).

The simulations that formed the analysis presented by the IPCC also showed that this warming was strongest in northern-hemisphere wintertime, particularly at high-latitudes, with temperatures increasing at twice the global average within the high-northern latitudes (IPCC, 2014), with the mean annual Arctic temperature being 1.5°C warmer than the 1971 to 2000 mean, more than twice the warming of lower latitudes (Overland *et al.*, 2013).

This observed disparity in global warming is due to the process of Arctic amplification, a process driven by, but not restricted to, positive sea-ice-albedo feedbacks within the Arctic region that alter the heat fluxes between the ocean and the atmosphere and snow cover, which affects the heat fluxes between land and the atmosphere. This positive feedback mechanism within the Arctic, causes the net surface albedo of the Arctic Ocean to decrease as sea-ice melts and atmospheric temperatures rise (Manabe and Stouffer, 1980). A similar process occurs when snow-cover melts and exposes more land. These elevated temperatures feedback upon the sea-ice and snow cover, thus reducing the net albedo in the Arctic further (Serreze and Barry, 2011).

These near-term temperature changes are also projected to extend into the mid-21st century, with global mean surface temperatures for the period 2081 to 2100, relative to 1986 to 2015, expected to increase by 0.3 to 0.7°C (RCP2.6), 1.1 to 2.6°C (RCP4.5), 1.4 to 3.1°C (RCP6.0) and 2.6 to 4.8°C (RCP8.5) (Stocker *et al.*, 2013). The likely consequences of this warming will be the continued modification of the Arctic environment, which will have localised and far reaching climatic impacts, unless a global governmental strategy is agreed upon and implemented.

The Arctic Ocean (Fig.1.1), situated between the Pacific and Atlantic Oceans, receives freshwater inputs from some of the largest rivers in the world, receiving 11% of

the worlds freshwater in the process and has an estimated liquid freshwater volume of 74,000km^3 (Serreze *et al.*, 2006). It also receives inputs in the form of annual net precipitation over the Arctic Ocean (~2000km^3), from the Pacific Ocean via the Bering's Strait (2500±300km^3) (Woodgate and Aagaard, 2005) and via the Norwegian Coastal Current (250±50km^3) (Blindheim, 1989). This large input of freshwater is predominantly stored within the top 200m of the Ocean. This allows the Arctic Ocean to be strongly stratified within its upper layers, decoupling forces the deeper, warmer waters from the surface, reducing heat transport through the ocean, and thus promoting the formation of sea-ice. This accounts for 10,000km^3 of freshwater (Serreze *et al.*, 2006) stored within the Arctic as sea-ice, across a large proportion of its surface throughout the year. However, with a recurring sequence of record or near record September sea-ice minima being observed within the Arctic Ocean over the past decade, the prospect of an ice-free Arctic Ocean during summer is becoming more plausible.

To balance these freshwater inputs to the Arctic Ocean, freshwater is exported to the North Atlantic, via the Fram Strait in the form of sea-ice (2300±340km^3) (Vinje *et al.*, 2004) and freshwater (2400±400km^3) (Meredith *et al.*, 2001). It is also exported via the Canadian Arctic Archipelago in liquid form (3200±300km^3) and to a lesser extent sea-ice (160±17km3) (Prinsenberg and Hamilton, 2005).

These exports of freshwater from the Arctic Ocean are an important coupling mechanism of the Arctic Ocean to the global oceanic circulation, via the Atlantic Meridional Ocean Circulation (AMOC). The AMOC plays an important role in regulating the Earth's climate by redistributing heat and salt around the world's oceans. Relatively warm, dense, saline waters are transported in near-surface currents, whereas cooler, less saline waters are transported in deeper layers of the ocean. At specific locations across the globe there are several sites where the near-surface waters descend to the deeper levels of the ocean when the density of the water is higher than the surrounding water masses. These sites are known as deep-water formation sites. Approximate well-known present-day locations of these sites include the Nordic Seas, the Labrador Seas, the Irminger Seas, the Mediterranean Seas and Antarctica (See Fig.1.2). Given that a site of deepwater formation is located in the Nordic Seas, an important location given the export of freshwater from the Arctic Ocean via the Fram Strait, directly into the Nordic Seas, it is likely that any variability of freshwater export via the Fram Strait would have an impact on deep water overturning in the Nordic Seas and thus impact regional and global climate. Indeed, it has been shown that Arctic freshwater exports affect deep-ocean convection in the North Atlantic (Haak *et al.*, 2003; Koenigk *et al.*, 2007).

Deep convection is a result of density variations, caused by differences in temperature and saline content of ocean waters. Relatively dense surface waters sink from the surface to the depths of the ocean, allowing for the transport of heat and saline waters within our oceans. Within the North Atlantic, an important site of deep convection is within the Nordic Seas. Within these seas, warmer waters transported northwards by the North Atlantic Current, are cooled by a combination of surface winds and cooler air temperatures. Eventually, their relative density, being greater than the vertical column

waters, causes these water masses to sink to the depths of the Nordic Seas, creating a branch of the AMOC or 'great ocean conveyor' (Broecker, 2010). Therefore, a freshwater perturbation applied to the North Atlantic Ocean will have an impact on the strength of this overturning.

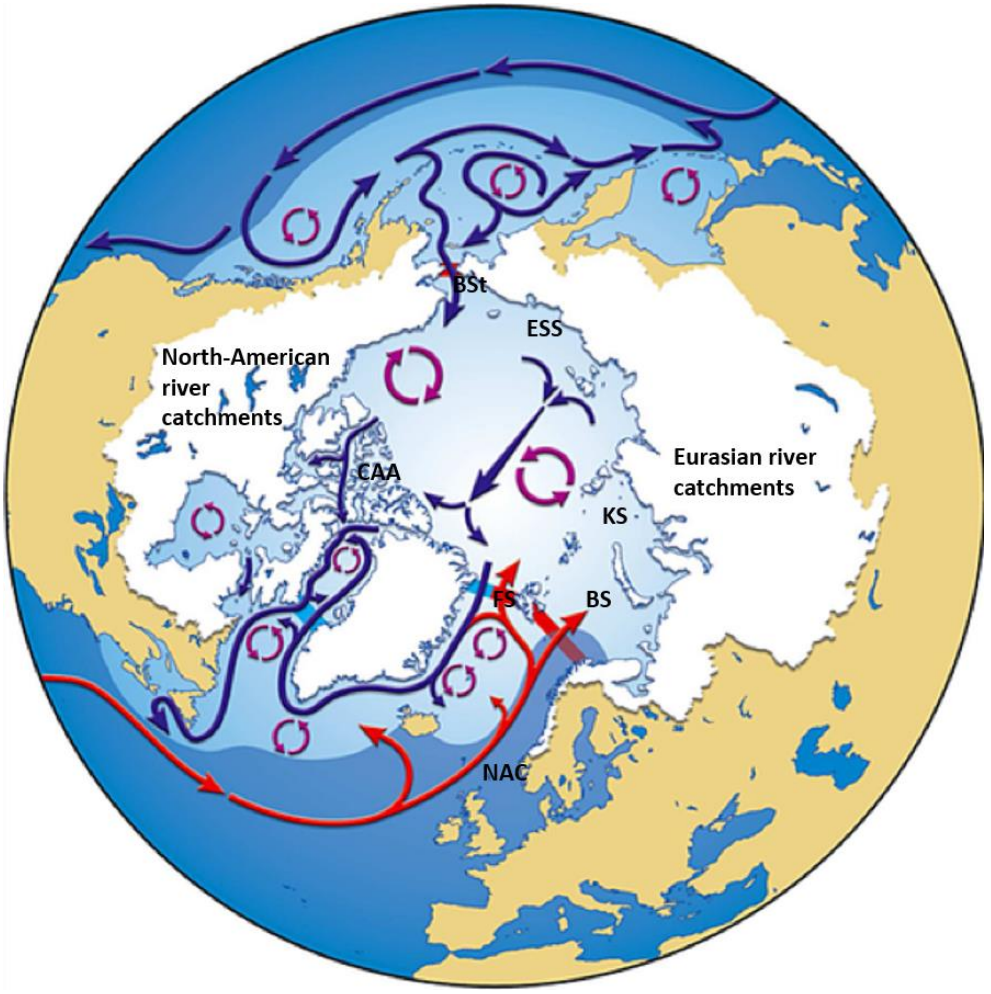

Fig.1.1. Arctic Ocean. The red (warm ocean currents) and blue (cold ocean currents) arrows represent the ocean currents. The white land areas highlight the Eurasian and North-American river catchments that drain into the Arctic Ocean. BSt = Bering Strait; ESS = East-Siberian Sea; KS = Kara Sea; BS = Barents Sea; NAC = North Atlantic Current; FS = Fram Strait; CAA = Canadian Arctic Archipelago (modified from Prowse 2016).

Recent studies have shown that since the 1990s the freshwater content of the Arctic Ocean has been increasing, particularly in the Western Arctic and the Beaufort Gyre (McPhee *et al.*, 2009, Rabe *et al.*, 2011 and Giles *et al.*, 2012), which has largely been driven by an increase in river runoff (Peterson *et al.*, 2002). In addition, we have

seen a 6% increase in the mean annual ice export via the Fram Strait since 1979 (Smedsrud *et al.*, 2017). As a result of these changes it is projected that the volumes of water passing through the various components that constitute the Arctic Ocean freshwater cycle will increase during the 21st century (Holland *et al.*, 2007, Koenigk *et al.*, 2007).

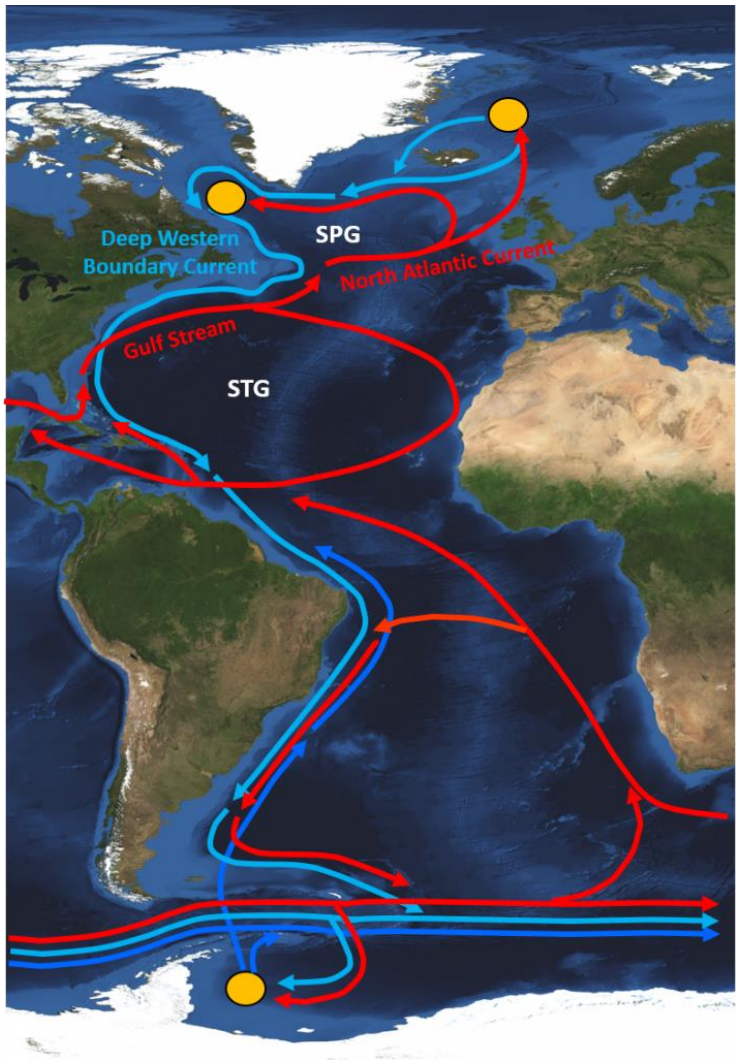

Fig.1.2. Schematic diagram of the Atlantic Meridional Overturning Circulation. Red arrows represent warm near-surface currents; Blue arrows represent cold-deep currents; Yellow circles represent sites of deep-water formation in the Labrador Sea, Norwegian-Greenland Sea, and Antarctic Weddel Sea respectively. The Subpolar Gyre (SPG) and Subtropical Gyre (STG) are also depicted. RACE Project Synthesis (2015) Synthesis.

Therefore, being cognisant of these changes occurring in the Arctic, this thesis focuses on investigating the freshwater budget of the Arctic Ocean during the Holocene, the present day and the 21st century. This is achieved through the application of modelling studies. This thesis forms part of a scientific collaborative project, drawing on the expertise of six institutes across Europe entitled: "CASE ITN: The Changing Arctic and Sub-Arctic Environment". Further information on the project and its partner institutions can be found at http://caseitn.epoc.u-bordeaux1.fr/index.php/home.html. The overreaching aim of this project was to ascertain and advance understanding of how observed climatic changes to the Arctic and Nordic Seas compare with past changes observed during the Holocene (~the past 11,700 years), and how do intrinsic changes of the climate system stand in the context of the present day human-influenced modulation of the climate system.

This introductory chapter serves to introduce a general background for the work presented in this thesis. Firstly, a description of the climate system (Section 1.2) is given, followed by an overview of the Milankovitch theory of orbitally driven climate change (Section 1.3), greenhouse gas concentrations (GHGs) (Section 1.4), ice sheets (Section 1.5), the Holocene (Section 1.6), and a description of climate modelling (1.7). This will be followed by a detailed description of LOVECLIM, the Earth System Model of Intermediate Complexity (EMIC) used throughout this thesis (Section 1.8) and its advantages (Section 1.9). Finally, this leads to an overview of the research questions I sought to address in this thesis (Section 1.10).

1.2 The Climate System

The climate is the longer-term conditions (defined as 30-year mean; WMO, 2007) of temperature, rain, humidity, winds etc. that we expect for any given location and time. Climate variability, defined as the variations in the mean state of the climate on all temporal and spatial scales, beyond single weather events, is the net result of external and internal forcings, and feedbacks within the climate system, which is a representation of the current state of the atmosphere, the hydrological cycle, the land surface, the cryosphere, and the biosphere.

The composition of the atmosphere has changed naturally throughout the history of the Earth. The main constituents of the atmosphere are Nitrogen (78.1%), Oxygen (20.9%) and Argon (0.93%), plus several trace gases, including carbon dioxide (CO_2), methane (CH_4), nitrous oxide (N_2O) and ozone (O_3). The trace gases, CO_2, CH_4, N_2O and O_3, known as greenhouse gases, absorb and emit infrared radiation and play an important role in modulating the Earth's energy budget. In addition, water vapour contained within the Earth's atmosphere also acts as a greenhouse gas.

The hydrological cycle comprises all fresh and saline water components on our planet including, the seas, oceans, lakes, wetlands, and underground stores. The Oceans cover 70% of the Earth's surface and store vast amounts of carbon dioxide (CO_2) and heat.

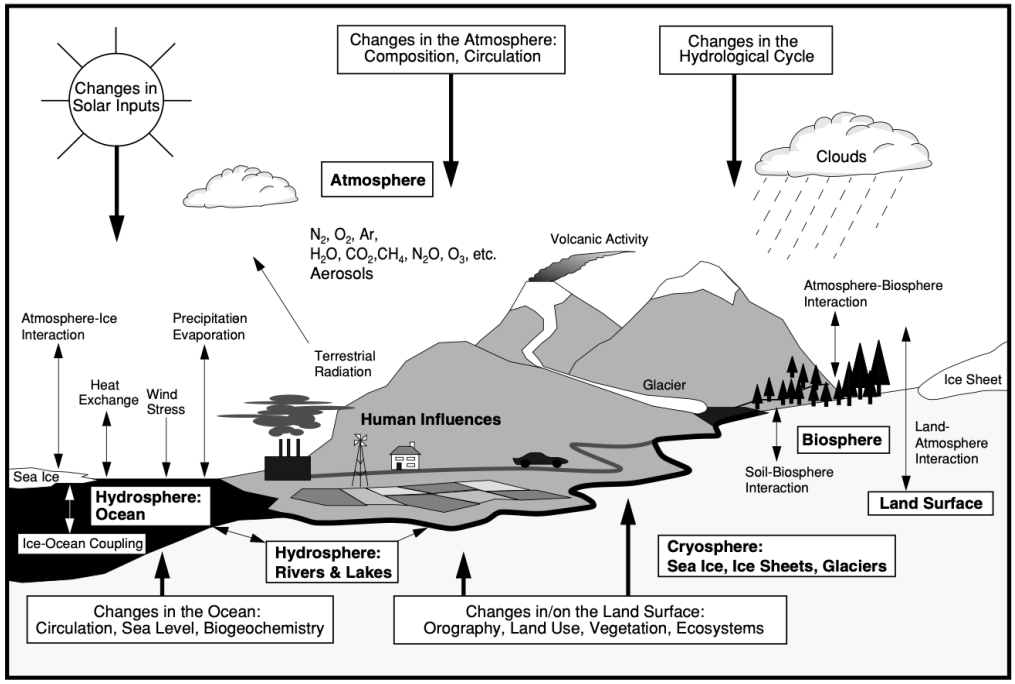

Fig.1.3. Schematic of the components of the global climate system (bold arrows), their processes and interactions (thin arrows) with the other elements of the climate system IPCC (2001).

Due to the high thermal inertia of the oceans, they regulate climatic variability over the longer-time scales.

The cryosphere is comprised of the world's large icesheets, The Greenland Icesheet, and the Antarctic Icesheet, along with the numerous smaller ice caps found in the high- and low-latitudes. It also includes sea-ice, permafrost, and snow fields. The high albedo for solar radiation of snow and ice, along with its low thermal conductivity, are the features of the cryosphere that form its strongest connection to the climate system.

These components that form the climate system are dynamic and undergoing constant change due to a series of forcings, feedbacks and boundary conditions. Forcings can be external or internal to a dynamical system and in the context of the Earth's climate system these include the orbital configuration of the Earth (the Milankovitch theory see section 1.3) and greenhouse gas concentrations (see section 1.4). Feedbacks are transfers of energy within the climate system and work to either amplify (positive feedback) or reduce (negative feedback) the effect of a forcings. Feedbacks operate over different timescales with those related to sea-ice, clouds, and atmospheric particles extending from weeks to decades, whereas processes such as vegetation growth and ice-sheets extend over centuries to millennia, with plate tectonics operating over millions of years. Boundary conditions are what defines the edges of the system. Together these operate, over a range of timescales, leaving us with a highly dynamic climate system.

An important aspect to consider, within the context of climate modelling studies, is whether a process should be defined as a feedback, a forcing, or a boundary condition. To do so, one must consider the length of time the climate process operates over and the length of the period of interest. If the period of interest is shorter than the timescale of the climatic process, then it can be defined as a boundary condition.

In the context of this thesis nearly all the simulations were conducted over the Holocene. Therefore, the orbital configuration and greenhouse gas concentrations were considered forcings, whereas icesheet configuration, sea-level and the solar constant were considered boundary conditions.

1.3 Milankovitch theory

It was not until the last 150 years that the variation of the Earth's orbital parameters were known to have a significant impact on the Earth's climate. Nowadays this theory is commonly known as the Milankovitch theory (Milankovitch, 1941). The theory is based on the assumption that surface temperatures vary in response to regular and predictable changes in the earth's orbit and axis, amplified by several positive feedbacks, thus the orbital configuration determines the distribution and amount of insolation upon the Earth's surface at all latitudes.

Planetary gravitational influences modify the shape of the Earth's orbit around the sun over a period of ~100ka (ka = thousand years) during which time the shape of the earth's orbit varies from an almost circular orbit to an elliptical one. This process is known as the eccentricity of the orbit (blue line in Fig.1.4).

In addition, the tilt of the Earth's axis varies between 21°39' to 24°36' over a period of ~41kyr (green line in Fig.1.4). It is the angle between the plane of the Earth's equator and the plane of the Earth's orbit around the sun and is known as the obliquity.

The third and final variable is due to the gravitational pull exerted by the sun and the moon which causes the earth to wobble on its axis. A consequence of this is that the equinoxes precess around the sun in a regular fashion and thus the season when the earth reaches perihelion (the point where the earth is closest to the sun) to the sun varies. Currently, the northern hemisphere winter occurs when the sun is in perihelion (the point where the earth is closest to the sun) and summer occurs when the sun is in aphelion (the point where the earth is furthest from the sun). It has been found that the periodicity with which this precessional cycle varies has both minor (~19kyr) and major (~21kyr) periodicities (red line in Fig.1.4).

The amount of incoming solar radiation received at the Earth's surface is partly determined by its eccentricity. The orbit of the Earth around the sun is not a perfect circle, but an ellipse, resulting in different lengths of the season when the Earth is closest or furthest away from the Sun. Modulated on top of this is the precession, which determines the time of the year when the earth is closest to the sun. Currently perihelion occurs in January and in approximately 10.5ka years' time it will occur in June. Finally, the greater the obliquity, or tilt of the earth around its axis is, the larger the seasonal contrast between the summer and winter is.

Yearly variations caused by the changes in insolation are relatively small, whereas over longer periods of time, centuries, millennia etc., they can amount to values that have a significant impact upon the climate. Therefore, in the context of this thesis and the papers contained within, it is important to include these variables within any experiments.

The Milankovitch theory, the theory that orbitally driven variability in the insolation at the Earth's surface is a major factor driving climatic cycles such as ice ages (Milankovitch, 1941), was originally met with strong resistance (Puetz *et al.*, 2016). It was not until the 1960s and 1970s when work on deep-sea sediments, specifically the work on oxygen isotope analysis on marine microfossils identified the three indices of global climate, eccentricity, obliquity, and precession (Hays *et al.*, 1976).

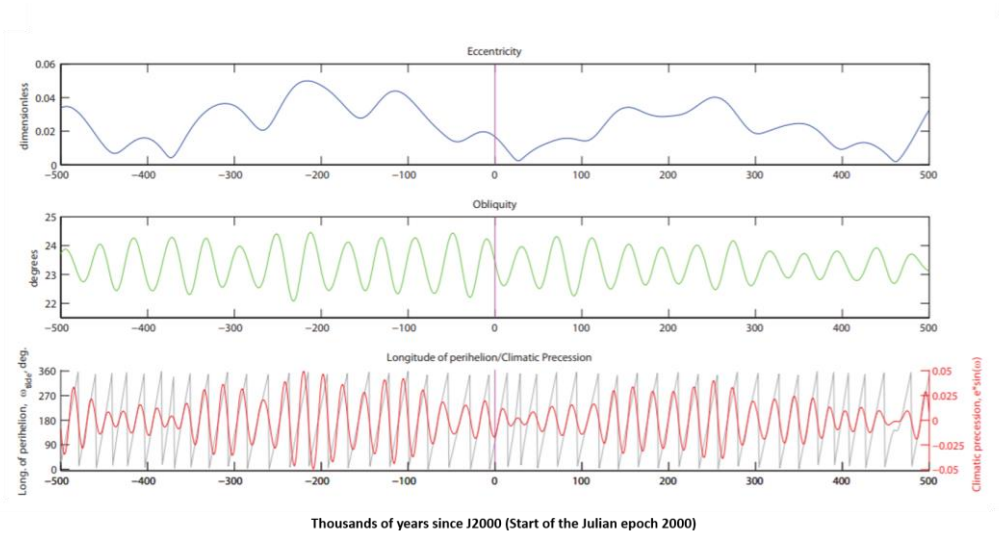

Fig.1.4. Plot of Milankovitch orbital parameters spanning 500 ka before and after present (J2000). Top time-series plot: eccentricity; Middle is obliquity; and the bottom figure is and longitude of perihelion and climatic precession (Kostadinov and Gilb, 2014).

1.4 Greenhouse gas forcing

The radiative properties of carbon dioxide (CO_2), methane (CH_4), and Nitrous Oxide (N_2O), allow them to absorb and re-emit long-wave radiation emitted by the Earth's surface, trapping heat within the atmosphere and preventing the loss of heat to space. Without this process, Earth would be uninhabitable, as the average global surface temperature would be -18°C (Ma and Tipping, 1998). This compares to ~14°C (NOAA, 2020) which is the 1901-2000 average combined land and ocean annual temperature.

If we were to look at proxy-based reconstructions of GHG concentrations, we would see they have varied consistently throughout the geological record (Fig.1.5). Over the Holocene atmospheric CO_2 concentrations have increased from 260ppm at 11ka, to 280ppm during the Pre-Industrial period (Monnin *et al.*, 2004). Today in August 2020 the global atmospheric CO_2 concentration stands at 412ppm. CH_4 levels were ~750ppb around 11ka, after which they decreased to ~550ppb 5ka. This was then followed by an increase to 750ppb pre-industrial (Kobashi *et al.*, 2007). Since then CH_4 levels have continued to increase and in August 2020 were upwards of 1875ppb. Throughout this study, we use reconstructed GHG concentrations as a forcing of our climate simulations throughout the Holocene and in the 21st century.

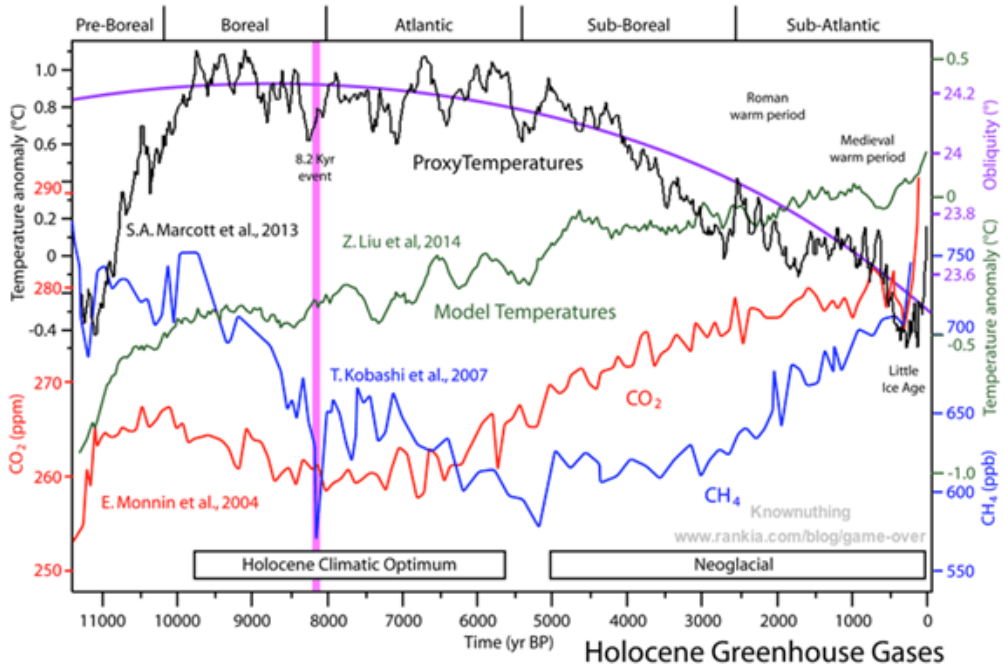

Fig.1.5. Temperature and atmospheric gas concentrations over the Holocene (Curry, 2017).

1.5 Icesheets

The Antarctic and Greenland Icesheets are the two largest icesheets on our planet. This has not always been the case because during the past ice age, icesheets covered large expanses of North America (the Laurentide Icesheet) and Scandinavia (the Fennoscandia Icesheet). The beginning of the Holocene, the current interglacial period which began ~11.7k, marked the end of the last major deglaciation, with a retreat of the Fennoscandian Icesheet. This icesheet extended from the UK north-eastwards over northern-Germany, Poland, the Baltics, Scandinavia, and Finland. At the same time, the Laurentide Icesheet which covered North-America, as far south as the Northern-Plains was also in retreat. But by 9.7ka and 7 to 8ka, respectively, they had all but disappeared (Dyke and Prest, 1987; Stroeven *et al.*, 2016).

It is known from modelling experiments that the configuration of icesheets have the ability to impact climate on a large scale (Singarayer and Valdes 2010). When used within modelling studies the way they are utilised often occurs in two ways. Firstly, the icesheets are fixed in spatial extent, height, geometry, and albedo. This allows an equilibrium icesheet response to the climate to be observed. Secondly, we can study the impact of icesheet melt by applying a freshwater forcing to a location in the ocean, as has been done when simulating the 8.2ka event (Matero *et al.*, 2017).

Incorporating icesheets into palaeoclimate modelling is not an easy task and often requires the user to define the icesheet as either a boundary condition or a forcing. Throughout this dissertation I choose to keep the Greenland and Antarctic Icesheets fixed

and use them as a boundary condition. Therefore, the configurations of the Greenland and Antarctic Icesheets were fixed with a modern-day configuration.

1.6 The Holocene

$\delta^{18}O$ reconstructions from ice cores recovered from five drilling sites on the Greenland Icesheet are interpreted as temperature reconstructions and show the stability of the temperature throughout the Holocene. Fig.1.6 shows the $\delta^{18}O$ records, which can be used as a proxy for temperature, from these five drill sites on the Greenland Icesheet. These five ice-core records show that temperatures increase during the early Holocene, followed by a thermal maximum in the early-to-mid Holocene, which is then followed by a gradual cooling over the remainder of the Holocene. Over the course of the Holocene the size of the Greenland and Antarctic ice-sheets have remained relatively constant, except for some thinning during the Holocene climate optimum ~9000 to 6000 years ago (Vinther, 2009), and the longer term climatic forcings have predominantly been accredited to the orbital parameters (Milankovitch theory, section 1.3 of this thesis) and natural variations of GHG concentrations (see section 1.4 of this thesis).

However, within the 'stable' climate there have been periods of rapid climate change, for example the 8.2ka event (Kobashi *et al.*, 2007), cold events such as The Little Ice Age (Mann *et al.*, 2009), warmer periods such as The Medieval Climate Anomaly (Mann *et al.*, 2009) and multicentennial climate variability, such as Bond cycles (Bond *et al.*, 1997).

The 8.2ka event is captured in all five of the Greenland ice cores shown in Fig.1.5 and was a relatively short-lived event (200-400years) that saw a decrease in global temperatures. The cause of this event is largely accredited to a large freshwater perturbation of the Atlantic Meridional Overturning Circulation that originated with a large release of freshwater from Lake Agassiz, which formed part of the Laurentide Icesheet (Kobashi *et al.*, 2007).

The Little Ice Age was a relatively recent period of cooling that can be split into three cooler periods, which began at 1650, 1770 and 1850 and were interspersed with warmer periods. The often-cited cause of these cold periods is solar minima (Eddy, 1979). Indeed, the Maunder minima (1645 to 1715) occurred during the Little Ice age, as did the Dalton Minima (1790 to 1830).

We have also seen that the Holocene climate optimum (9 to 6ka) was a period where global temperatures peaked (Renssen *et al.*, 2012). This warming was driven by orbital forcings with summer insolation 30 to 40 Wm^{-2} greater than present day (Renssen *et al.*, 2012). By this time, the Fennoscandia and Laurentide Icesheets had disappeared, and the configuration of icesheets was similar to present day.

It was also during the mid-Holocene that we observed an African humid period (deMenocal *et al.*, 2000; Kröpelin *et al.*, 2008). An orbitally enhanced summer monsoon led to a wetter period across northern Africa. This allowed for greater vegetation coverage across present day Sahara (deMenocal *et al.*, 2000). Drivers of this have been accredited

to orbital forcings which led to an orbital enhancement of the summer monsoon (deMenocal *et al.*, 2012).

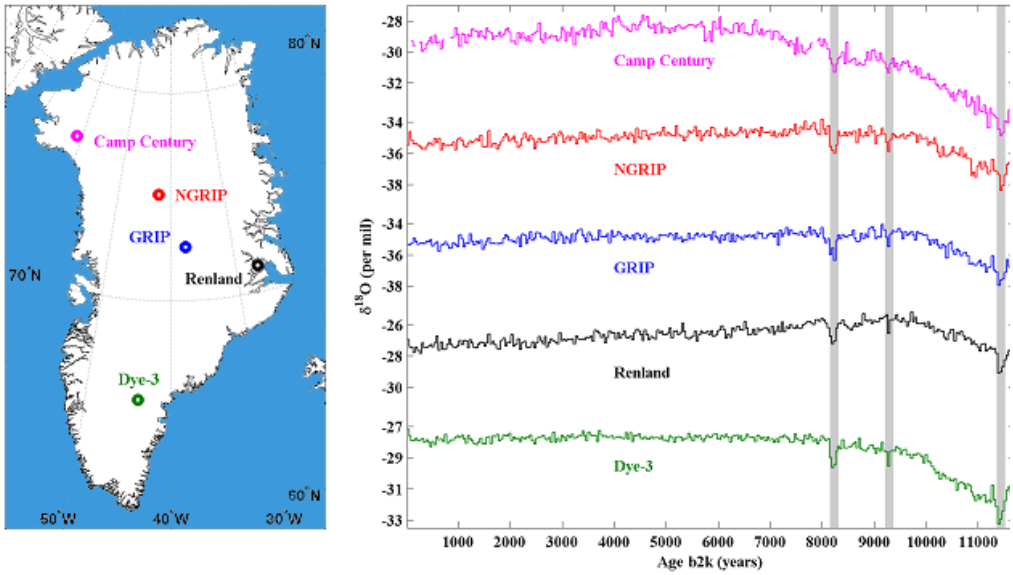

Fig.1.6. Map showing the 5 drill sites for the five ice cores spanning the entire Holocene, with the corresponding reconstructed Holocene temperature records, reconstructed from oxygen isotope analysis. b2k means before 2000AD. The 3 grey shaded areas represent the 3 cold events within the ice core oxygen isotope record (Ice and Climate, 2019). The one at ~8.2ka is known as the 8.2ka event, the one at 9.4ka is a weak cold event known as the Erdalen Event and the one at ~11.3ka is known as the Preboreal Oscillation.

Multicentennial climate fluctuations within the Holocene, more commonly referred to as Bond Cycles, are a record of ice-rafted detritus that show a ~1500-year cycle of climate variability over the course of the Holocene (Bond *et al.*, 1997). The Holocene has thus displayed significant climate variability which is important for understanding the impacts of anthropogenic climate change in the 21st century and beyond. This is particularly true for the warm periods such as the Mid-Holocene Climate Optimum along with the Medieval Climate Anomaly, which have both been proposed as analogues for 21st century temperature changes, owing to similar reconstructed warming for these periods.

1.7 Numerical climate modelling

Numerical climate models are mathematical representations of the physical, chemical, and biological components of the climate system. However, it is not possible to fully represent every aspect of the climate system due to computational limitations of the computers used to run the climate model. Therefore, aspects of the climate system must be approximated within the model. The most obvious process of all climate models that

is approximated is cloud dynamics. The processes governing cloud formation occur at scales that are below that of even the highest resolution models, meaning these processes need to be approximated, and all subsequent cloud related processes, such as precipitation and the radiation balance, need to be parametrised.

Due to the vast number of components that could potentially be used to construct a climate model, a distinct climate model hierarchy has developed over time. It is now widely considered that there are three distinct categories of climate models, beginning with zero-dimension energy balance models being the most simple, followed by Earth system Models of Intermediate Complexity (EMICs) being the middle-ground, with fully coupled Earth System Models (ESMs) classed as the most sophisticated within the climate modelling hierarchy (Claussen *et al.*, 2002). Fig.1.7 provides a schematic illustration of climate models as a function of their complexity and the processes within them (McGuffie and Henderson-Sellers, 2014).

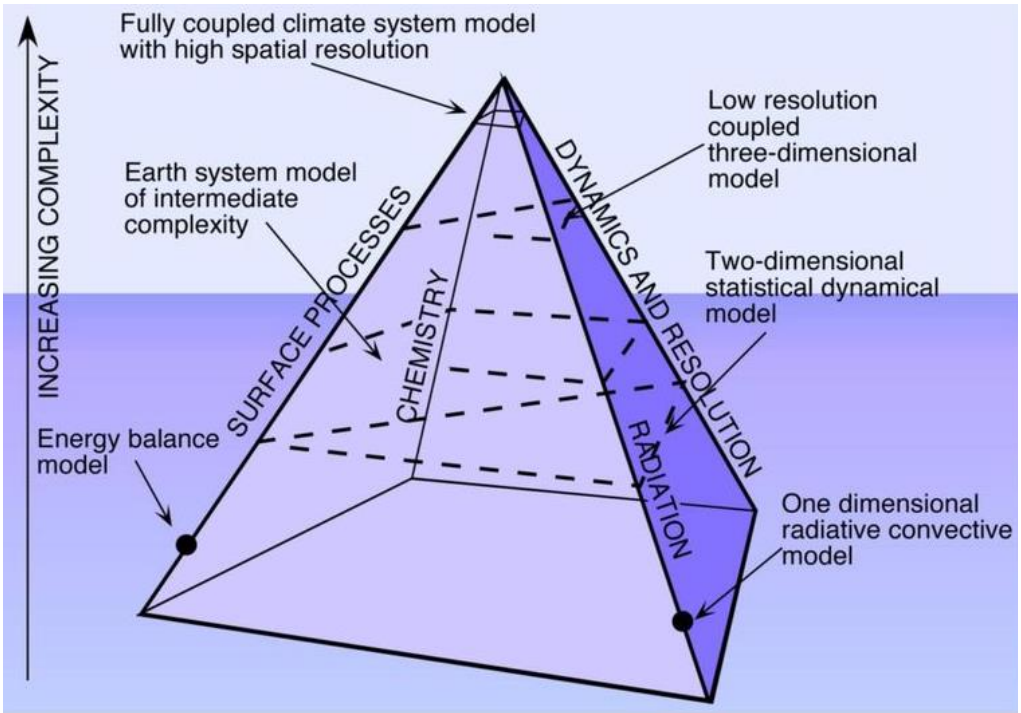

Fig.1.7. Schematic illustration of different types of climate models and their complexity (McGuffie and Henderson-Sellers, 2014).

As the climate pyramid visually demonstrates, no one model incorporates into its being all the processes over all the timescales, meaning that a decision needs to be made as to which category of climate model to use for your research. The most complex models, ESMs, provide the most detailed results of the current and future climate. However, these models are tuned to the present-day climate, and may not necessarily have the correct sensitivity to a large change in forcings. In addition, the time needed to run these for

relative short simulations (~100 years) is computationally expensive, i.e. it takes a long time. Therefore, they are not suited for multi-millennial climate simulations that are required to study climate changes over glacial/interglacial cycles. For this purpose, we need to employ an EMIC and throughout this thesis we employ the use of one EMIC, LOVECLIM.

A final, but important remark about climate models and their application is that it is important that results from climate models be compared and discussed alongside those of proxy-based reconstructions or contemporary data. By using these valuable resources in combination, research results will carry a greater degree of robustness when critiqued.

1.8 The LOVECLIM Earth Model of Intermediate Complexity

The LOVECLIM climate model, used throughout this thesis, is categorised as an Earth System Model of Intermediate Complexity (EMIC), meaning that the spatial resolution of the model is coarser than that of more complex Earth System Models (ESMs) and the physics employed in the model are more simplistic. This is particularly true for the atmosphere, because within ESMs the atmosphere is the most computationally expensive component, so by reducing this complexity allows simulations performed with LOVECLIM to be integrated faster. Therefore, it also means that LOVECLIM is ideally suited to perform long simulations, allowing for the investigation of centennial to millennial scale climate changes. Given that the main driver of climate over these timescales is the ocean, employing a model with a reduced atmosphere complexity is not considered a major hindrance.

LOVECLIM has been employed in a range of studies. It has been demonstrated that its modern-day climate is in good agreement with observations, including temperature, precipitation, and sea-ice cover in both the northern and southern hemisphere (Goosse *et al.*, 2010). LOVECLIM is able to simulate the features of deep convection in the high-northern latitudes in the Labrador Sea, Irminger Sea and south of Svalbard with reasonable skill (Goosse *et al.*, 2010). Within this thesis (Chapter 2) it has also been shown to be able to simulate a modern-day Arctic Ocean freshwater cycle (Davies *et al.*, 2014). At 6ka BP LOVECLIM simulates increased summer surface temperatures, particularly in the high-northern latitudes over the continents and the Arctic (Goosse *et al.*, 2010). In general, the results of the 6ka simulation performed with LOVECLIM capture similar characteristics of the climate that have also been observed in other models involved in the experiments performed within the Paleoclimate Modelling Intercomparison Project (PMIP 2014, Braconnot *et al.*, 2007). In addition, it has successfully been applied to simulate various past climates, including the last millennium (Goosse *et al.*, 2005), the last glacial maximum (LGM) (Roche *et al.*, 2007), the Holocene (Renssen *et al.*, 2009), the 8.2 ka event (Wiersma and Renssen, 2006), and the last interglacial (Bakker *et al.*, 2013). The results of these simulations are consistent with those of comprehensive GCMs (Goosse *et al.*, 2010; Bakker *et al.*, 2013; Nikolova *et al.*, 2013).

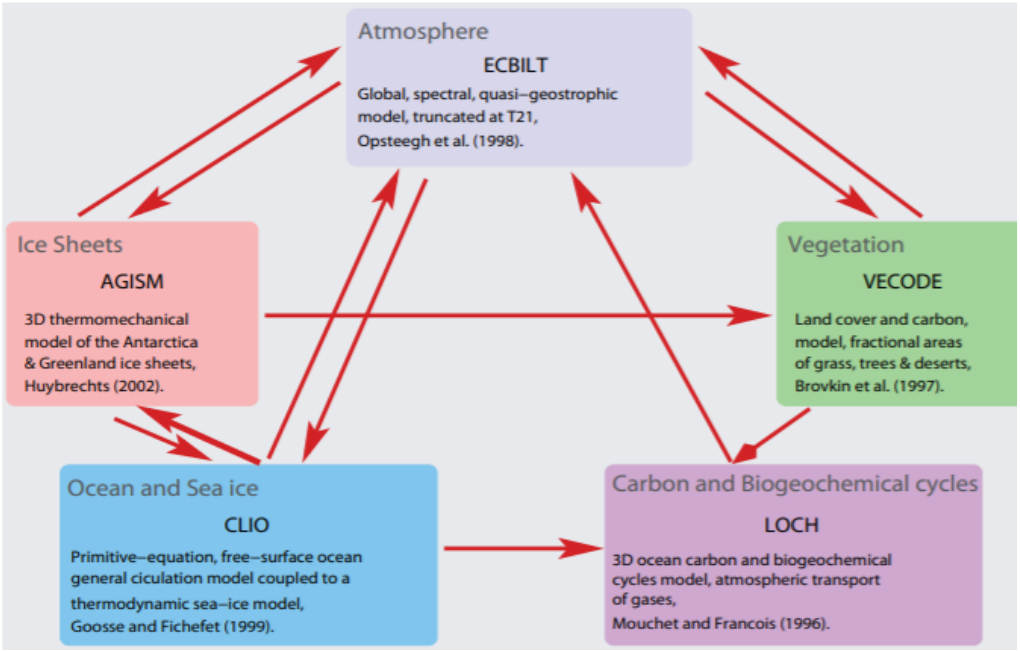

Fig.1.8. Schematic of the coupled components of LOVECLIM. In this study, only the ECBilt, CLIO and VECODE-LBM components are applied (Goosse *et al.*, 2010).

The version of LOVECLIM used in this thesis is composed of an atmosphere component (ECBilt) (Haarsma *et al.*, 1996; Opsteegh *et al.*, 1998), a coupled sea-ice-ocean component (CLIO) Goosse *et al.*, 1997 and a terrestrial biosphere model (VECODE) (Brovkin *et al.*, 2002).

The atmosphere component, ECBILT (Haarsma *et al.*, 1996; Opsteegh *et al.*, 1998) has three vertical layers (800hPa, 500hPa and 200hPa) a horizontal T21 truncation (5.6° x 5.6° latitude -longitude), a full hydrological cycle, and is governed by the equation for quasi-geostrophic potential vorticity within this space. The ageostrophic terms, included to improve the representation of circulation in the low latitudes, are obtained by computing the vertical velocity and the horizontal divergence (Opsteegh *et al.*, 1998). Within this atmospheric space, the radiative scheme and the thermodynamic exchange between the layers and the surface are computed. Temperature is calculated at the surface, at 650hPa and at 350hPa levels. Humidity is represented by a single prognostic variable, which is the total precipitable water between the surface and the 500hPa level. To account for the fact that humidity is generally higher closer to the surface, where wind speeds are lower, the prognostic variable for humidity is transported horizontally using a fraction of the sum (60%) of the geostrophic and ageostrophic winds at the 800hPa level. Above the 500hPa level, it is assumed that the atmosphere is completely dry, and thus, all water above this level is converted to precipitable water. Additionally, if the total precipitable water passes a specific threshold, defined as 0.83 times the vertically integrated saturated specific humidity, and assuming a constant relative humidity within the layer, precipitation also occurs below the 500hPa level (Goosse *et al.*, 2010).

In ECBilt, clouds are not resolved based on convection and condensation of evaporated precipitate; instead clouds are prescribed based on the modern day ISCCP D2 dataset (1983-1995) (Rossow *et al.*, 1996) with the total upward and downward radiative fluxes computed as a function of this dataset (Schaeffer *et al.*, 1998; Goosse *et al.*, 2010). In turn this means that clouds and precipitation are decoupled from one another within the model. This is an obvious limitation of the model, in that the radiative feedbacks between clouds, the atmosphere and the land surface may be simplified and affect planetary albedo.

The land surface component of the model is a subsection of ECBilt and has the same grid resolution as the atmospheric component. Additionally, river runoff is computed using a simple bucket method, in that the volume of water in the bucket is a function of the vegetation type. If the water level of the bucket is higher than the allowed capacity of the bucket after precipitation, evaporation and snow melting have occurred, then the excess water is transferred directly to the mouth of the corresponding river basin.

The oceanic component, CLIO (Goosse *et al.*, 1997), is a primitive-equation, free-surface ocean model that consists of a general ocean circulation model (Deleersnijder and Campin, 1995; Deleersnijder *et al.*, 1997) coupled to a thermodynamic-dynamic sea-ice model (Fichefet and Morales Maqueda, 1997 and 1999) with a 3°x3° latitude-longitude resolution. It includes realistic bathymetry, classical approximations (Boussineq, thin shell and hydrostatic), plus the eddy-induced advection term of Gent and McWilliams (1990). In addition, it is comprised of two spherical subgrids, to avoid North Pole singularity and allow more evenly sized grids at higher latitudes (Madec and Imbard, 1996). The resolution of the model does not allow for a realistic representation of flow through the Bering Strait, therefore it is determined by the sea-level difference across the strait, following the geostrophic control theory (Goosse *et al.*, 1997). Sea-ice is represented by a three-layer model where each floe of ice is divided into two homogenous layers upon which snow accumulates, when the surface temperature is below the freezing point and precipitation occurs. If sufficient snow accumulates upon the floe, it is depressed below the surface layer of the underlying water, whereby it becomes immersed in seawater. The combination of accumulating snow and freezing seawater allows for the ice floe to increase in thickness (Fichefet and Morales Maqueda, 1997). Even though the thermodynamic processes that govern the vertical decay and growth of sea-ice within CLIO are a simplified version of reality, the model has the ability to replicate the geographical extent of seasonal sea-ice in both hemispheres (Goosse *et al.*, 2010).

The vegetation component, VECODE (Brovkin *et al.*, 2002), is a reduced form dynamic global vegetation model which is capable of simulating the dynamics of two plant functional types (trees and grasses), in addition to a dummy type (desert). These interact with the atmosphere through only their albedo and do not affect other processes such as evapotranspiration (Goosse *et al.*, 2010).

1.9 Advantages of LOVECLIM

Amongst the spectrum of climate models, LOVECLIM falls within the middle ground in terms of complexity. As such it is classified as an Earth System Model of Intermediate Complexity (EMIC). However, this does not make it a lesser model to use in climate modelling studies. In fact, the context of the analysis is critical when choosing the correct model for climate modelling studies.

The most complex models are known as ESMs. These include a wide range of components of the climate system and are intended to provide the best possible representation of climate system dynamics. However, this comes at a cost, computation cost, which limits the temporal scale they can be used to study. Thus, choosing the model with the highest resolution is not always the best choice. This is where EMICs come into their own, as despite their often lower resolution, simplified dynamics and higher number of parameterisation of processes, they are often the most appropriate models to use for climate simulations spanning millennia, even glacial cycles. This allows multiple simulations, over large timescales, such as the Holocene to be performed within a relatively short time, and at no substantial impact to the quality of the results.

LOVECLIM has been used in numerous studies of palaeoclimate including studies ranging from the Millennium (Goosse *et al.*, 2005) to the last interglacial (Bakker *et al.*, 2013). In addition, the last Glacial Maximum (Roche *et al.*, 2007), the Holocene (Renssen *et al.*, 2009) and the 8.2 ka event (Wiersma and Renssen, 2006) are all but a few examples of other studies where LOVECLIM has been applied. The results of LOVECLIM have also been tested against those of ESMs and they have shown to be consistent with them (Goosse *et al.*, 2010; Bakker *et al.*, 2013; Nikolova *et al.*, 2013). Therefore, we have no doubt that LOVECLIM is a suitable model to use throughout this thesis.

1.10 Overview of research questions

Studying the Arctic freshwater cycle provides an opportunity to show how it responded to past warm climates and how natural intrinsic mechanisms controlling various aspects of the Arctic freshwater cycle have varied throughout the Holocene. This has led to structuring the thesis as follows:

Chapter 2: "*The Arctic freshwater cycle during a naturally and an anthropogenically induced warm climate*".

The projected temperature increase in the Arctic region during the 21st century is often compared to what occurred there during the mid-Holocene. However, the climates of these two periods evolved due to a very different set of forcings. Therefore, to solely focus on the response of the Arctic based on the change in temperature is not giving a full appreciation to the fact that the underlying state of the various components that comprise the Arctic freshwater cycle could respond differently to these forcings. In this chapter, we compared the response of the various components that comprise the Arctic Freshwater cycle between the mid-Holocene and the 21st century.

Chapter 3: *"An intrinsic mechanism of multicentennial variability of the Arctic Ocean freshwater content".*

In this chapter we further explored a result we observed in the previous chapter. We observed in our climate simulation of the modern period, that the Arctic Ocean freshwater content displayed a clear periodicity, between its maximum and minimum states, on the order of ~250-years. We wanted to understand this phenomenon further, in particular the mechanisms that were driving this variability. However, as our simulation in Chapter 2 included numerous external climate forcings, we had to perform a control simulation with fixed pre-industrial forcings which would allow us to understand the intrinsic mechanisms controlling the Arctic Ocean freshwater content.

Chapter 4: *"Simulating the multicentennial variability of the Arctic Ocean freshwater content over the Holocene with the LOVECLIM climate model".*

In this chapter we further explore the intrinsic mechanism of multicentennial variability of the Arctic Ocean explained in Chapter 3, but this time we use a transient climate simulation over the Holocene.

Chapter 5: *"The impact of Sahara desertification on Arctic cooling during the Holocene".*

As can be seen, this is a slight departure from the main theme of the thesis. However, it was included as it highlights that relative minor changes to the atmosphere, induced by a relatively large vegetation change in the Sahara, can have far reaching impacts in the Arctic. Studies show that the Sahara was vegetated during the early Holocene (9000 to 6000 years ago), however we are more familiar with a desert Sahara. There have been many studies that have sought to understand the reasons for this change, and these, along with the speed at which they occurred are still a hot topic of debate, and one which we do not try to resolve. Instead, we approached this problem from the opposite angle, instead of asking how did the climate impact the vegetation in the Sahara as many before have done, we wanted to know how the vegetation change in the Sahara effected the climate? Given that the Sahara is the world largest non-polar desert, it seemed a reasonable assertion that it would likely have some impact, either locally or globally.

"Everyday some new fact comes to light - some new obstacle which threatens the gravest obstruction. I suppose this is the reason which makes this game so well worth playing"

Robert Falcon Scott

Chapter 2: The Arctic Freshwater Hydrological Cycle during a naturally and an anthropogenically induced warm climate

Published as: Davies FJ, Renssen H, Goosse H (2014) The Arctic freshwater cycle during a naturally and an anthropogenically induced warm climate. Clim Dyn 42: 2099-2112. doi.10.1007/s00382-013-1849-y

Abstract

The Arctic freshwater hydrological cycle plays an important role in regulating regional and global climate. Current observations suggest that an intensification of the high-northern latitude hydrological cycle has caused a freshening of the Arctic and sub-Arctic seas, increasing the potential of weakening overturning strength in the Nordic Seas, and reducing temperatures. It is not known if this freshening is a recent phenomenon and a manifestation of the current anthropogenic warming, or if the Arctic freshwater hydrological cycle has exhibited a similar response to past, naturally induced periods of warming, for example during the mid-Holocene hypsithermal event. Thus, we have used an earth model of intermediate complexity, LOVECLIM, to investigate the response of the Arctic freshwater hydrological cycle, during two warm periods that evolved under different sets of forcings, the mid-Holocene and the 21st century. A combination of proxy reconstructions and modelling studies have shown these two periods to exhibit similar temperature profiles however, it has yet to be determined if the Arctic freshwater hydrological cycle and thus, the transport and redistribution of freshwater to the Arctic and the sub-arctic seas, during the two warm periods, is comparable. Here we provide an overview that shows that the response of the Arctic freshwater hydrological cycle during the early 21st century could be interpreted as an 'extreme' mid-Holocene hydrological cycle. Whilst for the majority of the 21st century, the Arctic freshwater hydrological cycle will likely transition into what can only be described as truly anthropogenic in nature.

2.1 Introduction

In recent decades, the Arctic has been warming at a rate far greater than any other region on the planet, drawing the attention of a broad scope of society. This amplification of warming in the high-northern latitudes is due to a series of complex positive feedbacks (Manabe and Stouffer, 1980) and it is likely to continue into the 21st century, with temperatures in the Arctic projected to rise anywhere between 2.8°C and 7.8°C (Christensen *et al*, 2007). With noticeable changes already being observed in the Arctic, it is vital to understand the effect this warming is likely to have upon the climate system, especially when the reach of these effects is likely to extend further afield than the Arctic. It has already been observed that, the extent and thickness of both the perennial and seasonal sea-ice has decreased (Comiso *et al.*, 2007; Stroeve *et al.*, 2007); the Arctic hydrological cycle is intensifying (Kattsov and Walsh, 2000); the Greenland Ice Sheet has shown increased melting at its periphery (Krabill *et al.*, 2004; Chen *et al.*, 2006; Luthcke

et al., 2006), which is being further enhanced by the acceleration of a number of its tidewater glaciers (Rignot and Kanagaratnam, 2006); river discharge into the Arctic Ocean from Eurasian and Canadian rivers has been increasing (Peterson *et al.*, 2002; Déry and Wood, 2005; Déry *et al.*, 2009; Shiklomanov and Lammers, 2009); and the southern extent of permafrost has been decreasing, which is accompanied with a deepening of the active layer (Kwong and Gan, 1994; Jorgenson *et al.*, 2001; Serreze *et al.*, 2003; Zhang *et al.*, 2005).

The Arctic Ocean is a unique feature, in that while only storing approx. 1% of the worlds water, it receives 11% of the worlds river runoff via the Eurasian and North American basins (Shiklomanov, 2000). Therefore, the observed and predicted changes in the Arctic are likely to have an impact upon the freshwater supply to the Arctic Ocean, which in turn will affect its water mass properties, and by association, the climate of the Arctic. In addition, the increase in freshwater entering the Arctic Ocean will then be transported southward close to the sites of deep convection that control climate on a larger scale through the Atlantic Meridional Overturning Circulation (AMOC). The collapse of which, due to increased freshwater flux, could affect regional and global climate (Vellinga and Wood, 2000). Although this is not expected, 21st century simulations show its likely decrease, which will in turn influence the climate (Gregory *et al.*, 2005). Therefore, it is of great relevance that we seek to explore how the future anthropogenic warming is likely to impact the Arctic Freshwater Hydrological Cycle (AFHC).

The projected warming of the future is unlike what the Earth has experienced in the recent past, making it difficult to draw any solid comparisons on how the climate is likely to respond to enhanced levels of greenhouse gases in the atmosphere. However, the current interglacial, although relatively benign when compared to the climatic variability of previous interglacials, provides us with an example of the most recent hypsithermal event to have occurred. This event, most commonly referred to as the Holocene Thermal Maximum (HTM), has been observed in a number of palaeoclimatic proxy records, such as marine and lake sediments, glacial records, ice-cores and speleothems (Wanner *et al.*, 2008; Ljunqvist, 2011). Reconstructions show that this period was characterised by a relatively warm, wet climate, particularly in the high-northern latitudes, and that sea surface temperatures were estimated to be 2-8°C higher than present day, (Levac *et al.*, 2001; Birks and Koç, 2002; Calvo *et al.*, 2002; Sarnthein *et al.*, 2003; Kaufman *et al.*, 2004), while terrestrial summer temperatures were 1-3°C higher (Kaufman *et al.*, 2004; Kerwin *et al.*, 2004). However, the timing of the initiation of the HTM is still unclear. According to the Milankovitch theory of orbitally driven climate change, the HTM would be most likely to occur during the onset of the Holocene, between 11-10ka (Berger, 1978). While the majority of proxy reconstructions show an initiation of the HTM during the early part of the Holocene (11-8ka), (Davis *et al.*, 1980; Ritchie *et al.*, 1983; Koerner and Fisher, 1990; Szeicz *et al.*, 1995; Hu *et al.*, 1998; Bennike, 2000; MacDonald *et al.*, 2000; Duplessy *et al.*, 2001; Levac *et al.*, 2001; Christiansen *et al.*, 2002; Marchal *et al.*, 2002; Wagner and Melles, 2002; Pisaric *et al.*, 2003; Kaufman *et al.*, 2004), there are also a noteworthy number of proxies that indicate its initiation was during the mid-Holocene (8-

4ka) (Koç and Jansen, 1992; MacDonald *et al.*, 1993; Korhola *et al.*, 2000; Kaplan *et al.*, 2002; Smith, 2002; Caseldine *et al.*, 2003; Kerwin *et al.*, 2004; Caseldine *et al.*, 2006). In addition to the temporal variation of the initiation of the HTM there appears to be a spatial element to it, with the HTM occurring earlier in Alaska, the Canadian Arctic Archipelago and northwest Canada, than it did so in southern Greenland and north east America (Kaufman *et al.*, 2004; Jansen *et al.*, 2007).

With temperatures during the mid-Holocene being comparable to those for the near future, the mid-Holocene has often been referred to as a useful analogy for the future (Macdonald, 2010). However, there are several important caveats that one must consider before doing so. The mid-Holocene and the 21st century have been shown, by proxy reconstructions and model simulations respectively, to be relatively warm periods, however the climate of each period evolved due to a combination of different forcings. Whilst both periods were preceded by increasing levels of atmospheric CO_2, this increase was not the reason for the mid-Holocene warming, as is primarily the case for current and future warming. Due to the surplus in summer insolation during the mid-Holocene (490 Wm^{-2} for 6ka and 468 Wm^{-2} for 2000 AD) the annual mean climate during this period was also warmer than present day at many locations in the Northern Hemisphere (Ljunqvist, 2011). Unlike the mid-Holocene, current warming is predominantly driven by an increase in the concentration of atmospheric trace gases that lead to an annual, instead of seasonal, forcing and with trace gas concentrations expected to continue to increase, this will result in an annual radiative forcing increase, by 2100AD, of between 4.3 and 7.5 Wm^{-2} (B1 to A2 scenarios) relative to 2000 AD from trace gases alone. In contrast, during the mid-Holocene the effect of GHG concentrations on radiative forcing was minor (-0.2 Wm^{-2} relative to 2000 AD). A final point to consider is that during the early Holocene (until 7ka BP), there were still remnants of the Laurentide Ice Sheet, which resulted in large temporal and spatial variations in the expression of the HTM (Renssen *et al.*, 2009; Renssen *et al.*, 2012). To avoid this spatiotemporal complexity, palaeoclimatological studies often take the mid-Holocene climate (6ka BP) as a benchmark to study the relatively stable warm conditions during the mid-Holocene.

Despite these caveats, the mid-Holocene climate is still a very useful reference, as it enables us to compare a naturally warm climate with a future anthropogenically induced one. In this study we focus our analysis on the AFHC, with the purpose to evaluate how the various components that comprise the AFHC respond in two different warm climates. With there being a lack of proxy evidence from which to reconstruct the AFHC during the mid-Holocene we shall use a global climate model to do so, after first establishing the relative merits of the model. In addition, we shall evaluate when the future climate is likely to equal and surpass that of the mid-Holocene.

2.2 Model and Methods

2.2.1 Model

The simulations were performed using LOVECLIM (Version 1.2), an Earth model of intermediate complexity (Goosse *et al.*, 2010), plus minor modifications. This global

climate model is comprised of an atmosphere, ocean, sea-ice, ice-sheet, carbon cycle, iceberg, land and vegetation components. In this study we have enabled the atmosphere, sea-ice, ocean and vegetation components.

The atmosphere component, ECBilt is a quasi-geostrophic dynamical atmosphere with a horizontal T21 truncation (5.6° x 5.6°) and three vertical layers, 800hPa, 500hPa and 200hPa (Haarsma *et al.*, 1996; Opsteegh *et al.*, 1998). It consists of a full hydrological cycle, where humidity is represented by the total precipitable water between the surface and 500hPa. Above 500hPa, it is assumed that the atmosphere is dry and all water that surpasses this level is converted to precipitation.

Clouds are prescribed based on the ISCCP D2 dataset of Rossow *et al.* (1996). The land surface component is part of ECBilt and has the same grid resolution as the atmosphere. River runoff is calculated using a simple bucket method, where the volume of water in the bucket is a function of vegetation. If after precipitation, evaporation and snow melting have occurred the water level is still higher than the maximum one allowed in the bucket, it is then added to the mouth of the river for the corresponding basin.

The Ocean is represented by CLIO (Goosse *et al.*, 1997). This is a primitive-equation, free-surface model that consists of a general ocean circulation model (Deleersnijder and Campin, 1995; Deleersnijder *et al.*, 1997) coupled to a thermodynamic-dynamic sea-ice model (Fichefet and Morales Maqueda, 1997 and 1999). It has a resolution of 3° in the longitude and latitude, realistic bathymetry, and contains some classical approximations, including the Boussineq approximation, the thin shell approximation, the hydrostatic approximation and the eddy-induced advection term of Gent and McWilliams (1990). It is also comprised of two spherical subgrids to avoid North Pole singularity (Madec and Imbard, 1996). Flow through the Bering Strait is determined by the sea-level difference across the strait, following the geostrophic control theory (Goosse *et al.*, 1997). The thermodynamic processes that govern the vertical decay and growth of sea-ice are represented in a three-layer model. The ice floe of each grid cell is a slab of ice, which is divided into two equal layers. Snow accumulates upon these floes when the surface temperature is below the melting point. If sufficient snow accumulates upon the floe, it is depressed below the surface level of the underlying water and, the floe is inundated with seawater. A combination of freezing seawater and snow then increases the thickness of the ice floe (Fichefet and Morales Maqueda, 1997). Although natural conditions are not fully represented in the model, the ability of the model to simulate the geographical extent of sea-ice in both the Northern and Southern hemispheres is reasonably good (Goosse *et al.*, 2010).

The vegetation component of LOVECLIM is represented by VECODE (Brovkin *et al.*, 2002). This is a reduced form dynamic global vegetation model, and is capable of simulating the dynamics of two plant functional types, trees and grasses, as well as desert as a dummy type, and these only have an effect upon the surface albedo and not on other processes such as evapotranspiration (Goosse *et al.*, 2010).

LOVECLIM is shown to reproduce the main characteristics of the present-day climate with reasonable accuracy (Goosse *et al.*, 2010). After a doubling of CO_2 the surface

temperature in LOVECLIM increases by 1.9°C after 1000 years, which when compared to GCMs (Randall *et al.*, 2007), places the climate sensitivity of LOVECLIM at the lower end of values. In addition, LOVECLIM requires a precipitation flux correction, including a 25% reduction in the Arctic. Without this correction applied, the simulated precipitation is too high, resulting in an excess of freshwater entering the Arctic Ocean and weakening the meridional overturning circulation. Precipitation produced in the model is removed before it enters the Arctic Ocean and transferred directly to the Pacific Ocean. LOVECLIM is able to simulate the features of the high-northern latitudes reasonably well, including deep convection in the Labrador Sea, Irminger Sea and south of Svalbard, and the present-day extent of sea-ice (Goosse *et al.*, 2010).

At 6ka BP LOVECLIM simulates increased summer surface temperatures, particularly in the high-northern latitudes over the continents and the Arctic (Goosse *et al.*, 2010) (Fig.2.1). It also captures the increases in precipitation over Northern Africa and the Middle East. In general, the results of the 6ka simulation performed with LOVECLIM capture similar characteristics of the climate that have also been observed in other models involved in the PMIP series of experiments (Braconnot *et al.*, 2007). For a more detailed description of model performance at the time periods discussed above, as well as for the recent decades, the last millennia, and the last glacial maximum, the reader is referred to Goosse *et al.* (2010).

For the experiments performed here, there were some minor modifications to the setup of LOVECLIM. As mentioned above, in accordance with geostrophic control theory (Toulany and Garrett, 1984), the flow across the Bering Strait is parameterised as a linear function of the cross-strait sea-level difference. This parameter was tuned to be a better representation of the modern day Bering Strait throughflow. Additionally, the land catchments areas were critically evaluated and adjusted to give a more realistic representation of modern-day river basins.

2.2.2 Experimental Setup

The climates of the pre-industrial (PI), modern day (MOD) and 21st century (A1B, A2 and B1) were derived from a series of transient experiments covering the period 1ka to 2100AD. Values calculated for the pre-industrial era, were averaged over the period 1251 to 1750 and for the modern era, values were averaged over the period 1951 to 2000. This transient simulation was forced with annually changing orbital parameters (Berger, 1978), total solar irradiance (Wang *et al.*, 2005; Delaygue and Bard, 2009), volcanic forcings (Crowley *et al.*, 2008), tropospheric ozone (Nakicenovic and Swart, 2000), aerosol sulphates (Nakicenovic and Swart, 2000) and GHG concentrations (PMIP3). The trace gas reconstructions reach levels of 370ppm (CO_2), 1752ppb (CH_4) and 316ppb (N_2O), by 2000AD.

For the 21st century simulations (A1B, A2 and B1) we followed the IPCC Special Report on emissions Scenarios (SRES) A1B, A2 and B1. In scenarios A1B, A2 and B1, by the year 2100AD, the additional radiative forcings, relative to 2000AD, due to the increase in trace gas concentrations were 5.9, 7.5 and 4.3 Wm^{-2}, respectively.

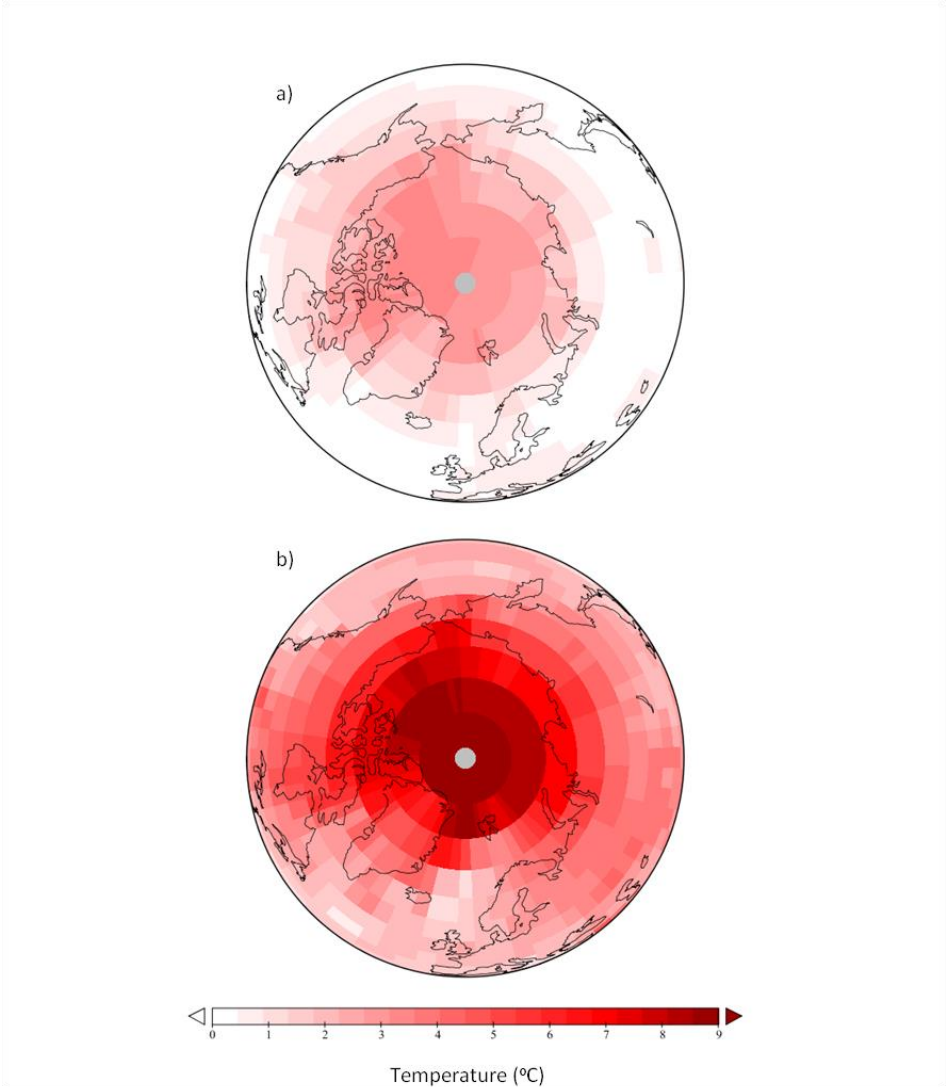

Fig. 2.1. Mean annual surface temperature anomaly plots of a) 6ka - PI; and b) A1B – PI. (A1B is averaged over the years 2051-2100AD).

Additionally, ozone and sulphates forcings were applied. Volcanic forcing was held constant at 2001 levels, and total solar irradiance was held at 1365 Wm^{-2}. These scenarios were chosen because they cover the full range of future trace gas emissions scenarios as defined by the IPCC and allow for comparison with other studies. The values presented in the text for each scenario are averaged over the period 2051-2100.

The climate of the mid-Holocene (6ka) was simulated following the guidelines of the PMIP3 Protocol (http://pmip3.lsce.ipsl.fr/). The major difference between the

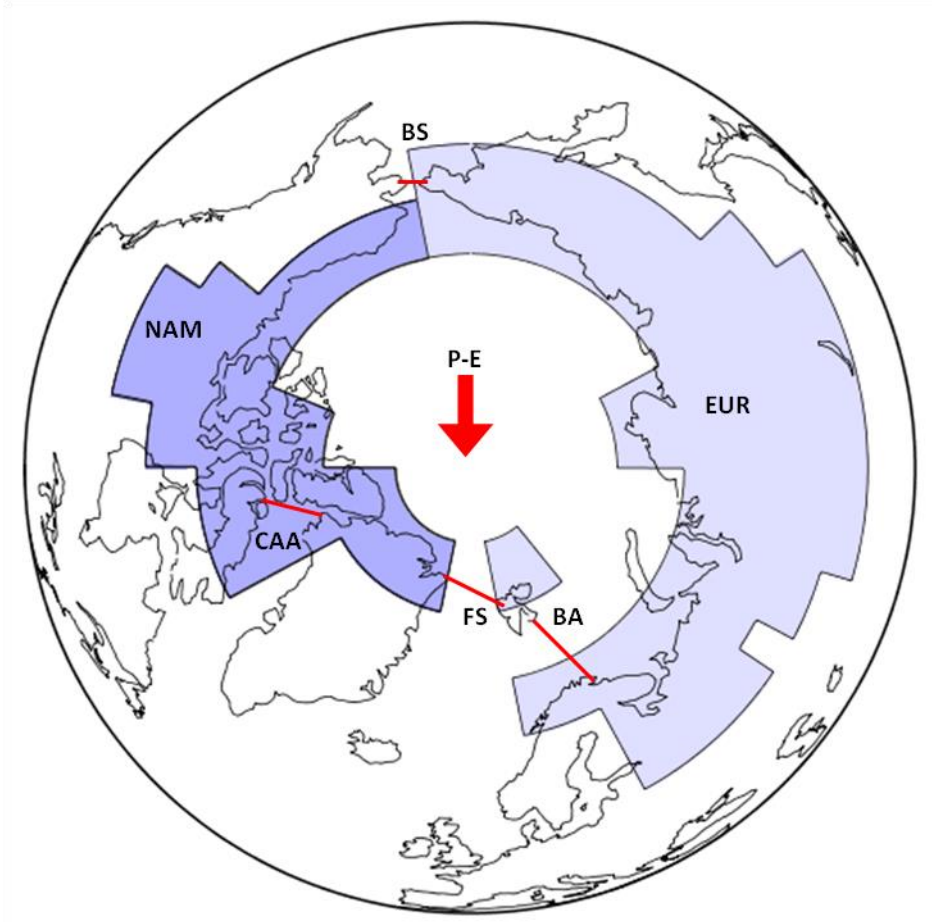

Fig.2.2. A map of the Arctic domain as used in this study, including the locations of where freshwater and sea-ice fluxes are calculated: Fram Strait (FS); Barents Sea boundary (BA); Canadian Arctic Archipelago (CAA) and the Bering Strait (BS); The river catchments of the Eurasian (EUR) and North American (NAM) basins; and net precipitation (P-E), which was calculated for the area enclosed by the boundaries defined above.

forcings for 6ka and PI are the orbital parameters. This would suggest that any climatic variation between the two periods is due to the effects of the orbital forcings. Volcanic and solar forcings were not modified compared to the preindustrial period. The simulation was initiated from a PI control simulation and was run for 2500 years to allow the model, in particular the deep oceans, to reach a quasi-equilibrium state. The data presented for the mid-Holocene are mean annual values of the last 500 years of the simulation.

2.2.3 Calculating Freshwater Fluxes

To analyse the AFHC in detail, we modified the CLIO code to allow for the computation of liquid freshwater fluxes (F_W) and ice fluxes (F_i) at each time step and at a number of predefined boundaries (Fig.2.2): Fram Strait (FS), Bering Strait (BS), Kara-

Barents Sea boundary (KS), and Canadian Arctic Archipelago (CAA), the following equation (2.1) was used to calculate the freshwater flux (F_w):

$$F_w = \int_{L_1}^{L_2} \int_{Z_1}^{Z_2} v_w \frac{S_{ref} - S_o}{S_{ref}} \, dz \, dL \qquad (2.1)$$

Where v_w is the velocity of the water, which is computed perpendicular to the length of the transect L, through which it passes. S_{ref} is a reference salinity (taken to be 34.8 psu to allow for comparison with other studies) and S_o is the salinity of the ocean at that location. These are computed over the entire depth of the water column at the corresponding point in the ocean (Z_2 to Z_1) to give a freshwater flux (km^3yr^{-1}).

The freshwater content of the ice and snow (F_i) (km^3yr^{-1}) was calculated using equation (2.2):

$$F_i = \int_{L_1}^{L_2} v_i h_i \frac{(S_{ref} - S_i)}{S_{ref}} \frac{\rho_i}{\rho_w} \, dL + \int_{L_1}^{L_2} v_i \, h_s \frac{(S_{ref} - S_w)}{S_{ref}} \frac{\rho_s}{\rho_w} dL \qquad (2.2)$$

Where v_i is the velocity of the ice floe, S_i is the salinity of Ice (6 p.s.u), S_w is the salinity of snow (0 p.s.u), ρ_w is the density of water (1000 kgm^{-3}), ρ_i is the density of sea ice (900 kgm^{-3}), ρ_s is the density of snow (330 kgm^{-3}), and h_i and h_s are the thickness of the ice and snow respectively. The salinity of sea-ice, S_i, is taken as 6 psu, as opposed to the usual value of 4 psu (Aagaard and Carmack, 1989; Serreze *et al.*, 2006; Holland *et al.*, 2007). This is because in LOVECLIM the salinity of first year ice is approx. 6 psu and is well adapted to the Southern Ocean, where the exact value has a larger impact than in the Arctic. Liquid Freshwater content (F_c) of the Arctic Ocean (km^3) is defined as:

$$F_c = \int dV \frac{(S_{ref} - S_o)}{S_{ref}} \qquad (2.3)$$

Where dV is the change in volume over the entire depth of the water column. The volume of freshwater contained within the sea-ice (F_{ic}) (km^3) is calculated with respect to the volume of sea-ice (V_i):

$$F_{ic} = V_i \frac{(S_{ref} - S_i)}{S_{ref}} \qquad (2.4)$$

Equation (2.4) neglects the freshwater contained in snow upon the ice it is small and has a negligible effect on the overall AFHC.

As already noted, equations (2.1) to (2.4), take the reference salinity (S_{ref}) of the Arctic Ocean to be 34.8 psu, which is in-keeping with the literature, and allows for comparison with other studies (Häkkinen and Proshutinsky, 2004; Serreze *et al.*, 2006;

Holland *et al.*, 2007). While the choice of reference salinity is somewhat discretionary, it is important to consider the implications of choosing an appropriate one. An adequate estimate of the salinity of the Arctic Ocean is taken to be 34.8 psu (Aagaard and Carmack, 1989), therefore the relative effect of a freshwater flux upon the overall freshwater budget of the Arctic Ocean is in relation to this reference value. For example, Atlantic derived waters, entering the Arctic Ocean via the Barents Sea, have a salinity of approx. 35 psu (Dickson and Blindheim, 1984). Therefore, with a reference salinity of 34.8 psu this is classed as a freshwater sink and its tendency effect is to increase the overall salinity of the Arctic Ocean. However, if a reference salinity of 35.2 psu is taken, as in Dickson *et al.* (2007), then the Atlantic inflowing waters would now be classed as a freshwater source, and the net effect upon the salinity of the Arctic Ocean would be a freshening.

2.3 Results and Discussion

2.3.1 Hindcast Simulation of the Arctic Freshwater Hydrological Cycle (1951-2000)

The Arctic freshwater hydrological cycle was simulated from 1951 to 2000, and compared to best estimate values (Table. 2.1). For this period, the total inflow (5976±189 km^3yr^{-1}) is at the lower range of estimates of both *in situ* studies: 6120 km^3yr^{-1} (Aagaard and Carmack, 1989); 8450 km^3yr^{-1} (Serreze *et al.*, 2006); and modelling studies: 7044 km^3yr^{-1} (Holland *et al.*, 2007); and 7486 km^3yr^{-1} (Arzel *et al.*, 2008). The total freshwater input to the Arctic is mostly comprised of river runoff (49%) and net precipitation (35%). With the remainder being accounted for by Bering Strait throughflow (16%). The simulated river runoff (2912±118 km^3yr^{-1}) is comprised of input from the North American (831±54 km^3yr^{-1}) and Eurasian (2081±127 km^3yr^{-1}) basins. The total input from river runoff is slightly lower than observations (Table. 2.1), whereas precipitation (2078±105 km^3yr^{-1}) is in excellent agreement with observations, which would be expected due to the flux correction. It must be noted that LOVECLIM is not able to capture the 7% increase in Eurasian river discharge over the late 20th century (Peterson *et al.*, 2002).

The lower-than-expected simulated total freshwater input to the Arctic Ocean can, in part, be accredited to a lower than observed Bering Strait liquid freshwater flux (933±144 km^3yr^{-1}). However, with the Bering Strait volume flux throughflow tuned to observations (0.83±0.66Sv Roach *et al.*, 1995), this lower-than-expected value is due to a too high salinity in the Bering Strait throughflow waters. Typically, observational based freshwater fluxes are calculated assuming a salinity of 32.5 psu while in our simulations we see a salinity that is 0.5-1.5 psu greater than this, leading to a reduced freshwater flux.

The total outflow (5944±909 km^3yr^{-1}) is well within the range of both other *in situ* studies: 5230 km^3yr^{-1} (Aagaard and Carmack, 1989) and 9160 km^3yr^{-1} (Serreze *et al.*, 2006), and modelling studies; 5578 km^3yr^{-1} (Holland *et al.*, 2007), and 6955 km^3yr^{-1} (Arzel *et al.*, 2008). It is dominated by freshwater exiting the Arctic via the Fram Strait (67%), in the form of both liquid (53%) and ice (14%). Additional liquid freshwater outflows occur through the Kara Sea (24%) and the CAA (9%). Simulated liquid Fram Strait export (3140±378 km^3yr^{-1}) compares well with observations (Table. 2.1). However, the Fram Strait ice flux (808±246 km^3yr^{-1}) is a significant underestimation. This can partially be

explained by a weaker than observed East Greenland Current (EGC) (3.13±0.44Sv) compared to observations (7 to 14Sv) (Schlichtholz and Houssais, 1999; Schauer *et al.*, 2008). In addition, LOVECLIM is not able to simulate winds of sufficient strength in the Arctic region, which significantly reduces the efficiency of the model in transporting sea-ice. Also, liquid freshwater flux through the CAA (536±253 km^3yr^{-1}) is poorly represented in LOVECLIM.

Over the period of the simulation the mean annual Arctic Ocean Freshwater Content (46,400±1897 km^3) showed a decreasing trend (13 km^3yr^{-1}). Freshwater stored in the form of sea-ice (13,722±1768 km^3) also showed a small decreasing trend (100 km^3yr^{-1}) over the period.

Because of the approximations included in the computation of the fluxes (for instance the diffusion terms are neglected), our estimate of the freshwater budget of the Arctic is not completely closed. Nevertheless, the imbalance is negligible in the present framework as it amounts to only 2% of the total inflow for the period 1951-2000.

A noticeable feature of this hindcast simulation is the late 20th century response of the AFHC. Temperatures in the Arctic begin to increase from the early 20th century (Fig.2.3a), although they do not exceed the range of values shown between 1250 and 1950 until mid-20th century. In conjunction, there is a response beyond the PI variability in sea-ice volume (Fig.2.3b), Fram Strait freshwater ice export (Fig.2.3c), net precipitation over the Arctic Ocean (Fig.2.3d), Fram Strait liquid freshwater export (Fig.2.3e), and the Nordic Seas overturning strength (Fig.2.3f).

To explain this late 20th century response seen in our simulations, it would seem that the rise in temperatures in the Arctic (Fig.2.3a) resulted in increased melting of sea-ice (Fig.2.3b). Consequently, there was reduced Fram Strait freshwater ice export (Fig.2.3c), but an increase in Fram Strait liquid freshwater export (Fig.2.3e), which in turn contributes to the reduction of the overturning in the Nordic Seas (Fig.2.3f). Subsequently, the North Atlantic Deep Water exported southward in the Atlantic at 20°S (hereinafter referred to as the Atlantic Meridional Overturning Circulation (AMOC)) is weakened, although this response seems to be delayed until the early part of the 21st century (Fig.2.4a). It would be expected that the reduction in both the AMOC and the Nordic Seas overturning strength, would decrease the northwards heat flux (Fig.2.4b), however, this is not the case, as between 1951 and 2000, its variability is indistinguishable from the natural variability shown over the 1250 to 1900 period (0.2±0.04 PW; Electronic Supplementary Information (ESM) T1). Therefore, this means that despite a reduction in the strength of the AMOC, the heat flux to the North Atlantic is maintained primarily by the warming of the ocean.

2.3.2 Projected Arctic Freshwater Hydrological Cycle (2051-2100)

The Arctic freshwater hydrological cycle was simulated over the period 2050-2100 following the A1B, A2 and B1 IPCC scenarios. Most notably we see a freshening of the Arctic Ocean (Fig.2.5) over the 21st century in scenarios A1B (6.4%) and A2 (4.9%), whilst in scenario B1, the Arctic Ocean becomes more saline (6.5%). The freshening of

the Arctic Ocean can be accredited to three main factors. Firstly, river runoff (Fig.2.6) increases steadily (9-10%) over the 21st century, indicating that the hydrological cycle in the high-northern latitudes is intensifying (Kattsov and Walsh, 2000). Additionally, Fram Strait freshwater ice export (Fig.2.3c) decreases (58-59%), due to diminished sea-ice cover (Fig.2.3b) (63-68%). A direct consequence of the aforementioned processes is an increase in liquid freshwater export via the Fram Strait (2-4%), which is contrary to the net effect on the total Fram Strait freshwater export from the Arctic over the course of the 21st century, which sees an overall decrease (8-10%).

The current and future freshening of the Arctic Ocean and North Atlantic has been shown in previous studies (Peterson *et al.*, 2002; Karcher *et al.*, 2005; Holland *et al.*, 2006; Holland *et al.*, 2007; Arzel *et al.*, 2008), bringing our results in line with these. In addition, the strengthening of the hydrological cycle shown over the 21st century is also consistent with other studies (Miller and Russell, 2000; Holland *et al.*, 2006; Holland *et al.*, 2007).

A key consideration with regards to the freshening of the Arctic and the North Atlantic is how the changes to the AFHC will affect the formation of North Atlantic Deep Water at the main deep convection sites, and subsequently, how this freshening is likely to impact the AMOC effect on regional and global climate. It is expected that additional freshwater added to the North Atlantic will reduce the salinity of the waters, whilst inflowing warmer Atlantic waters will have a complementary effect, reducing the density gradient in the water column and weakening the overturning strength. This is indeed what is observed in our future simulations (Fig.2.3f), which show that for the 21st century, the Nordic Seas overturning strength decreasing by approx. 1Sv (Fig.2.3f). Additionally, there is a reduction in the AMOC by approx. 1Sv (Fig.2.4a).

The observed reduction in the AMOC that we see in our simulations is similar to that observed by Gregory *et al.* (2005), who evaluated the performance of an ensemble of climate models of varying complexity and analysed the potential causes of the decrease in the AMOC in addition to the freshwater inflow at high latitudes. They found that in none of the simulations, the increase in freshwater input to the North Atlantic during the 21st century was enough to completely shut down the AMOC, which is consistent with our findings. However, it must be noted that in all our simulations, and in the ones analysed by Gregory *et al.* (2005), there is no dynamic-thermodynamic Greenland Ice sheet, therefore omitting a potentially important source of future freshwater input to the North Atlantic. However, studies involving models that do include an interactive Greenland Ice Sheet suggest that its potential freshwater melt flux in a warming climate is not sufficient to induce a complete shutdown of the AMOC during the 21st century (Jungclaus *et al.*, 2006; Driesschaert *et al.*, 2007; Hu *et al.*, 2009).

2.3.3 Comparing the Arctic Freshwater Hydrological Cycle of the mid-Holocene and 21st Century anthropogenic warm climates

In all scenarios the surface temperature in the Arctic (Fig.2.3a) at the beginning of the 21st century (until 2010) was within the natural variability ($\pm 2\sigma$) of the mid-Holocene mean. However, by 2010, surface temperature in the Arctic surpasses that seen during the 'extreme' mid-Holocene, and by the end of the 21st century, temperatures exceed the mid-Holocene mean by 3°C (B1) to 6°C (A2). Additionally, it can be seen that the influence of anthropogenic warming in the Arctic was first visible during the early half of the 20th century, and modern-day temperatures are approx. 1.5°C warmer than the mid-1900s which is consistent with the findings of Serreze *et al.* (2000). These observations enable us to say that whilst the majority of the 21st century is likely to exhibit a temperature that is greater than that seen during the mid-Holocene, the first decade of the 21st century is a better analogy, with respect to the surface temperature, to the mid-Holocene, albeit in an enhanced state.

In conjunction with the increase in temperatures, there is a considerable reduction of northern hemisphere sea-ice volume over the 20th and 21st centuries (Fig.2.3b). By the beginning of the 21st century, sea-ice volume had decreased by 34% of its PI mean. However, this value is equivalent to the mid-Holocene sea-ice volume mean. By the end of the 21st century, sea-ice volume has decreased even further, 66% to 76% of its PI mean. Interestingly, current sea-ice volume is comparable to that which occurred during the mid-Holocene. There is a clear negative correlation between Fig.2.3a and Fig.2.3b, suggesting that the reduction in sea-ice volume since the early 1900s and over the course of the 21st century is driven by the increasing temperatures in the Arctic and the ice-albedo, ice-insulation feedbacks.

By the end of the 21st century all scenarios show an increased liquid freshwater export via the Fram Strait (Fig.2.3e). Interestingly, both A2 and surprisingly B1 show increases that, by the end of the 21st century, are equivalent to 33% of the mid-Holocene mean, whilst A1B increases by 22%. The increase in liquid freshwater export via the Fram Strait is greater than the upper 2σ level of the mid-Holocene in all scenarios. It must be noted that while liquid freshwater export via the Fram Strait in scenario B1 does show an extreme increase, this variability is not statistically significant, as it does not lie outside the natural variability of the A1B and A2 scenarios. Fram Strait ice export lies outside the range shown during the mid-Holocene, with ice export in scenarios A1B and A2, 62% less than the mid-Holocene mean (ESM T1).

Although melting sea-ice is partly responsible for the freshening of the Arctic Ocean during the 21st century, there is also a significant contribution of freshwater input from continental river runoff (Fig.2.6). It can be seen that the mid-Holocene and early 21st century mean annual runoff from the Eurasian and North American continents were similar (ESM T1). However, by the mid-21st century, runoff increases by 8% in all scenarios. After which, scenario B1 plateaus, whilst scenarios A1B and A2 continue to increase over the 21st century (14%). This suggests an intensification of the hydrological

cycle over the continental land masses. Interestingly, in all scenarios the increase in runoff is due entirely to an increase in Eurasian river runoff. The intensification of the hydrological cycle is not only a phenomenon we observe over land, with P-E over the Arctic Ocean also increasing (Fig.2.3e). It can be seen that P-E over the Arctic Ocean during the late 21st century relative to the mid-Holocene, increases by 4.8%, 6.5% and 6.5% for scenarios B1, A1B and A2, respectively.

2.3.4 The Arctic during the mid-Holocene an analogy for the 21st Century

Establishing if the mid-Holocene is a good analogy for the 21st century, with respect to the AFHC, first requires us to define a period when the temperature profiles for the two periods were equivalent. From 1990 to 2010, the temperature in the Arctic was within the $\pm 2\sigma$ range of the mid-Holocene mean surface temperature, therefore we can say that these two periods were analogous. However, during this period the Arctic Ocean freshwater content, the Fram Strait Freshwater liquid and ice export, and river runoff were all in a state that was an enhancement of the mid-Holocene, and were excessively beyond the natural variability of the mid-Holocene. A direct result of this is that the Arctic Ocean is fresher and the Nordic Seas overturning strength is weaker, than during the mid-Holocene. Conversely, between 1990 and 2010, sea-ice volume was greater than what occurred during the mid-Holocene. The remaining fluxes and oceanographic parameters, which included the AMOC, northwards heat flux at 30°S, and net precipitation, are all within the natural variability of the mid-Holocene.

These results suggest that between 1990 and 2010 the AFHC was in a state that was not reminiscent to the mid-Holocene. After 2010, it is clear that temperature in the Arctic will exceed those seen during the mid-Holocene and the AFHC will also continue to exceed the mid-Holocene natural variability, with no sign of it being suppressed by the freshening of the Arctic.

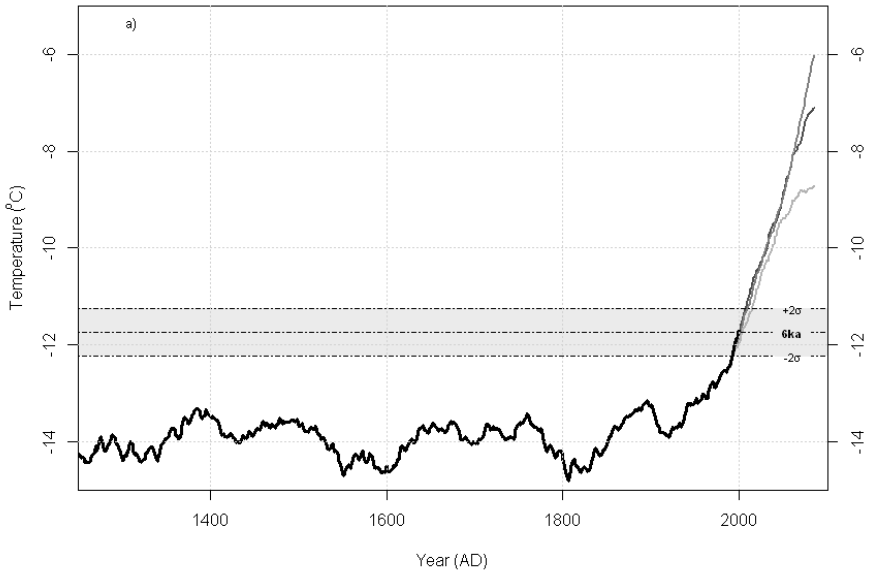
a)
Temperature (°C)
-6
-8
-10
-12
-14
+2σ
6ka
-2σ
1400
1600
1800
2000
Year (AD)

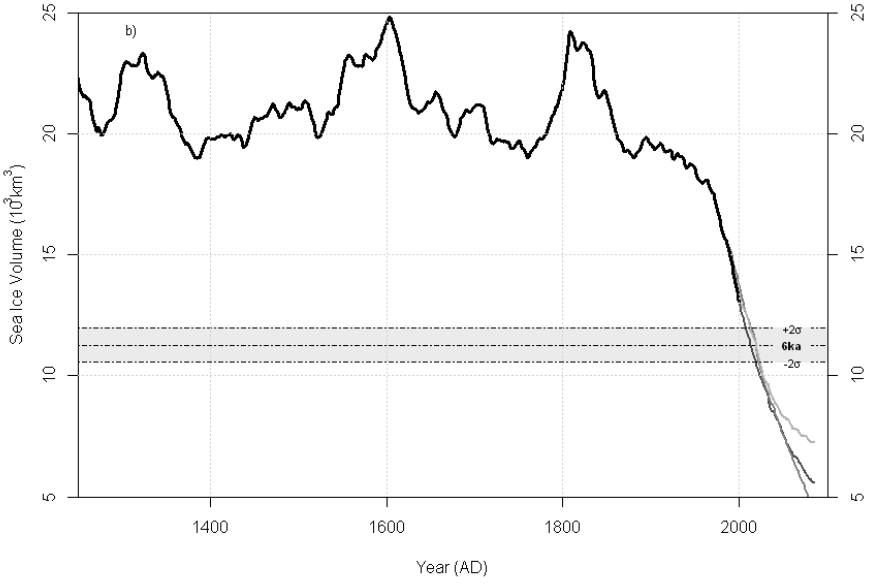
b)
Sea Ice Volume (10³km³)
25
20
15
10
5
+2σ
6ka
-2σ
1400
1600
1800
2000
Year (AD)

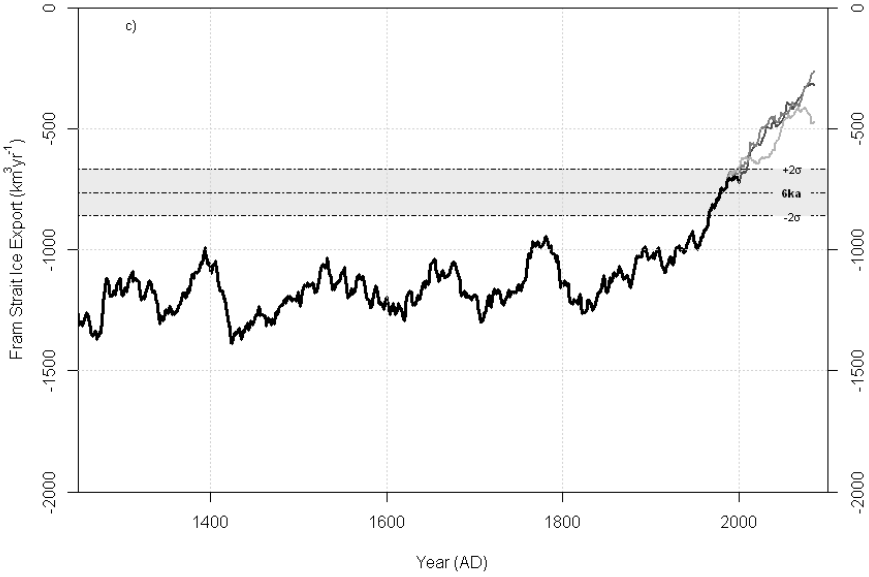
c)
Fram Strait Ice Export (km^{3}yr^{-1})
0
-500
-1000
-1500
-2000
+2σ
6ka
-2σ
1400
1600
1800
2000
Year (AD)

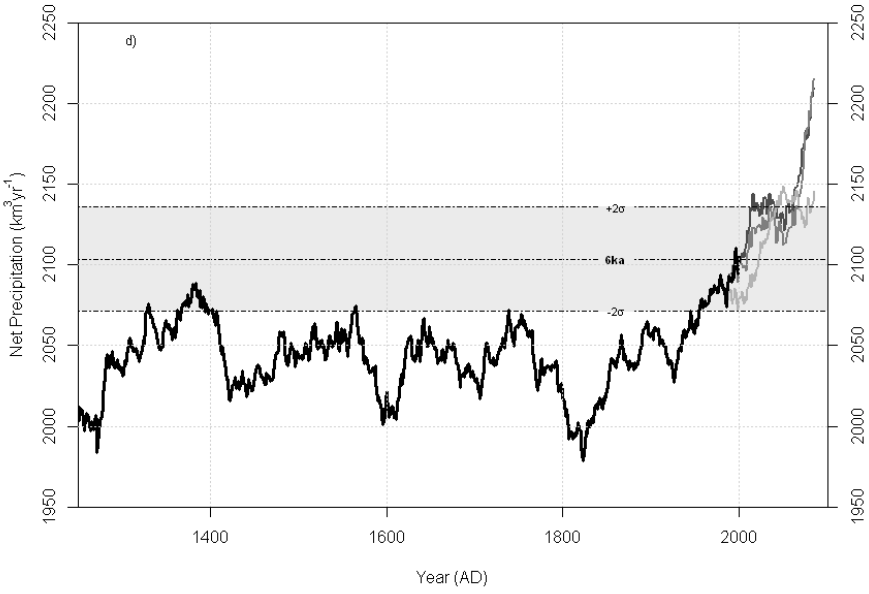
d)
Net Precipitation (km^{3}yr^{-1})
2250
2200
2150
2100
2050
2000
1950
+2σ
6ka
-2σ
1400
1600
1800
2000
Year (AD)

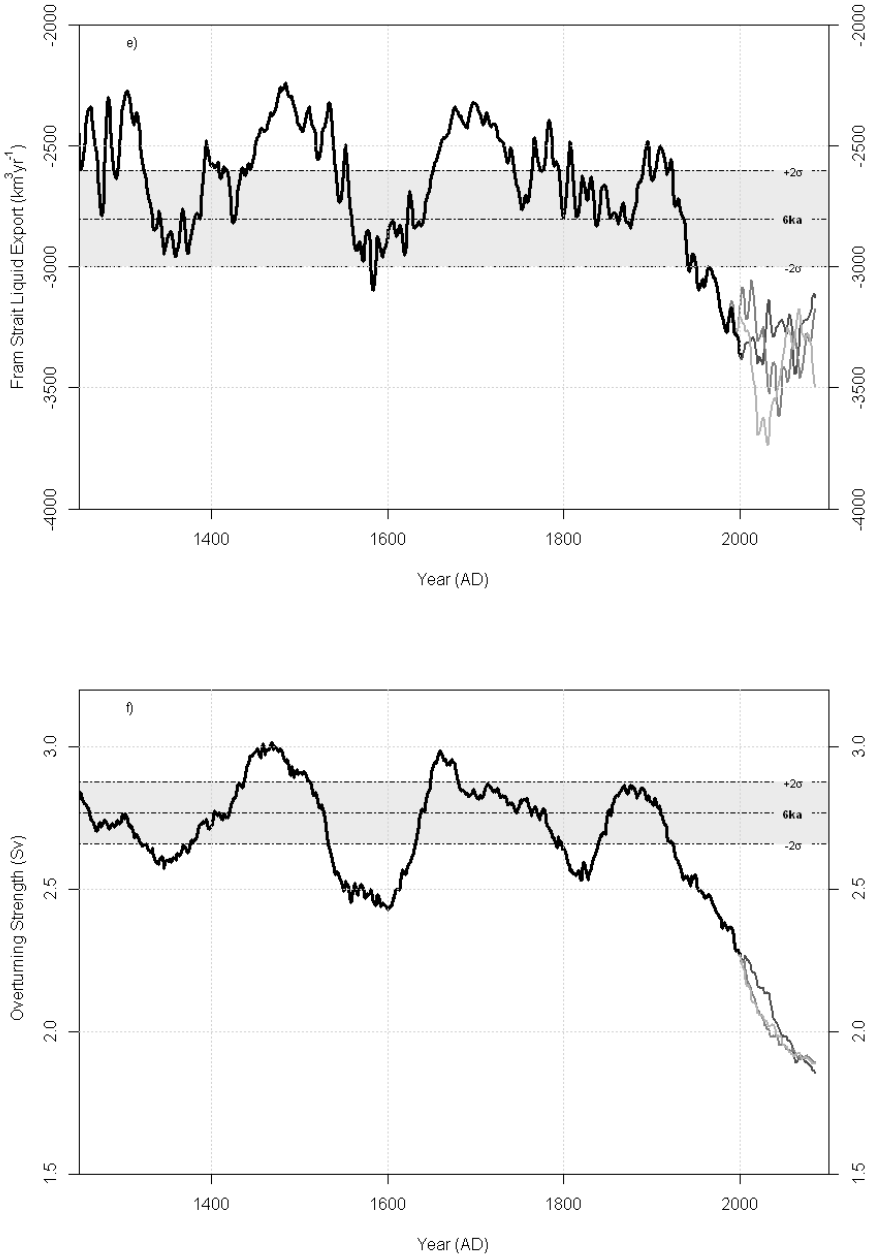

Fig.2.3. Time series (31-year running mean) of the a) Arctic surface temperature; b) Sea-Ice volume; c) Fram strait Ice export; d) Net Precipitation over the Arctic Ocean; e) Fram Strait liquid export; and f) The Nordic Seas overturning strength; from 1250 to 2100AD for SRES scenarios A1B (Dark Grey), A2 (Grey), B1 (light Grey). The shaded background represents the mid-Holocene (defined as 6ka).

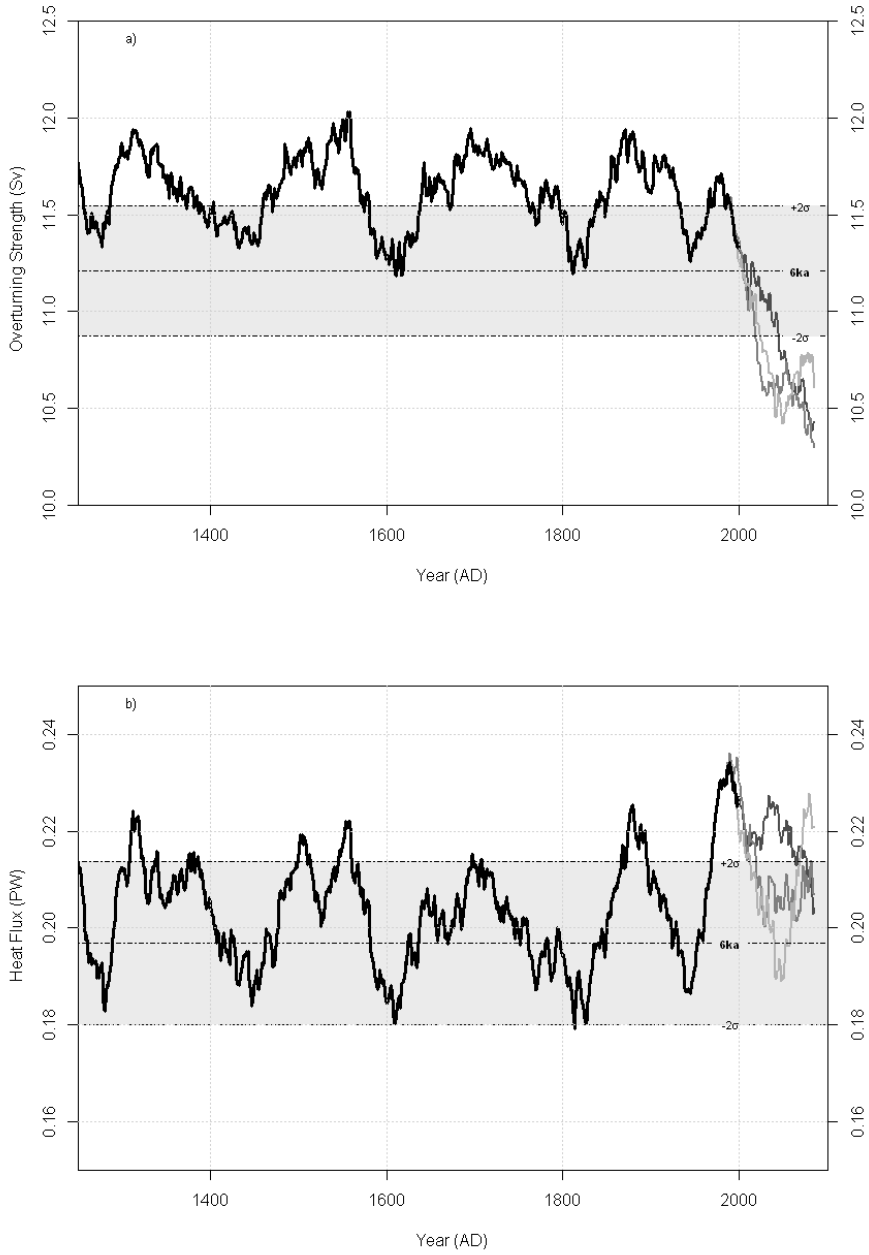

Fig.2.4. Time series (31-year running mean) of the a) AMOC Strength b) Northwards heat flux; from 1250 to 2100AD for SRES scenarios A1B (Dark Grey), A2 (Grey), B1 (light Grey). The shaded background represents the mid-Holocene (defined as 6ka).

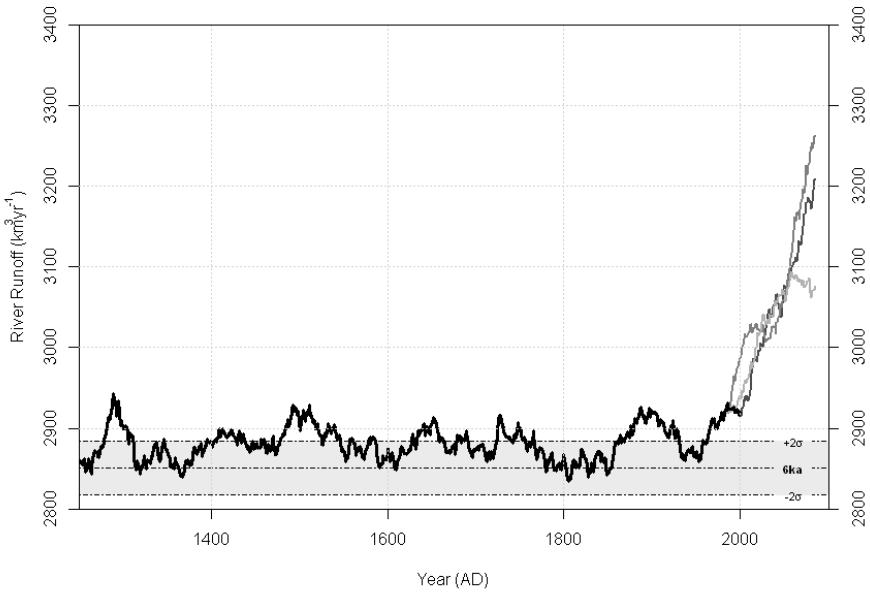

Fig.2.6. Time series (31-year running mean) of the River Runoff; from 1250 to 2100AD for SRES scenarios A1B (Dark Grey), A2 (Grey), B1 (light Grey). The shaded background represents the mid-Holocene (defined as 6ka).

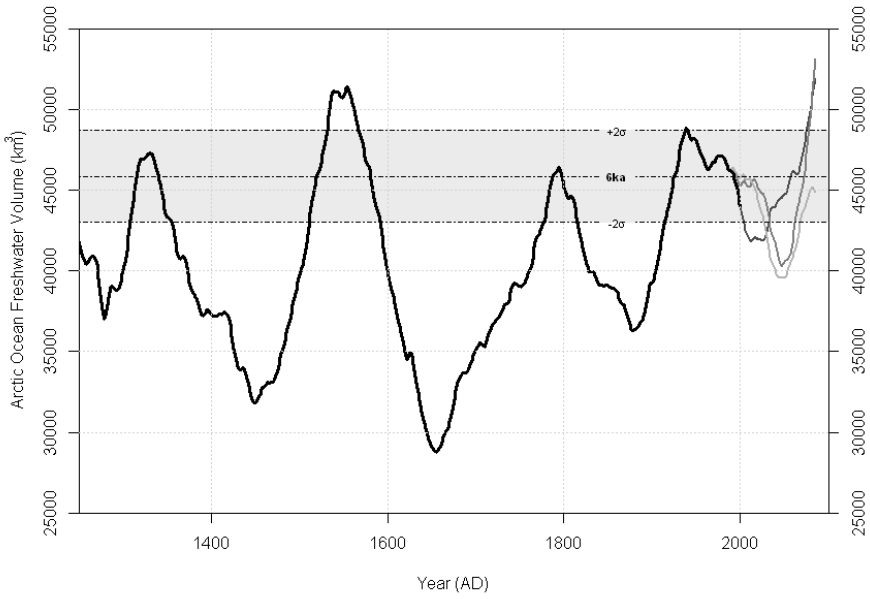

Fig.2.5. Time series (31-year running mean) of the Arctic Ocean freshwater content; from 1250 to 2100AD for SRES scenarios A1B (Dark Grey), A2 (Grey), B1 (light Grey). The shaded background represents the mid-Holocene (defined as 6ka).

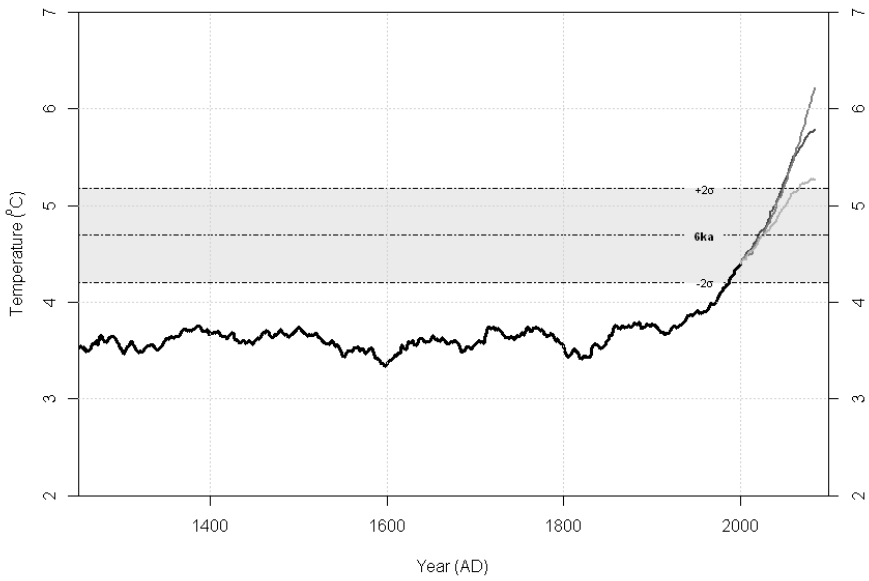

Fig.2.7. Time series (31-year running mean) of the mean summer (JJA) surface temperatures in the Arctic; from 1250 to 2100AD for SRES scenarios A1B (Dark Grey), A2 (Grey), B1 (light Grey). The shaded background represents the mid-Holocene (defined as 6ka).

2.4 Conclusions

In our study we have used LOVECLIM, an Earth Model of Intermediate Complexity to evaluate the differences between the AFHC of two warm periods, the mid-Holocene and the 21st century, each of which has evolved due to different climatic forcings. An initial test was to evaluate the performance of the model in simulating modern day (1951-2000AD) freshwater sources and sinks of the Arctic in both liquid and ice forms. In this respect, the model performed reasonably well, freshwater ice export and CAA liquid freshwater export, giving significant underestimations, most notably for the CAA, with net precipitation, river runoff and Fram Strait liquid freshwater export showing good agreement with the published literature. However, LOVECLIM was not able to accurately capture the Fram

We observed that during the late 20th century, sea-ice volume and Fram Strait freshwater ice export decrease, net precipitation over the Arctic Ocean and Fram Strait liquid freshwater export increase, and the Nordic Seas overturning strength weaken, all as a response to anthropogenic forcings, and enter a state that is beyond that of the PI natural variability. As a result, freshwater export increases and subsequently, there is a delayed weakening of the AMOC, although not enough to cause a complete suppression of it. By the end of the 21st century the Arctic Ocean has freshened considerably, with a noticeable decrease in sea-ice volume, which over the course of the 21st century decreases

by 55-68 % of its 1951-2000 mean. Additionally, river runoff increases by a maximum of 10% (A2) over the course of the 21st century, which is beyond mid-Holocene levels, with the observed increase being entirely dominated by an intensification of the hydrological cycle over the Eurasian continent. Additionally, there is an intensification of the hydrological cycle over the Arctic Ocean with increase of P-E of 2.4%, 4.8% and 7% for scenarios B1, A1B and A2, respectively. This intensification of the hydrological cycle in the Arctic is clearly viable in the AFOC, which also transitions to a state where the volume and throughflow of freshwater is enhanced. As a result, liquid freshwater export via the Fram Strait steadily increases over the entire duration of the 21st century, with the increase ranging from 22%- 33% of its PI mean, which is comparable to an extreme mid-Holocene export. Additionally, over the same period, Ice export via the Fram Strait decreases by $700 km^3 yr^{-1}$ in all scenarios.

The main focus of the study was to compare two warm periods, the mid-Holocene and the 21st century, with respect to the response of the AFHC during these periods. Firstly, it can be seen from our analysis that in all scenarios up until 2010, that the surface temperature in the Arctic is within the bounds of natural variability that was exhibited during the mid-Holocene (Fig.2.7). However, the temperatures are more an extreme representation of the mid-Holocene climate. After 2010, surface temperatures surpass those of an extreme mid-Holocene warm climate and are no longer comparable to the mid-Holocene. Therefore, we can say that with respect to temperature, only the first decade of the 21st century is analogous to the mid-Holocene. This leads to say that overall, the response of the AFHC prior to 2010 is within the natural variability that was observed during the mid-Holocene however, it is more representative of an extreme mid-Holocene AFHC. Therefore, after 2010 it is likely that the response of the AFHC to anthropogenic warming is likely to be one that sees it move to a state that exceeds that of the mid-Holocene.

Acknowledgements

This work was supported with funding from the 'European Communities 7th Framework Programme FP7/2013, Marie Curie Actions, under grant agreement No. 238111: CASEITN', and is greatly appreciated. H.G. is Senior Research Associate with the Fonds de la Recherche Scientifique (F.R.S.- FNRS-Belgium).

"And I tell you, if you have the desire for knowledge and the power to give it physical expression, go out and explore"

Apsley Cherry-Garrard

Chapter 3: The driving mechanisms of multicentennial variability of the Arctic Ocean freshwater content with the LOVECLIM climate model

Authors: Frazer, J. Davies, Hans Renssen and Hugues Goosse

Abstract

We investigated the mechanisms driving multicentennial variability of the Arctic Ocean freshwater content in a 10,000-year preindustrial control simulation performed with the LOVECLIM climate model. Spectral analysis reveals the existence of a distinct multicentennial intrinsic Arctic Ocean freshwater content variability with a significant peak periodicity at 165-years. This variability is driven by a series of oceanic processes that regulate the heat and saline fluxes reaching the Arctic Ocean, via the Barents and Kara Seas in the form of the North Atlantic Current. A weakening of this relatively saline current leads to a freshening of the Arctic Ocean, where freshwater is stored in both liquid and solid forms. In this enhanced freshwater state, the export of freshwater from the Arctic in liquid form increases through the Fram Strait, acting to suppress the Nordic Seas deepwater formation, leading to regional cooling. Eventually, the volume of freshwater stored as sea-ice becomes the dominant store of freshwater, resulting in a decrease of liquid export via the Fram Strait. This leads to the reinvigorating of the Nordic Seas deepwater, and the strengthening of both heat and saline fluxes to the Arctic Ocean, in the form of the North Atlantic current. These results highlight the importance of fully understanding how the intrinsic variability of the climate system modulates the anthropogenically driven changes we are observing.

3.1 Introduction

The Arctic climate is controlled by the interactions between a number of complex components. Wide ranging changes have been observed in the Arctic region in recent years (Stroeve *et al.*, 2012; Döscher *et al.*, 2014; Lindsay and Schweiger, 2015), with this trend set to continue during the present century. For example, the combination of increasing global temperatures and the Arctic amplification of this signal (Manabe and Stouffer, 1980) have led to the mean annual Arctic temperature being 1.5°C warmer than the 1971-2000 mean, which is more than twice the warming of lower latitudes (Overland *et al.*, 2013). Enhanced poleward atmospheric moisture transport due to an intensification of the high-latitude hydrological cycle (Kattsov and Walsh, 2000; Zhang *et al.*, 2012) have resulted in increased river runoff into the Arctic Ocean from Eurasian and North American rivers (Peterson *et al.*, 2002; Déry and Wood, 2005; Déry *et al.*, 2009; Shiklomanov and Lammers, 2009). In addition, we have also seen a retreat of the extent of permafrost in the high-northern latitudes and as a result, the deepening of its active layer (Kwong and Gan, 1994; Jorgenson *et al.*, 2001; Serreze *et al.*, 2003; Zhang *et al.*, 2005). In terms of sea-ice, we have seen a continuing downward trend in both the extent and thickness of both perennial and seasonal sea-ice (Stroeve *et al.*, 2007; Comiso *et al.*, 2008; Kwok and Rothrock, 2009; Overland *et al.*, 2013) with a 6% increase in the mean annual ice export

via the Fram Strait since 1979 (Smedsrud *et al.*, 2017). As a result of these changes it is projected that the volumes of water passing through the various components that constitute the Arctic Ocean freshwater cycle will increase during the 21st century (Holland *et al.*, 2007).

Because of the aforementioned observations and increases in freshwater delivery to the high-northern latitudes environment, the freshwater content of the Arctic Ocean, particularly within the Western Arctic and the Beaufort Gyre, has been increasing since the 1990s (McPhee *et al.*, 2009, Rabe *et al.*, 2011 and Giles *et al.*, 2012). However, when viewed from a broader perspective, observations of the freshwater content of the Arctic Ocean, particularly the central Arctic, show that it has become more saline between 1920 and 2003 (Polyakov *et al.*, 2008). This disparity sharply brings into focus the important role that understanding the natural variability of the Arctic Ocean freshwater budget plays when trying to ascertain the roles internal and external forcings have on any recent, present and future observed climatic variations. The inconsistent findings of the trend of the freshwater content of the Arctic Ocean when analysing different periods make not only for an interesting narrative, but also highlights the difficulties encountered when trying to attribute observed changes of the climate system to either an internal or external forcing.

Given that the Arctic Ocean is stratified due to its saline content, as opposed to its thermal properties, with increased freshwater delivery to the Arctic, we are likely to see profound changes to the upper-ocean layer stratification within the Arctic Ocean. The upper ocean plays an important role in the transfer of energy between the ocean and the atmosphere (Aagaard *et al.*, 1981). Freshwater inputs to the Arctic allow the upper layers of the Arctic Ocean to become decoupled from the warmer and more saline waters of Atlantic origin below. In turn, this allows sea-ice to form more easily, which is then transported southwards to the sub-Arctic Seas and the sites of deep convection that ultimately drive the deep ocean circulation in the North Atlantic. Therefore, any substantial modification in the hydrological cycle is likely to result in further changes to the Arctic environment, with implications for the weather and climate on a wide range of scales (Overland *et al.*, 2016). However, in conjunction with observing these projected changes, it is important to disentangle and fully understand how much of the variability we observe around us can be attributed to internal or external climate variability.

In this framework, we sought to investigate the mechanisms driving the intrinsic low-frequency variability of the Arctic Ocean freshwater content, focussing on multicentennial timescales. However, due to the complexity of the climate and the numerous feedbacks and forcings, it is not possible to explain these mechanisms from the observational or palaeoclimate record alone. In addition, the observational record is too short, and the paleoclimate records are relatively scarce, making it difficult to use these sources to study multicentennial variability. Therefore, in order to provide greater clarity of the natural drivers of climate variability over periods extending beyond the instrumental record, and within the finer timescales that are not captured by palaeoclimate records, it is extremely useful to use a climate model.

In a previous study using the climate model LOVECLIM, it was established that the Arctic Ocean freshwater content displayed multicentennial variability in a transient simulation of the last millennium (Davies *et al.*, 2014; Chapter 2 of this thesis). However, it was not possible to decipher to what extent this variability was due to internal variability, as this observation occurred within a transient simulation with varying external forcings (i.e. greenhouse gas concentrations, volcanic aerosols) for the last millennium. Therefore, in order to explore the centennial scale variability of the Arctic Ocean freshwater content, and to specifically understand the mechanisms driving it, we performed a 10,000-year long preindustrial control simulation using the LOVECLIM climate model, and analysed the results. The length of this simulation allows a robust analysis of multicentennial variability.

3.2. Model Description and Experimental Design

3.2.1 Model Description

We applied LOVECLIM (Version 1.2), an Earth system model of intermediate complexity (Goosse *et al.*, 2010), that has a fully coupled, dynamically enabled atmosphere, ocean, sea-ice, land and vegetation components, whilst the ice-sheets were prescribed to modern day conditions.

The atmospheric component, ECBilt (Haarsma *et al.*, 1996; Opsteegh *et al.*, 1998), has a quasi-geostrophic dynamical atmosphere with a horizontal T21 truncation (5.6° x 5.6° longitude-latitude), three vertical layers, 800hPa, 500hPa and 200hPa, and includes a full hydrological cycle, where humidity is represented by the total precipitable water between the surface and 500hPa. Above 500hPa, it is assumed that the atmosphere is dry and all water that surpasses this level is converted to precipitation. The model does not dynamically simulate clouds; instead clouds are prescribed based on the modern day ISCCP D2 dataset (Rossow *et al.*, 1996), which is an obvious limitation of the model. The land surface component of the model is part of ECBilt and has the same grid resolution as the atmospheric component. Additionally, river runoff is computed using a simple bucket method, in that the volume of water in the bucket is a function of the vegetation type. If the water level of the bucket is higher than the allowed capacity of the bucket after precipitation, evaporation and snow melting have occurred, then the excess water is transferred directly to the mouth of the corresponding river basin.

The oceanic component, CLIO (Goosse and Fichefet, 1999), is a primitive-equation, free-surface ocean model that consists of a general ocean circulation model (Deleersnijder and Campin, 1995; Deleersnijder *et al.*, 1997) coupled to a thermodynamic-dynamic sea-ice model (Fichefet and Morales Maqueda, 1997 and 1999) with a 3° x 3° (latitude-longitude) resolution. It includes realistic bathymetry, classical approximations (Boussineq, thin shell and hydrostatic), plus the eddy-induced advection term of Gent and McWilliams (1990). The resolution of the model does not allow for a realistic representation of flow through the Bering Strait, therefore it is determined by the sea-level difference across the strait, following the geostrophic control theory (Goosse *et al.*, 1997). Sea-ice is represented by a three-layer model where each floe of ice is divided

into two homogenous layers upon which snow accumulates when the surface temperature is below the freezing point and precipitation occurs.

The vegetation component, VECODE (Brovkin *et al.*, 2002), is a reduced form dynamic global vegetation model which is capable of simulating the dynamics of two plant functional types (trees and grasses), in addition to a dummy type (desert). The vegetation types influence the surface albedo, soil moisture content, and net precipitation (Goosse *et al.*, 2010).

LOVECLIM is able to simulate climate that is in reasonable agreement with modern day observations. For the period 1980-2000, the maximum annual Atlantic Meridional Overturning Circulation strength as simulated in an earlier version of LOVECLIM is 22Sv (Goosse *et al.*, 2010), which compares to 20.61±1.01Sv (1 s.d.) in our pre-industrial (PI) control simulation. These values are slightly higher than suggested by observations, 17.2Sv (2004-2012) (Smeed *et al.*, 2014) and modelling studies (Gregory *et al.*, 2005). Additionally, the sites of deep convection in the North Atlantic occur within LOVECLIM in the Labrador Sea, the Irminger Sea and south of Svalbard in the Greenland-Norwegian Sea (Goosse *et al.*, 2010). The seasonal maxima and minima sea-ice extent in the Northern Hemisphere are close to observations (Goosse *et al.*, 2010) and overall, the magnitude of temperature and precipitation is simulated reasonably well (Goosse *et al.*, 2010). To a doubling of the atmospheric CO_2 level, LOVECLIM demonstrates a climate sensitivity of 1.9°C, which when compared to more complex models, is at the lower end of the range (Flato *et al.*, 2013). Furthermore, LOVECLIM has successfully been employed in numerous studies, covering a variety of temporal scales, including simulating the last millennium (Goosse et al. 2005), the Holocene (Renssen *et al.*, 2009), the 8.2ka event (Wiersma and Renssen, 2006), the last glacial maximum (Roche *et al.*, 2007), and the last interglacial (Bakker *et al.*, 2013). The results of these simulations show a high level of consistency with more complex models (Goosse *et al.*, 2010; Bakker *et al.*, 2013; Nikolova *et al.*, 2013). Therefore, LOVECLIM is an effective tool to study the mechanisms ruling centennial variations of the Arctic Ocean freshwater content.

A pre-industrial (PI) 10000-year long equilibrium simulation was performed, using fixed forcing parameters, as outlined by the PMIP3 protocol (http://pmip3.lsce.ipsl.fr/), where orbital parameters (Eccentricity = 0.016724, Obliquity = 23.446°, Precession = 102.04°), trace gas concentrations (CO_2: 280ppm, CH_4: 760ppb, N_2O: 270ppb) and solar constant (1365Wm^{-2}) forcings were kept constant for the entirety of the simulation. The forcings were kept fixed to allow for an analysis of the intrinsic variability of the climate system in our model. The simulation was initiated from a 2500-year control simulation to allow the model, particularly the deep oceans, to reach a quasi-equilibrium state.

3.2.2 Calculating freshwater fluxes

In order to complete a full analysis of the Arctic freshwater cycle, new diagnostics were introduced into the CLIO code to allow for the computation of both liquid freshwater (F_w) and ice (F_i) fluxes at all boundaries of the Arctic Ocean. These have been

explained in detail in Davies *et al.* (2014), but for completeness we shall include once again. To calculate the freshwater flux (F_w):

$$F_w = \int_{L_1}^{L_2} \int_{-h}^{0} v_w \frac{(S_{ref} - S_0)}{S_{ref}} dz dL$$

Where v_w is the water velocity, which is computed perpendicular to the length of the transect (L_1 to L_2) through which it passes. S_{ref} is a reference salinity of the Arctic Ocean (taken to be 34.8 psu) and S_0 is the salinity of the ocean. These fluxes are computed over the entire depth of the water column to give a freshwater flux (km^3 year^{-1}).

The freshwater flux of the sea-ice and snow (F_i) (km^3 year^{-1}) is calculated as follows:

$$F_i = \int_{L_1}^{L_2} v_i \, h_i \frac{(S_{ref} - S_i)}{S_{ref}} \frac{\rho_i}{\rho_w} \, dL + \int_{L_1}^{L_2} v_i \, h_s \frac{(S_{ref} - S_w)}{S_{ref}} \frac{\rho_s}{\rho_w} \, dL$$

Where v_i represents the ice flow velocity, S_i the salinity of the ice (6 psu), S_w is the salinity of the snow (0 psu), ρ_w is the density of the water (1000 kg m^{-3}), ρ_i the density of ice (330 kg m^{-3}), h_i the thickness of the ice, and h_s the thickness of the snow.

The liquid freshwater content (F_c) of the Arctic Ocean (km^3) is defined as follows:

$$F_c = \int dV \frac{(S_{ref} - S_0)}{S_{ref}}$$

With dV representing the change in volume over the entire depth of the water column. The volume of freshwater contained within the sea-ice (F_{ic}) (km^3) is calculated with respect to the volume of sea-ice (V_i):

$$F_{ic} = V_i \frac{(S_{ref} - S_i)}{S_{ref}}$$

The above equation does not include the freshwater contained in snow upon the sea-ice as its overall effect is negligible with respect to the overall Arctic freshwater cycle.

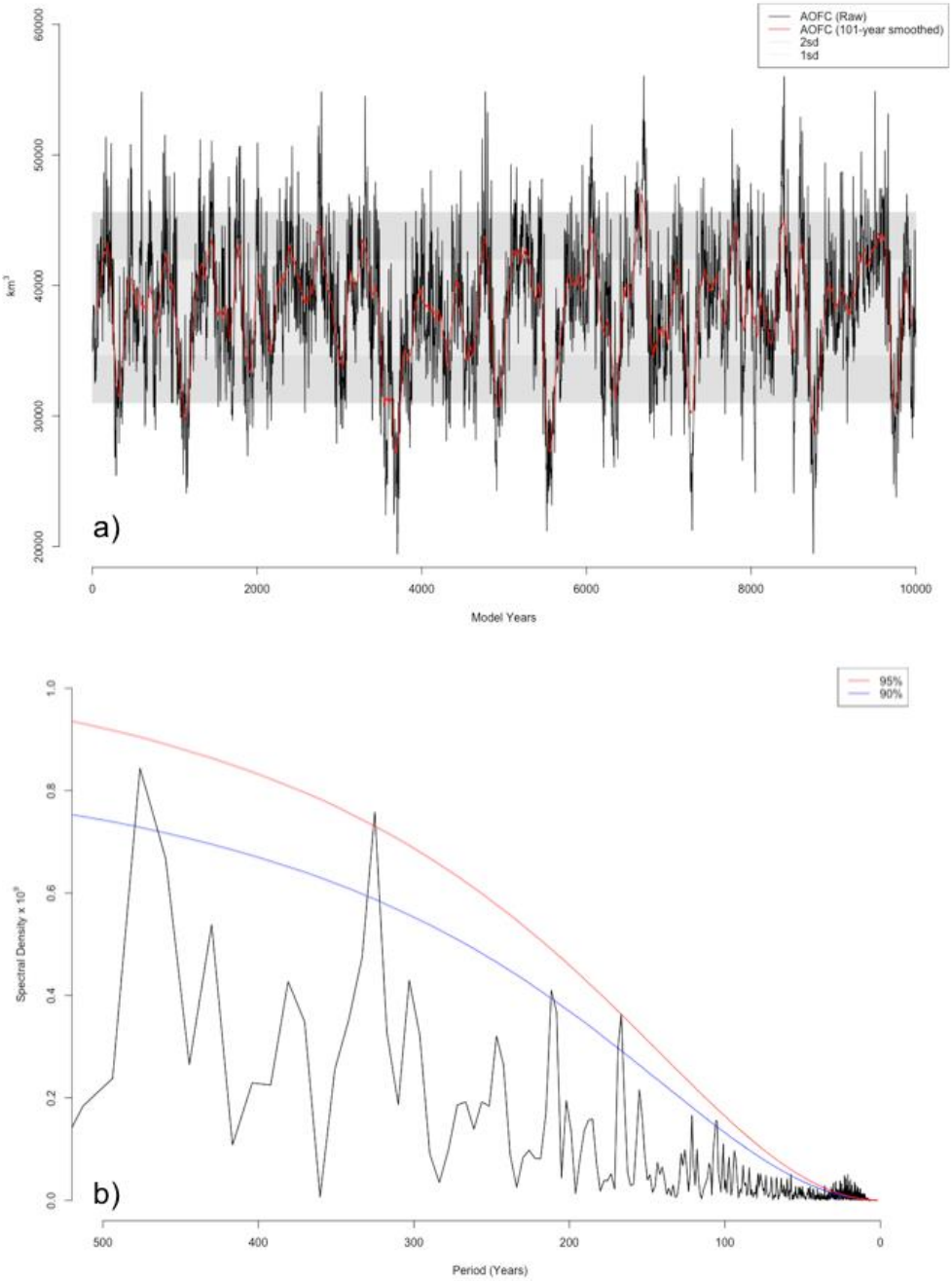

Fig.3.1. a) The annual Arctic Ocean freshwater content (AOFC) time series, both unfiltered (black line) and filtered with a 101-year moving average (red line). (b) A Lomb Periodogram of the annual Arctic Ocean freshwater content (AOFC) unfiltered time-series with both 90% (blue line) and 95% (red line) significance levels.

3.3. Statistical analysis of the Arctic Ocean freshwater content

The simulated time series of the mean annual Arctic Ocean freshwater content reveals clear multicentennial periodicity (Fig.3.1a) which is similar to the variability reported by Davies *et al.* (2014). Here the results of the complete 10000-year time series of Arctic Ocean freshwater content variability are shown, both in its unfiltered and filtered forms (a 101-year moving average was performed to reduce the high-frequency variability of the data, whilst still allowing the low-frequency, multicentennial scale signals to be visible). Spectral analysis of the unfiltered Arctic Ocean freshwater content data, shown as a Lomb Periodogram (Fig.3.1b), reveals a mostly red spectrum. There are only two peaks in the spectrum that are at or above the 95% significance level and these occur at approximately 165 and 325-years. These results suggest there is a dominant mode of intrinsic multicentennial variability of the Arctic Ocean freshwater content, with the 325-year signal merely representing double the periodicity of the 165-year signal.

Cross-correlation is a commonly applied method of assessing the degree to which the variance of one time series can account for the variance of another time series, as a function of a lag between the time series. This makes it a suitable method with which to investigate the mechanics driving the simulated multicentennial variability of the Arctic Ocean freshwater content. Initially, ~30 ocean and atmospheric variables were cross-correlated with each other, totalling >500 cross-correlations being performed. From this multitude of cross-correlations, the Arctic Ocean freshwater content (AOFC); the Nordic Seas overturning strength (NSOS); Fram Strait ice freshwater volume export (FS_I); North Atlantic Current (NAC); Fram Strait liquid volume export (FS_V); and East-Siberian Shelf sea-ice thickness (ESS) were the variables that showed the strongest correlations with one another. Thus, these pairs of correlations form the basis of our analysis. To achieve a statistically robust result, the cross-correlations were performed on the entire 10,000-year time series.

To perform a cross-correlation test, it is assumed that the data is normally distributed and stationary (meaning the mean, variance, median etc. remain the same throughout the time series and the dataset does not possess a trend). To test if the variables we used in our statistical analysis were stationary we applied three widely known tests that test for stationarity of a time series. These were the Ljung-Box test (Ljung and Box, 1978; Box and Pierce, 2012); the Augmented Dickey-Fuller test (Dickey and Fuller, 2012); and the Kwiatkowski-Phillips-Schmidt-Shin test (Kwiatkowski *et al.*, 2012). All variables used in our analysis were shown to be stationary across all three tests. To test if each time series was normally distributed the skewness, kurtosis and Box-Cox values were calculated. The skewness of a dataset is a measure of its symmetry around its mean values, with a value of zero indicating a normally distributed dataset. Kurtosis is a measure of the shape of the distribution in relation to its tails, with a value of three showing normality in a dataset. The Box-Cox value is a measure of the transformation that is required to make a dataset normally distributed, with a value of one indicating no transformation is required. For our variables, the skewness values range from -0.29 to 0.35; Kurtosis values range from 2.65 to 3.65; and Box-Cox values range from 0.48 to 1.99 (all at the 95% confidence level)

(Table 3.1). Given these results, we can assume with a high-degree of confidence that the data is normally distributed. These results, combined with the results from stationary tests, and also assuming that given the variables we are cross-correlating are clearly different from a dynamical point of view and have differing units (hence drawn from different populations), shows that the time series used are suitable for cross-correlation analysis.

Table 3.1. Sampled statistics of the different time series variables. Arctic Ocean freshwater content (**AOFC**); Nordic Seas overturning strength (**NSOS**); Fram strait liquid volume export ($\mathbf{FS_v}$); North Atlantic Current (**NAC**); Fram strait ice freshwater volume export ($\mathbf{FS_i}$); and East-Siberian shelf sea-ice thickness (**ESS**).

Variable	Skewness (95%)	Kurtosis (95%)	Box-Cox value (λ) (95%)
AOFC	-0.18	3.13	0.48
NSOS	-0.29	3.05	1.52
FS_v	0.35	3.12	1.99
NAC	-0.22	3.53	0.91
FS_i	-0.29	3.65	0.57
ESS	0.23	3.02	0.53

3.4. Drivers of Arctic Ocean freshwater content multicentennial variability

The Nordic Seas are a site of overturning in the high-latitude North Atlantic. The strength of which, along with the subpolar gyre (Hátún *et al.*, 2005), determine the amount of heat and salinity that is delivered to the Arctic Ocean, via the Barents and Kara Seas and the Fram Strait. In reality, as well as in LOVECLIM, Atlantic-derived waters entering the Arctic Ocean, as a branch of the North Atlantic Current, have a salinity of approximately 35 psu (Dickson and Blindheim, 1984), which is greater than the mean Arctic Ocean salinity, for which an adequate estimate is taken to be 34.8 psu (Aagaard and Carmack, 1989). Therefore, the North Atlantic Current represents a net freshwater sink to the Arctic Ocean and its tendency effect is to increase the overall salinity of the Arctic Ocean. Hence, the North Atlantic Current and the Nordic Seas overturning strength are strongly linked to the oceanic properties of the Arctic Ocean.

In Table 3.2, we observe that the Nordic Seas overturning strength is positively correlated ($r = 0.52$) with the North Atlantic Current, lagging by approximately 5 to 7 years. Thus, as the strength of the Nordic Seas overturning strength abates, the North Atlantic Current also weakens (Fig.3.2), leading to a decrease of heat and saline waters flowing northwards, via the Barents and Kara Seas to the Arctic Ocean. A consequence of this is that there is a decrease in saline waters reaching the Arctic Ocean, thus the role of the North Atlantic Current as a heat and saline source to the Arctic Ocean is diminished and the freshwater content of the Arctic Ocean begins to increase (Fig.3.3). In addition, this leads to lower temperatures across the Barents Sea (Fig.3.4) which are positively

correlated (r = 0.77) with the Arctic Ocean freshwater content, with the surface temperature of the Barents Sea and showing a lagged response of approximately 109 to 114 years.

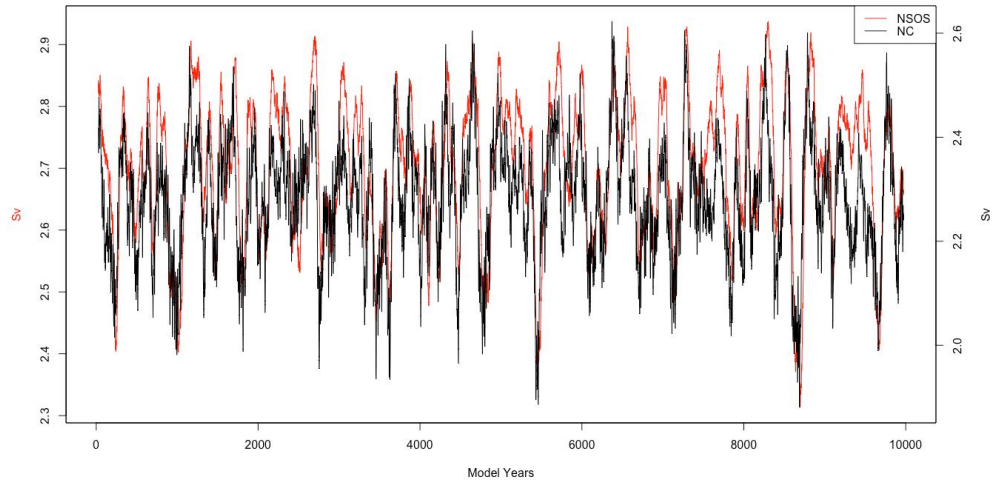

Fig.3.2 Time series (51-year running mean) of the simulated Nordic Seas overturning strength (Sv) (red line) v North Atlantic Current (Sv) (black line).

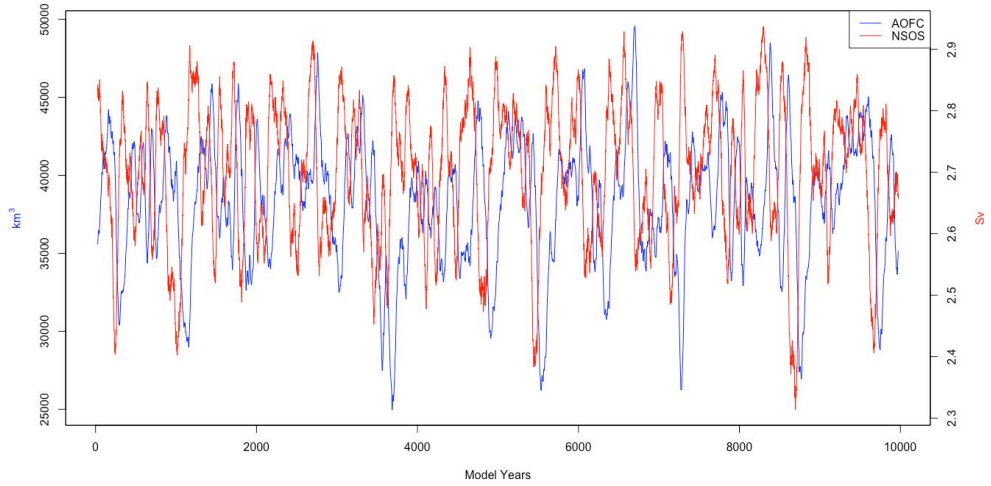

Fig.3.3. Time series (51-year running mean) of the simulated Arctic Ocean freshwater content (km^3) (blue line) v Nordic Seas overturning strength (Sv) (red line).

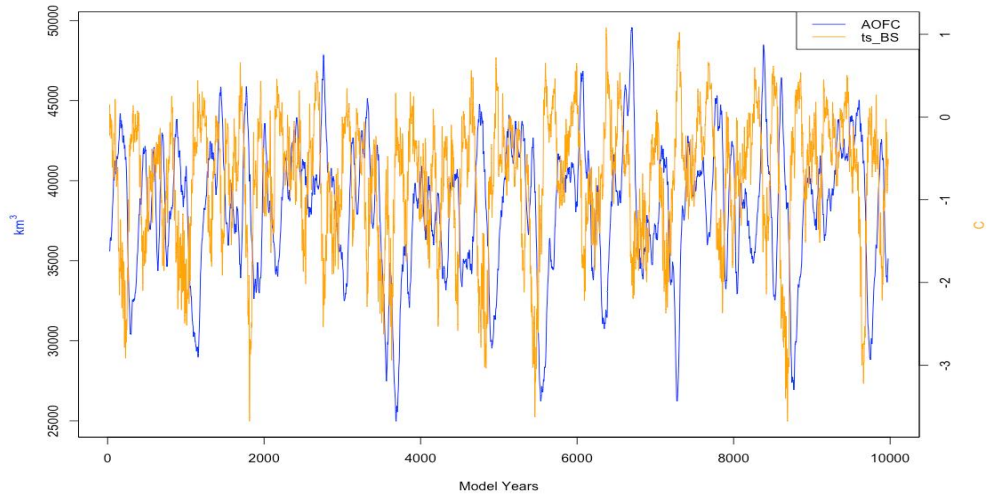

Fig.3.4. Time series (51-year running mean) of the simulated Arctic Ocean freshwater content (km^3) (blue line) v Barents Sea surface temperature (°C) (orange line).

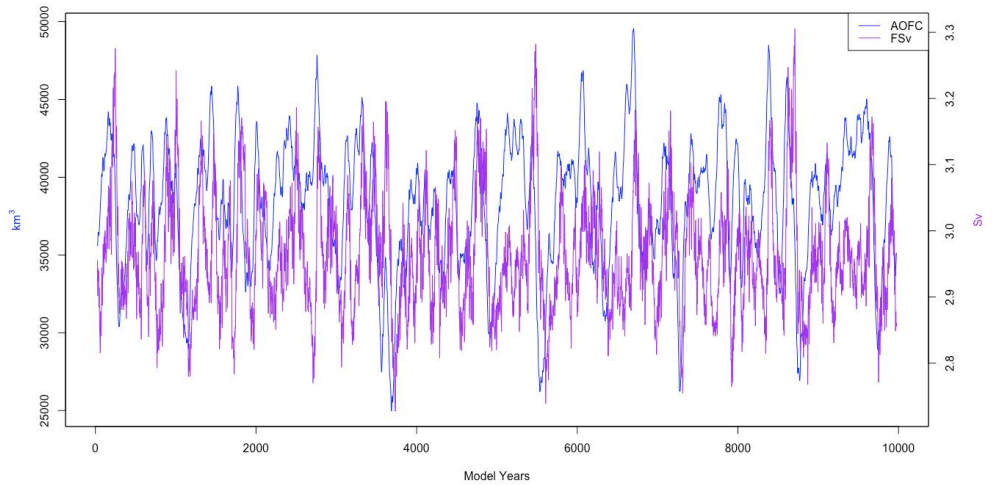

Fig.3.5. Time series (51-year running mean) of the simulated Arctic Ocean freshwater content (km^3) (blue line) v Fram Strait liquid volume export (Sv) (purple line).

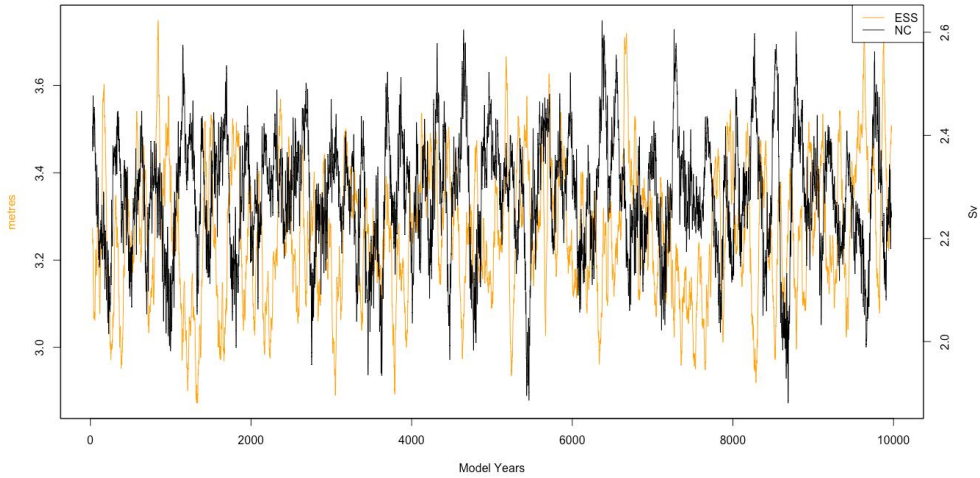

Fig.3.6. Time series (51-year running mean) of the simulated East-Siberian Shelf Ice thickness (ESS) (m) (orange line) v North Atlantic Current (NAC) (Sv) (black line).

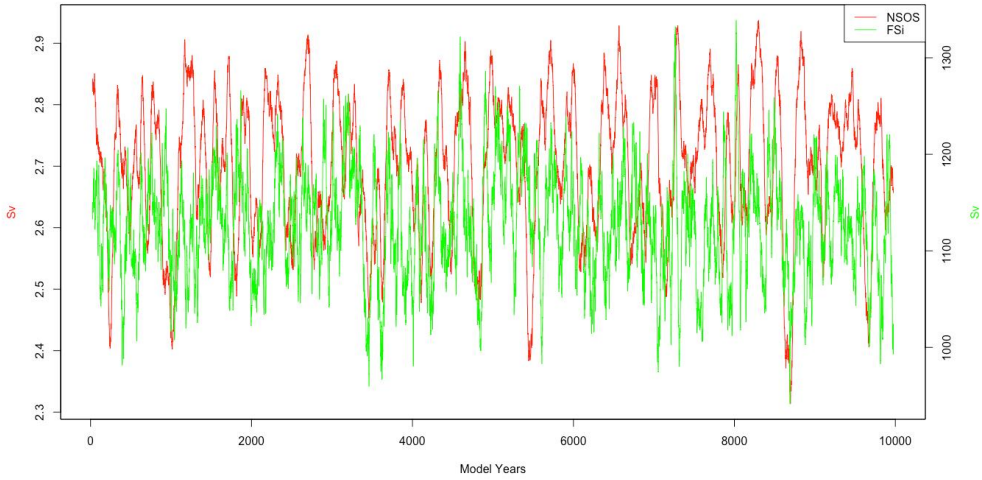

Fig.3.7. Time series (51-year running mean) of the simulated Nordic Seas overturning strength (Sv) (red line) v Fram strait freshwater ice volume export (km^3) (green line).

The main oceanic driver of the multicentennial variability we observe is the relationship between the Arctic Ocean freshwater content and the Nordic Seas overturning strength. Cross-correlation of these variables show that the peak correlation occurs at 69 to 85 years ($r = 0.48$, the Nordic Seas overturning strength lags Arctic Ocean freshwater content). As a result of the increased Arctic Ocean freshwater content, the export of liquid freshwater via the Fram Strait increases (Fig.3.5), lagging the response of the Arctic Ocean freshwater content by 2 to 4 years ($r = 0.39$). This export of freshwater into the Nordic Seas feeds back on the salinity within the Nordic Seas and acts to keep the Nordic Seas overturning strength reduced during the phase of increased Arctic Ocean freshwater content.

Table. 3.2. Data table of the statistical analysis we performed on our data. Showing the variables (**Var1** and **Var 2**) that were correlated with one another. Each time series was fitted with an 11-year **filter**. The **t-stat** shows the result of the Welch t-test that was performed, and the adjusted degrees of freedom (**df**) that were calculated using the methods outlined in the text. The **p-value** and **quantile** values were calculated in order to help in either accepting or rejecting the null hypothesis. The **correlation at maximum lag**, the year at which the **maximum lag** occurred, as well as the **lag range** are also included. Variables include: Nordic Seas Overturning Strength (**NSOS**); North Atlantic Current (**NAC**); Fram Strait Ice Export ($\mathbf{FS_I}$); Arctic Ocean Freshwater Content (**AOFC**); Fram Strait Freshwater Liquid Volume Export ($\mathbf{FS_V}$); and East-Siberian Shelf sea-ice thickness (**ESS**)

Var 1	Var 2	Filter (years)	t-stat (95%)	df	p-value (95%)	Tabulated t-stat (97.5%)	Correlation at maximum lag (95%)	Max lag (years)	Lag Range (years)
NSOS	NAC	11	152	1436	$<2.2e^{-16}$	1.96	0.52	6	5 to 7
NSOS	FS_V	11	2583	1406	$<2.2e^{-16}$	1.96	-0.58	-4	-5 to -3
NSOS	FS_I	11	878	1165	$<2.2e^{-16}$	1.96	0.20	6	5 to 7
AOFC	NSOS	11	791	391	$<2.2e^{-16}$	1.97	0.48	74	69 to 85
AOFC	FS_V	11	792	1173	$<2.2e^{-16}$	1.96	0.39	-3	-4 to -2
AOFC	NAC	11	791	1203	$<2.2e^{-16}$	1.96	-0.42	6	5 to 7
AOFC	FS_I	11	815	930	$<2.2e^{-16}$	1.96	-0.25	6	5 to 7
NAC	ESS	11	282	1454	$<2.2e^{-16}$	1.96	-0.20	-3	-3 to -2

The coupled effect of a freshening, cooling Arctic Ocean, as result of a weakened North Atlantic Current and the subsequent reduction of warm, saline waters flowing northwards, alters this high-northern latitude ocean environment. We observe an increase in sea-ice thickness when the North Atlantic Current weakens, particularly across the East-Siberian Shelf (Fig.3.6), although the negative correlation with East-Siberian Shelf sea-ice thickness is relatively weak (-0.20, Table 3.2). One explanation for this is that due to a reduced strength of the North Atlantic Current, and the subsequent reduction of heat travelling northwards, the Arctic Ocean is now able to stratify far easier as the cooler, less dense freshwater layers on top of the ocean and below the existing sea-ice, deepens. Therefore, we can say that the increase in sea-ice thickness is a consequence of the cooling ocean and we see a near instantaneous response of the sea-ice to this cooling of the ocean.

Eventually, the formation of sea-ice in the Barents Sea leads to a decoupling of the deeper warmer waters from the atmosphere (Fig.3.4), however which such a long response time (109 to 114 years) it can clearly be seen that this is not a driver of the process. However, the reduced heat exchange between the ocean and atmosphere would eventually aid the formation of sea-ice in the Arctic.

Overall, the increase in the volume of freshwater in the Arctic Ocean, as a result of weaker Atlantic inflow, leads not only to an increase in the amount of freshwater stored within the Arctic Ocean itself, but also in the amount being converted to a freshwater store of sea-ice when the ice thickens. Over time, we observe that the proportion of freshwater that is stored as sea-ice in the Arctic becomes more significant, leading to a decrease in freshwater export via the Fram Strait (Fig.3.5). This relationship is also clear from the negative correlation of -0.58 between the Fram Strait liquid volume export and the Nordic Seas overturning strength (Table 3.2, Fig.3.10). As a result, the salinity of the Nordic Seas begins to increase again, which also strengthens the Nordic Seas overturning strength.

It would be expected that exports of sea-ice from the Arctic via the Fram Strait would play a significant role in suppressing the Nordic Seas overturning strength during the freshening phase of the Arctic Ocean, given that we observe an ice build-up in the Eastern Arctic. However, this is not truly the case. Whilst we do observe episodes of large exports of sea-ice from the Arctic to the Nordic Seas, via the Fram Strait (Fig.3.7), the response of the Nordic Seas overturning strength is not consistent to this input of sea-ice. At approximately 4550 to 4600, 4950 to 5000 and 5300 to 5350 model years, we see a sudden increase in sea-ice export via the Fram Strait of approximately 20-25% (Fig.3.7), yet during these three periods, the response of the Nordic Seas overturning is a slight increase, a sharp increase and a sharp decrease, respectively. The cross-correlation was performed over the entire 10,000-year time-series and reveals a small positive correlation ($r = 0.20$) between the Nordic Seas overturning strength and Fram Strait ice freshwater volume export, where one would expect a negative correlation if enhanced export of sea-ice would significantly reduce the deepwater formation. This limited correlation between the Nordic Seas overturning strength and Fram Strait ice freshwater volume export is explained by an increase in wind speed during the freshening phase of the Arctic Ocean, through the Fram Strait region and along the Eastern Greenland coast (Fig.3.8), leading to enhanced southward sea-ice transport here. Additionally, we see an overall stronger atmospheric circulation in the Arctic Ocean during the decreasing phase, leading to a minimum Arctic Ocean freshwater content. This increase in winds through the Fram Strait is associated with a more pronounced ridging effect occurring within the atmospheric column, up to the 800hPa geopotential height level (Fig.3.9), but not at the 500hPa level (not shown). This suggests that the effects are mostly felt within the planetary boundary layer. Therefore, one of the conclusions we can draw is that the lack of a negative correlation occurs because the majority of the sea-ice that is exported via the Fram Strait does not melt near the main site of deepwater formation in the Nordic Seas, but instead is transported further south along the coast of Eastern Greenland, due to the enhanced

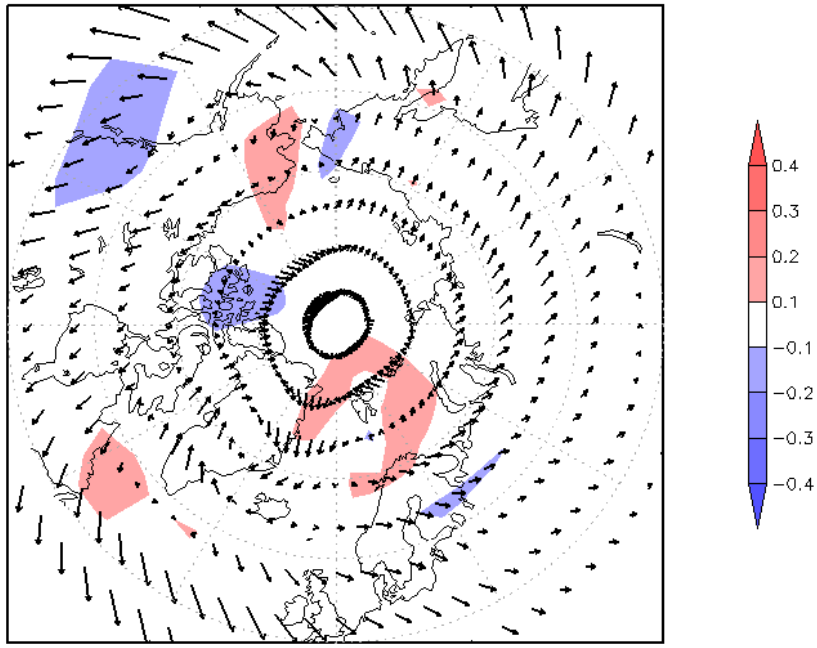

Fig.3.8. Composite anomaly plot of surface winds (ms^{-1}) between $AOFC_{MAX}$ (4774 to 4784 model years) - $AOFC_{MIN}$ (4902 to 4922 model years). Background colours relate to the magnitude anomaly of the wind between the $AOFC_{MAX}$ and $AOFC_{MIN}$ phases, while the arrows represent the direction of the winds.

winds. Hence, Fram Strait sea-ice export does not directly lead to a weakening of the Nordic Seas overturning strength.

The increase in liquid freshwater export through the Fram Strait diminishes the volume of excess freshwater stored in the Arctic. Eventually this leads to a decrease in the Arctic Ocean freshwater content when the liquid freshwater export is larger than the freshening effect of reduced inflow of relatively saline Atlantic waters, associated with the Nordic Seas overturning strength weakening. When the Arctic Ocean freshwater content is reduced beyond a critical point, the liquid freshwater export starts to decline again, leading to an increase in salinity in the Nordic Seas and a reinvigorating of the Nordic Seas overturning strength (Fig.3.10). This marks the beginning of the second-half of the cyclicity. As the Nordic Seas overturning strength increases, there is an increase in the volume of warm, saline waters transported to the Arctic Ocean, in the form of the North Atlantic Current via the Barents and Kara Seas. This reduces the Arctic Ocean freshwater content and the subsequent export of freshwater from the Arctic Ocean, to the Nordic Seas via the Fram Strait, and helps keep the Nordic Seas overturning strength strong. Additionally, with an increase of warmer waters reaching the Arctic Ocean, temperatures begin to rise (Fig.3.10), the sea-ice begins to melt, reducing its thickness, and the freshwater that had been stored in the form of sea-ice becomes remobilised. Therefore, the proportion of freshwater stored as sea-ice decreases, whereas the amount stored as freshwater in the Arctic Ocean increases. After a period, the freshwater export via the

Fram Strait begins to increase once again, which now acts to supress the Nordic seas overturning, competing the full cycle. The mechanisms controlling the Arctic Ocean freshwater content increasing and decreasing phases are depicted in Fig.3.11.

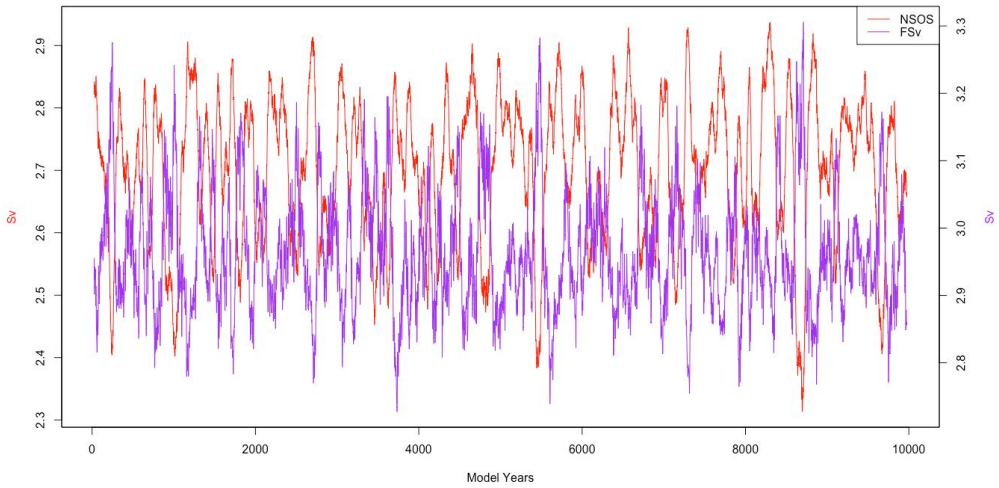

Fig.3.10. Time series (51-year running mean) of the simulated Nordic Seas overturning strength (Sv) (red line) v Fram Strait liquid volume export (Sv) (purple line).

The mechanism we propose relies on a series of cross-correlations, meaning that it is entirely plausible that the variability of the overturning in the Nordic Seas is due to another driving mechanism, and that the correlation we observe with the Arctic Ocean freshwater content is just a consequence of this variability with no impact on the mechanism itself. Still, we believe that the statistical robustness we have applied to our analysis gives some weight to our conclusions. However, the only way to confirm the casual link between the variability in the Nordic Seas overturning strength and the Arctic Ocean freshwater content is to conduct a series of sensitivity studies. Unfortunately, this is beyond the scope of this chapter.

Despite this limitation of our study, we do have a good degree of confidence that our research is pointing in the correct direction. Additionally, in a previous study (Davies *et al.*, 2014; Chapter 2 of this thesis) a similar period of variability was observed in the Arctic Ocean freshwater content. Therefore, we do believe that the mechanism we propose is fundamentally correct, but a more detailed understanding of it would require further sensitivity studies to be performed.

3.5. Discussion

Our results add to the growing body of work that has identified low-frequency intrinsic climate variability within the high northern latitudes. These include the Atlantic Meridional Oscillation (65 to 70 years) (Schlesinger and Ramankutty, 1994); the Arctic Oscillation (1500 years) (Darby *et al.,* 2012); the North Atlantic Oscillation (170 and 300 years) (Olsen *et al.*, 2012); the heat transported by the Atlantic Meridional Overturning

Circulation (300 to 400 years) (Park and Latif, 2008); and sea-ice cover in the Kara Sea (400 and 950 years) (Hörner *et al.*, 2017). We can add Arctic Ocean freshwater content (165 and 325 years) to the list. In an ideal world, we would compare our results with those of observations. However, time series of adequate length and resolution of each of component of the hydrological cycle, that are relevant to the multicentennial variability Arctic Ocean freshwater content mechanism, are not available. In addition, to our knowledge this is the first investigation of its kind (understanding the mechanisms behind intrinsic multicentennial variability of the Arctic Ocean freshwater content), so there are no comparable modelling studies either. Therefore, with respect to our results it is important to put the observed changes into context. One study that allows us to do this is the study by Polyakov *et al.* (2008). In this study, 100 years of *in situ* data recorded during the 20th century across the central Arctic Ocean were analysed. These results showed that the Arctic Ocean became more saline at a rate of 239±270 km^3 decade^{-1}, whilst the East-Siberian shelves became fresher at a rate 29±50km^{3}decade^{-1} (Polyakov *et al.*, 2008). If we analyse the rates of change of the Arctic Ocean freshwater content over the entire control simulation (Fig.3.1) we see that during a decreasing Arctic Ocean freshwater content phase, the Arctic Ocean became more saline at a rate of 313±273 km^{3}decade^{-1} and freshened at a rate of 314±244 km^{3}decade^{-1}. This comparison shows the rates of freshening and increased salinity we observe within our control simulation are comparable to the rates of changes observed by Polyakov *et al.*, (2008).

To bring further context to our results we can compare them to more recent climate observations. For example, the temperature changes we observe (Fig.3.4) over

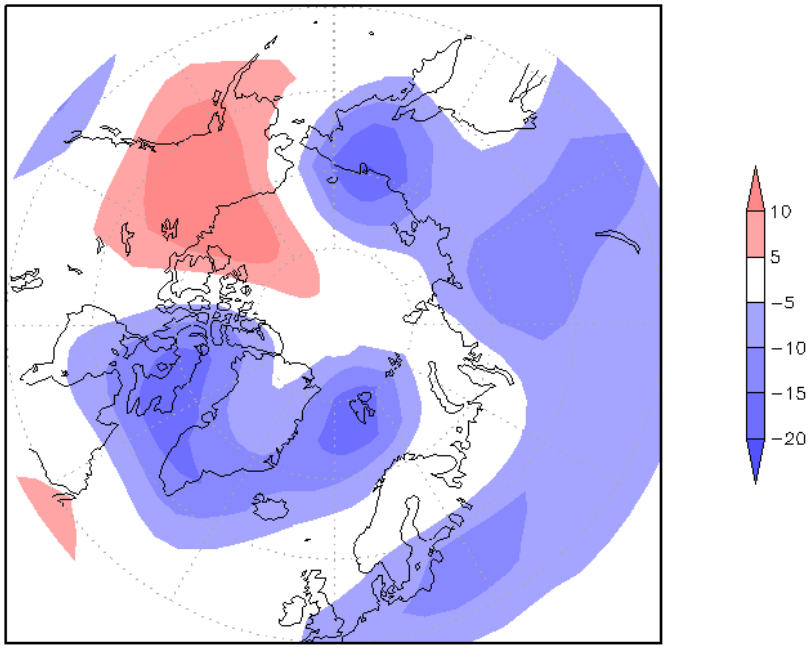

Fig.3.9. Composite anomaly plot of 500hPa geopotential height (m) between $AOFC_{MAX}$ (4774 to 4784 model years) - $AOFC_{MIN}$ (4902 to 4922 model years).

large parts of the Eastern Arctic, most notably the Barents and Kara Seas show a temperature change of up to 1.6°C between the Arctic Ocean freshwater content maximum phase ($AOFC_{MAX}$) and Arctic Ocean freshwater content minimum phase ($AOFC_{MIN}$). In comparison, the mean annual temperature across the whole of the Arctic was 1.5°C higher between 2001 and 2012 than the 1970-2000 mean (Overland *et al.*, 2013). To clarify, in no way are we trying to attribute variations between $AOFC_{MAX}$ and $AOFC_{MIN}$ as a casual mechanism to recent observed temperatures changes in the Arctic. The comparison is made to highlight that the changes we observe between the $AOFC_{MAX}$ and $AOFC_{MIN}$ phases in our simulation are significant in terms of their amplitude and are not just background noise. In relation to the observed variations in sea-ice thickness in the north-eastern Arctic, incorporating the East-Siberian Seas, we observed variations of sea-ice thickness of up to 0.5m. Studies in the Laptev Sea in 1995 and 1996 showed a change in thickness of 0.6m between these years (Hass and Eicken, 2001). If we look at the upper atmosphere, at the 500hPa geopotential level (Fig.3.10), the thickness change between the $AOFC_{MAX}$ and $AOFC_{MIN}$ phases, reaches a maximum of 80m. If one compares the thickness changes observed within our simulation and those occurring during a phase of the Arctic Oscillation using the NCEP/NCAR products, the changes we observe are significant. For other comparison, i.e. the Fram Strait freshwater and liquid exports, as well as the Nordic Seas overturning strength, the reader is referred to a previous study (Davies *et al.*, 2014), where it was shown that LOVECLIM is able to represent the mean annual freshwater cycle with a good degree of accuracy. Overall, these examples show that the amplitude of the variability observed within our results are comparable to contemporary climatic variability.

Whilst LOVECLIM has been shown to both accurately reproduce the climate of numerous interglacials, as well as perform well when pitted against more complex models, there are nevertheless weaknesses that pertain to this study that should be noted. In particular, the resolution of the ocean (3° x 3°) results in channels from the Arctic to the sub-Arctic Sea, particularly the Fram Strait and the Canadian Arctic Archipelago (CAA), being somewhat unrealistic in their width. However, the complex nature of the CAA makes it an inherently difficult channel to replicate in global climate models, therefore it is omitted in several of these models. LOVECLIM does includes a CAA, albeit it at an unrealistic scale, but when compared to *in situ* observations it is found to perform reasonably well (Davies *et al.*, 2014). However, whilst we do have confidence in our results and analysis, performing a similar simulation as ours with a higher resolution ocean model would be a welcome advance in our study. As a next step it would also be insightful to perform a transient simulation over the Holocene and to test whether this mechanism is robust. One branch of the mechanism that we believe would be relevant of further scrutiny is the seemingly lack of correlation between sea-ice transported via the Fram Strait into the Nordic Seas and the Nordic Seas overturning strength. Given current knowledge and from our understanding, one would expect a stronger correlation between the two. The only plausible explanation is that with a transient simulation, we would see a greater variability of Arctic sea-ice volume, due to summer insolation changes and

perhaps this branch of the mechanism we have described in our paper would respond differently.

3.6. Conclusion

We have analysed the output of a 10,000-year control simulation of the LOVECLIM climate model and have shown the presence of a distinct multi-centennial pattern of variability of the Arctic Ocean freshwater content, with a periodicity of both 165 and 325-years. The variability of the Arctic Ocean freshwater content (with maximum and minimum values of 56,100km^{3}yr^{-1} (+46% of the mean) and 19,400km^{3}yr^{-1} (-49%) respectively), is driven by multi-centennial variability of the Nordic Seas overturning circulation strength, (with a mean strength of 2.7±0.26Sv, with maximum and minimum values of 3.5Sv (+30%) and 1.6Sv (-41%) respectively) and the subsequent variability of heat and saline transported to the Arctic Ocean by the North Atlantic Current, via the Barents and Kara Seas. Essentially, the Arctic Ocean freshwater content increases when the inflow of relatively saline Atlantic waters is reduced due to a weakened Nordic Seas overturning, while the export of freshwater through Fram Strait is relatively small.

The significance of our findings suggests that the Arctic Ocean freshwater content has an intrinsic variability, which is driven by the low-frequency modulation of the transport of heat and saline to the high-northern latitudes. Our findings also allow us to expand the temporal frame of reference when discussing the recent observations of a freshening Arctic Ocean (McPhee *et al.*, 2009; Rabe *et al.*, 2011; Giles *et al.*, 2012). Additionally, our study along with others (Park and Latif, 2008; Darby *et al.*, 2012; Olsen *et al.*, 2012; Hörner *et al.*, 2017), show that there are a variety of low-frequency mechanisms driving the longer-term climate system that need to be incorporated into the present-day discussions about the attributional causes of climate variability. As the Arctic moves ever closer towards a time when it will be seasonally ice free, potentially having a large-scale effect on global climate, the need to fully understand all forcings that are changing the Arctic environment cannot be understated.

Acknowledgements

FD and HR were supported with funding from the 'European Community's 7th Framework Programme FP7/2013, Marie Curie Actions, under grant agreement No. 238111: CASEITN'. HR and HG were also supported by the European Union's 7th Framework programme (FP7/2007-2013) under grant agreement No. 243908, "Past4Future. Climate change - Learning from the past climate". HG is Research Director with the Fonds de la Recherche Scientifique (F.R.S.- FNRS-Belgium). All support is greatly appreciated.

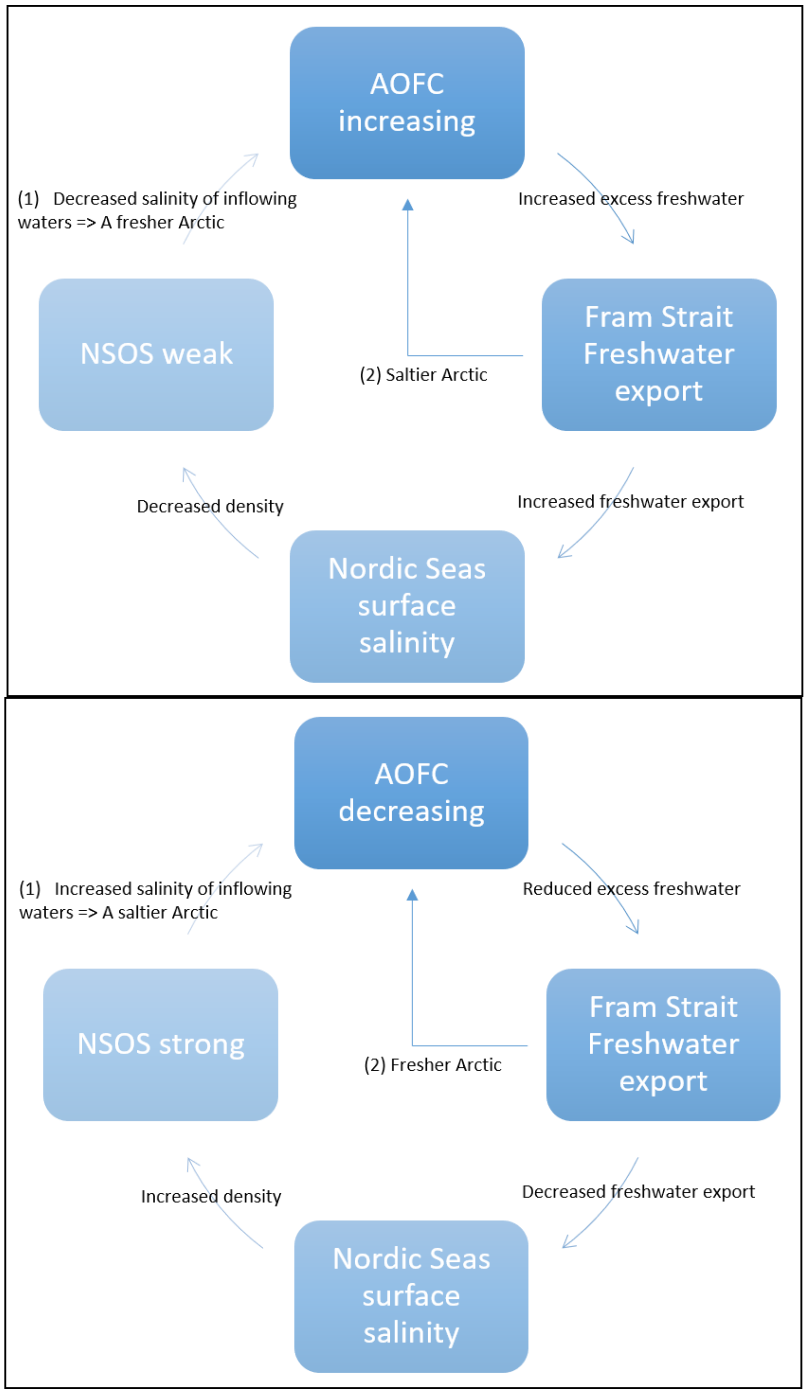

Fig.3.11. Schematic of the mechanism controlling the Arctic Ocean freshwater content (AOFC) phases for a) AOFC increasing and b) AOFC decreasing. For a) AOFC increases ONLY if (1) is stronger than (2). For b) AOFC decreases ONLY if (1) is stronger than (2).

"The difficult is what takes a little time; the impossible is what takes a little longer"

Fridtjof Nansen

Chapter 4: Simulating the Multicentennial variability of the Arctic Ocean freshwater content over the Holocene with the LOVECLIM climate model

Authors: Frazer.J.Davies and Hans Renssen

Abstract

In a previous study we investigated the oceanic and atmospheric mechanisms driving multicentennial variability of the Arctic Ocean freshwater content in a 10,000-year control simulation with fixed preindustrial forcings, performed with the LOVECLIM climate model. This study revealed an intrinsic Arctic Ocean freshwater content variability with a peak periodicity of 165-years. This variability was driven by a series of oceanic processes that regulate the heat and saline fluxes reaching the Arctic Ocean, via the Barents and Kara Seas, in the form of the North Atlantic Current. Here we have built upon this body of work and have investigated the same mechanism in a transient simulation of the last 8000-years with relevant forcings (orbital parameters and greenhouse gas concentrations). We find that the mechanisms driving the Arctic Ocean freshwater content in the previous study also determine multicentennial-scale variability in this Holocene transient simulation. In addition, we find that the sea-ice export via the Fram Strait into the North Atlantic Ocean, does play a significant role in the driving mechanism of multicentennial-scale variability. This is contrary to our findings in Chapter 3 and allows us to present a more complete picture of the mechanism driving the intrinsic variability of the Arctic Ocean freshwater content over the Holocene.

4.1. Introduction

The freshwater hydrological cycle of the Arctic Ocean is an extremely important part of the global climate system, as it has the potential to alter climate on both a regional and global scale through its interaction with the North Atlantic overturning circulation. Currently, we are seeing the impacts of climate change more acutely within the Arctic. Already we are observing a decrease in both the extent and thickness of perennial and seasonal sea-ice (Comiso *et al.*, 2007; Stroeve *et al.*, 2007); the Greenland Ice Sheet shows increased melting at its periphery (Krabill *et al.*, 2004; Chen *et al.*, 2006; Luthcke *et al.*, 2006), river discharge into the Arctic Ocean from Eurasian and Canadian rivers has been increasing (Peterson *et al.*, 2002; Déry and Wood, 2005; Déry *et al.*, 2009; Shiklomanov and Lammers, 2009); the extent of the permafrost has been moving northwards and active layer has deepened (Kwong and Gan, 1994; Jorgenson *et al.*, 2001; Serreze *et al.*, 2003; Zhang *et al.*, 2005). These changes will impact the Arctic Ocean hydrological cycle. With this in mind, our aim was to further understand the natural variability of the Arctic Ocean freshwater content, particularly the low-frequency mechanism controlling it.

In Chapter 3 of this thesis, we identified an intrinsic mode of variability and its driving mechanism of the Arctic Ocean freshwater content. This mechanism was driven by a series of oceanic processes that regulate the heat and saline fluxes reaching the Arctic Ocean, via the Barents and Kara Seas, in the form of the North Atlantic Current.

However, this control simulation was performed with fixed preindustrial forcings and therefore we can question to what extent this driving mechanism of low-frequency Arctic Ocean freshwater content variability would be affected by transient Holocene forcings, which would capture a more realistic scenario. This was clearly highlighted in Chapter 3 as our simulation failed to fully capture the relationship between the total Fram Strait freshwater export (ice and liquid volumes) and the Nordic Seas overturning circulation, which given our understanding of the Arctic Ocean hydrological cycle, one would expect.

Therefore, in this paper we have performed a Holocene simulation with transient forcings that closely capture reality. Transient forcings are known to impart important impacts on the background Arctic climate during the Holocene. In particular, the long-term decrease in summer insolation at 60°N, associated with the orbital forcing, is known to have caused a long-term cooling in the Arctic. Therefore, this simulation allows us to fully capture and explain the driving mechanisms behind the Arctic Ocean freshwater content.

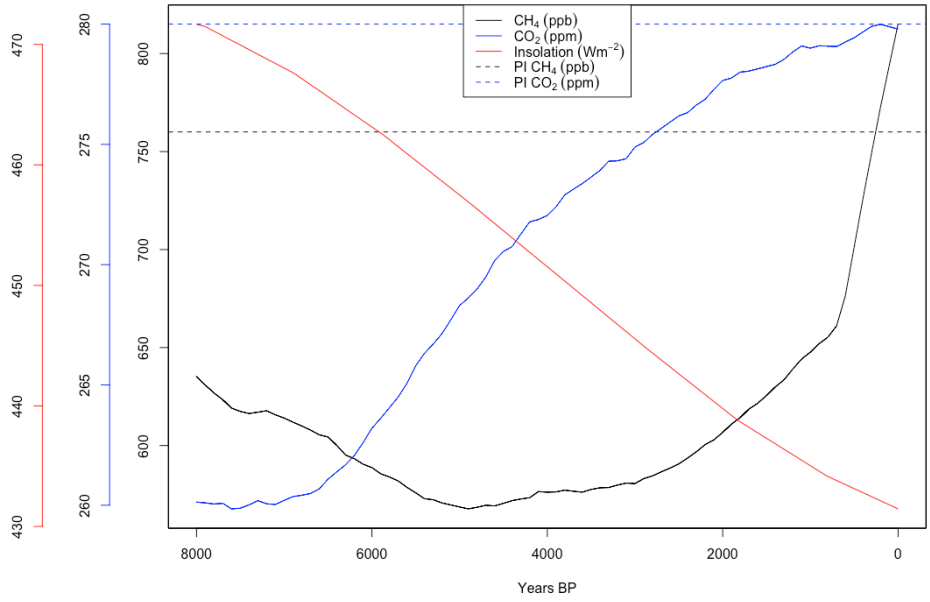

Fig.4.1. The forcings used in the transient simulation (solid lines) showed against the Pre-Industrial (PI) forcings (dashed lines) used in the control simulation of our previous paper (Chapter 3 of this thesis). Summer (JJA) insolation is provided for 65°N (Berger, 1978).

4.2. Model Description and Experimental Design

In this study we have applied LOVECLIM (Version 1.2), an Earth system model of intermediate complexity (Goosse *et al.*, 2010). It has a fully coupled, dynamically enabled atmosphere, ocean, sea-ice, land and vegetation components. The model does

have the option of dynamic ice-sheets, however in this study they were fixed and prescribed to modern day conditions. For a full description of the model please see Goosse *et al.* (2010). LOVECLIM has been shown to simulate modern day climate with a reasonable accuracy (Goosse *et al.*, 2010), in addition it has also been used in a variety of studies covering different temporal and spatial extents. A full description of these is given in Chapter 3 of this thesis.

In this study a 8000-yearlong Holocene transient simulation (from 8ka to 0ka) was performed. This was forced with appropriate orbital parameter settings (Berger, 1978) and greenhouse gas concentrations, thereby following the PMIP3 protocol, (Loulergue *et al.*, 2008; Schilt *et al.*, 2010) (Fig.4.1), whilst the solar, volcanic forcings and icesheets were fixed at preindustrial conditions. The simulation was initiated from a 2500-year long control simulation to allow the model, particularly the deep oceans, to reach a quasi-equilibrium state.

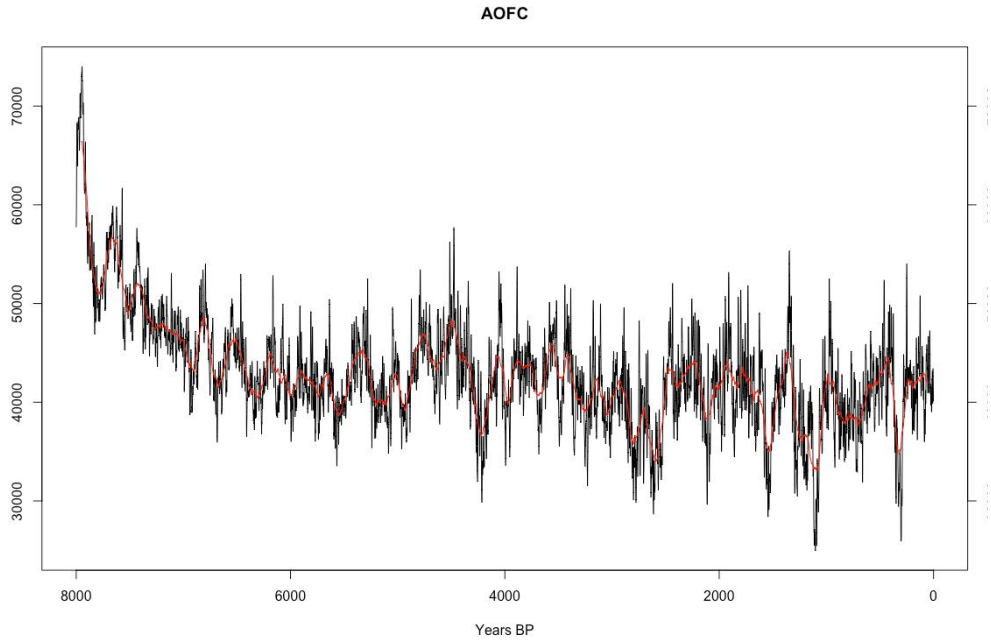

Fig.4.2. a) The annual Arctic Ocean freshwater content (AFOC) time series, both unfiltered (black line) and filtered with a 101-year moving average (red-line).

4.3. Statistical analysis of the Arctic Ocean freshwater content

The simulated 8000-year timeseries of the annual-mean Arctic Ocean freshwater content shows a clear multicentennial variability (Fig.4.2). Here we can see the raw and the smoothed data (101-year smoothing). Spectral analysis of the raw data spectrum reveals (Fig.4.3) one significant peak above the 95% significance level peak at ~220 years.

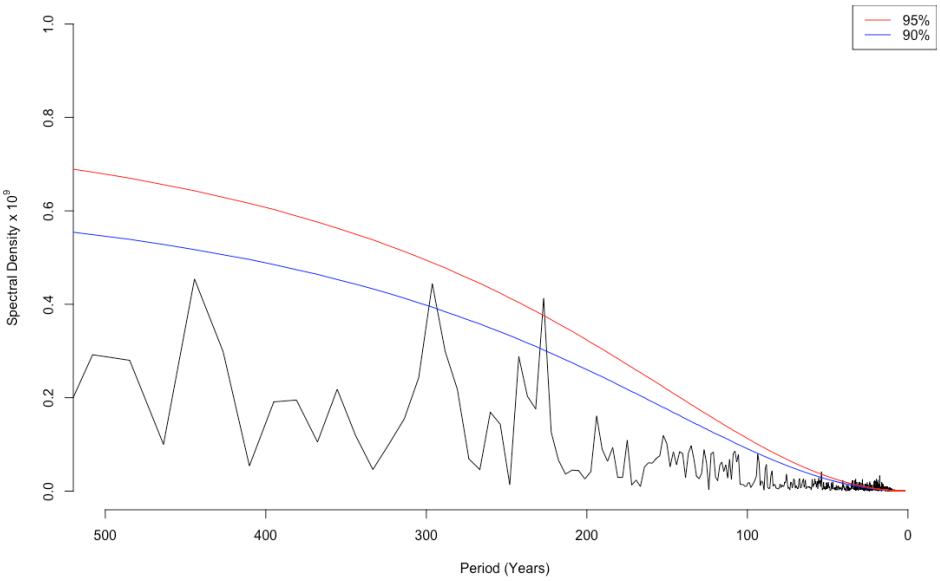

Fig.4.3. Lomb periodogram of the annual Arctic Ocean freshwater content unfiltered time-series with both 90% (blue line) and 95% (red line) significance levels.

Table. 4.1. Sampled statistics of the different time series variables. Arctic Ocean freshwater content (AOFC); Nordic Seas overturning strength (NSOS); Fram Strait liquid volumes export (FS_v); North Atlantic Current (NAC); Fram Strait ice freshwater volume (FS_i); and East-Siberian shelf sea-ice thickness (ESS). I performed the tests of the data from 500-7500 years of the dataset. I performed a qqplot on each variable and after transformation, the dataset did not change indicating it was ok to use the raw data in these tests.

Var 1	Var 2	Filter (years)	t-stat (95%)	df	p-value (95%)	Tabulated t-stat (97.5%)	Correlation at maximum lag (95%)	Maximum lag (years)	Lag Range (years)
NSOS	NAC	11	156	1088	<2.2e-16	1.96	0.51	6	5 to 7
NSOS	FS_V	11	2833	1053	<2.2e-16	1.96	-0.51	-4	-5 to -3
NSOS	FS_I	11	472	521	<2.2e-16	1.96	-0.25	199	197 to 200
AOFC	NSOS	11	849	348	<2.2e-16	1.97	0.36	78	75 to 81
AOFC	FS_V	11	849	809	<2.2e-16	1.96	0.32	-4	-5 to -3
AOFC	NAC	11	849	845	<2.2e-16	1.96	-0.3	6	5 to 6
AOFC	FS_I	11	868	273	<2.2e-16	1.96	-0.6	6	5 to 7
NAC	ESS	11	201	823	<2.2e-16	1.96	-0.2	-1	-2 to -1

As in Chapter 3, we performed a series of cross-correlation analyses with the following variables (Table 4.1): the Arctic Ocean freshwater content (AOFC); the Nordic Seas overturning strength (NSOS); Fram Strait ice freshwater volume export (FS_I); North Atlantic Current (NAC); Fram Strait liquid volume export (FS_V); and East-Siberian Shelf sea-ice thickness (ESS), and it is these pairs of variables that form the basis of our analysis and allow direct comparison with Chapter 3. To achieve a significantly robust result, prior

to performing the cross-correlations, a quantile-quantile plot was produced from each of the raw datasets. These tests revealed that transforming the data was not necessary and thus we could work directly with the raw data. As a further step, to make sure there was no trend within each timeseries, we also removed the first and last 500 years of each timeseries and performed all the cross-correlations on the data from 7.5ka to 0.5ka. The composite plots used in the analysis for the $AOFC_{MAX}$ and $AOFC_{MIN}$ years were made up of 118 and 190 years respectively, and defined by being +2 (for max) and –2 (for min) standard deviations from the mean.

4.4. Results and discussion

4.4.1 Similarities with the previous study

When comparing the results of the transient simulation with those of the pre-industrial control run (Chapter 3 of this thesis), we see many similarities from a dynamical and a statistical point of view. Firstly, the statistical relationship between the following pairs of variables are the same: the Nordic Seas overturning strength and the North Atlantic Current; the Nordic Seas overturning strength and the Fram Strait liquid volume export; The Arctic Ocean freshwater content and the Nordic Seas overturning strength; The Arctic Ocean freshwater content and the Fram Strait liquid volume export; The Arctic Ocean freshwater content and the North Atlantic Current; The Arctic Ocean freshwater content and the Fram Strait ice freshwater volume export; The North Atlantic Current and East-Siberian Shelf sea-ice thickness. The correlation at maximum lag, the maximum lag in years, and the range of the lag in years are all extremely similar between the simulations (Table 4.1).

Table 4.2. Sampled statistics of the different time series variables for both the preindustrial control (Chapter 3 of this thesis) and transient simulations. Arctic Ocean freshwater content (AOFC); Nordic Seas overturning strength (NSOS); Fram Strait liquid volumes export (FS_v); North Atlantic Current (NAC); Fram Strait ice freshwater volume (FS_i); and East-Siberian shelf sea-ice thickness (ESS).

			Control			Transient		
Var 1	Var 2	Filter (years)	Correlation at maximum lag (95%)	Maximum lag (years)	Lag Range (years)	Correlation at maximum lag (95%)	Maximum lag (years)	Lag Range (years)
NSOS	NAC	11	0.52	6	5 to 7	0.51	6	5 to 7
NSOS	FS_V	11	-0.58	-4	-5 to -3	-0.51	-4	-5 to -3
NSOS	FS_I	11	0.2	6	5 to 7	-0.25	199	197 to 200
AOFC	NSOS	11	0.48	74	69 to 85	0.36	78	75 to 81
AOFC	FS_V	11	0.39	-3	-4 to -2	0.32	-4	-5 to -3
AOFC	NAC	11	-0.42	6	5 to 7	-0.3	6	5 to 6
AOFC	FS_I	11	-0.25	6	5 to 7	-0.6	6	5 to 7
NAC	ESS	11	-0.2	-3	-3 to -2	-0.2	-1	-2 to -1

4.4.2 Differences with the previous study

The main difference between the simulations occurs in the relationship between the Nordic Seas overturning strength and the Fram Strait ice freshwater volume export

(Table 4.2). In the pre-industrial control simulation this pair of variables show a correlation of 0.2 with the Nordic Seas overturning strength lagging the Fram Strait ice freshwater volume export by 6 years. However, in the transient Holocene simulation this pair of variables show a correlation of -0.25 with the Nordic Seas overturning strength lagging the Fram Strait ice freshwater volume export by 199 years, implying the response of increased ice flow from the Arctic Ocean to the North Atlantic, via the Fram Strait, reduces the strength of the Nordic Seas overturning strength.

This difference in the Fram Strait ice freshwater volume export is linked to the change in East-Siberian shelf sea-ice volume, which in our transient simulation, doubles over the course of the Holocene (Fig.4.4) and is due in part to the surface cooling that occurs in the Arctic during the 8000-year simulation (Fig.4.5), which itself is driven by the decreasing summer insolation in the Arctic over the same period (Fig.4.1). But the main takeaway from the analysis of the ocean variables is that more sea-ice, in the form of ice originating from the East-Siberian shelf, leads to a greater export of sea-ice through the Fram-Strait, and thus leads to a greater interaction between the Nordic Seas overturning strength and the Fram Strait ice freshwater volume export, than we saw in the simulation with fixed preindustrial forcings.

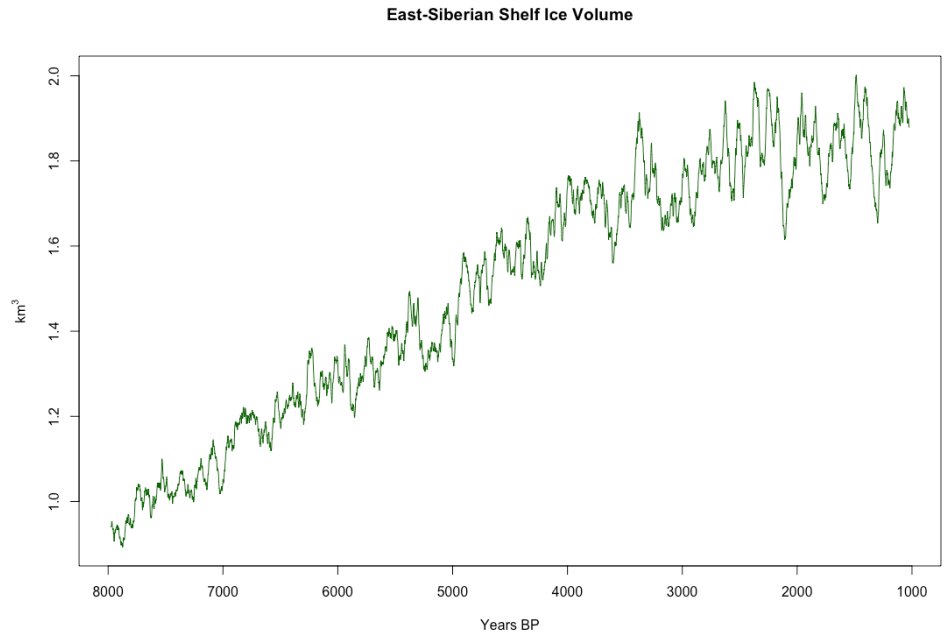

Fig.4.4. Time series (51-year running mean) of the simulated East-Siberian Shelf sea-ice thickness (ESS) (green line) over the course of the simulation.

4.4.3 Implications of results

The mechanism controlling the Arctic Ocean freshwater content in the Arctic that was first discussed in Chapter 3 is shown to be robust and is also present in our transient Holocene simulation. Beginning with the Nordic Seas overturning strength, the strength of which determines the amount of heat and salinity that is delivered to the Arctic Ocean via the Barents and Kara Seas, it is observed to lag the North Atlantic Current by 5 to 7 years (Fig.4.6). Meaning that as the strength of the Nordic Seas overturning strength decreases the strength of the North Atlantic Current also decreases. This also leads to a decrease of heat and saline waters flowing northwards and entering the Arctic via the Barents and Kara Seas to Arctic Ocean. Therefore, heat and saline being delivered to the Arctic Ocean is reduced and the freshwater content of the Arctic Ocean increases. A direct result of this is lower temperatures across the Barents Sea, which are positively correlated with the Arctic Ocean freshwater content but with a lagged response of 109 to 114 years (Fig.4.7). The main driver of the multicentennial variability we observe is the relationship between the Arctic Ocean freshwater content and the Nordic Seas overturning strength, which has a peak correlation occurring between 75 to 81 years (Fig.4.8). As a result of the increased Arctic Ocean freshwater content, the export of liquid freshwater via the Fram Strait increases, lagging the response of the Arctic Ocean freshwater content by 2 to 4 years (Fig.4.9). This export of liquid freshwater via the Fram Strait acts to keep the Nordic Seas overturning strength reduced during the phase of an elevated Arctic Ocean freshwater content. The coupled effect of a freshening, cooling Arctic Ocean, due to a weakened North Atlantic Current and the subsequent reduction of warm, saline waters flowing northwards, alters the high-northern latitude environment. A consequence of this is that throughout our transient simulation we observe an increase in sea-ice thickness across the Arctic Ocean (Fig.4.10a) and specifically the East-Siberian Shelf (Fig.4.10b), which is being driven by the longer-term orbital climate drivers. This is different to what we observed in Chapter 3 of this thesis.

In Chapter 3 of this thesis, we observed the role of reduced heat transport to the Arctic Ocean, which enables the waters of the Arctic Ocean to stratify easier, thus resulting in the less dense, cooler freshwater layers forming in the top layer of the ocean, which subsequent provide an increased cooling effect to the Arctic environment. The increased volume of freshwater in the Arctic Ocean not only leads to an increase in the amount of freshwater stored in the Arctic Ocean basin itself, but also in the amount being converted to a freshwater store of sea-ice. Over time we observe the proportion of freshwater that is stored in the Arctic as sea-ice becomes more significant, leading to a decrease in freshwater export via the Fram Strait, resulting in the salinity of the Nordic Seas to increase again, strengthening the Nordic Seas overturning strength.

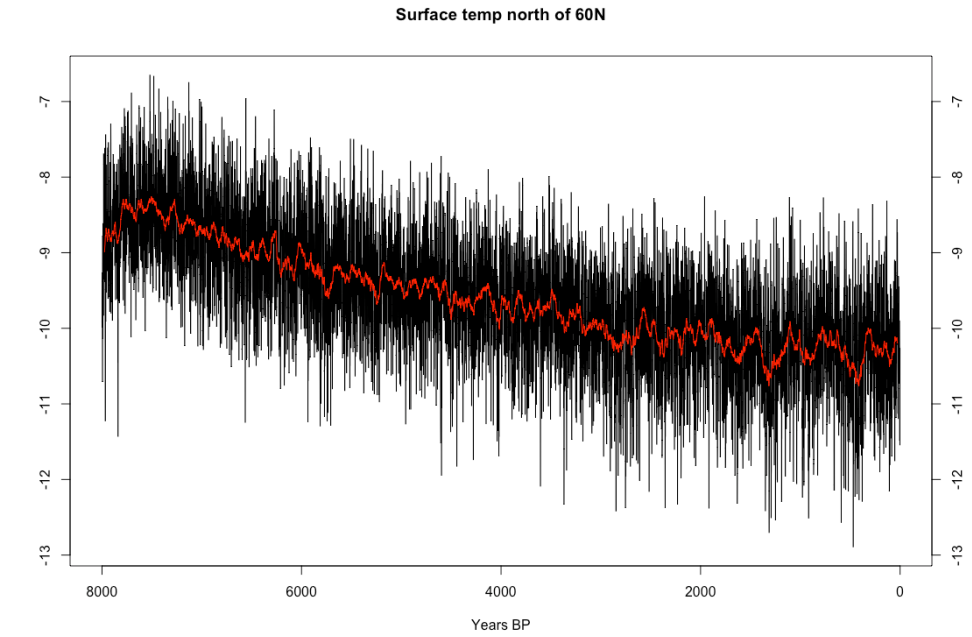

Fig.4.5. The mean annual surface temperature in the Arctic (defined north of 60°N) over the past 8000 years (black line) and filtered with a 51-year moving average (red-line).

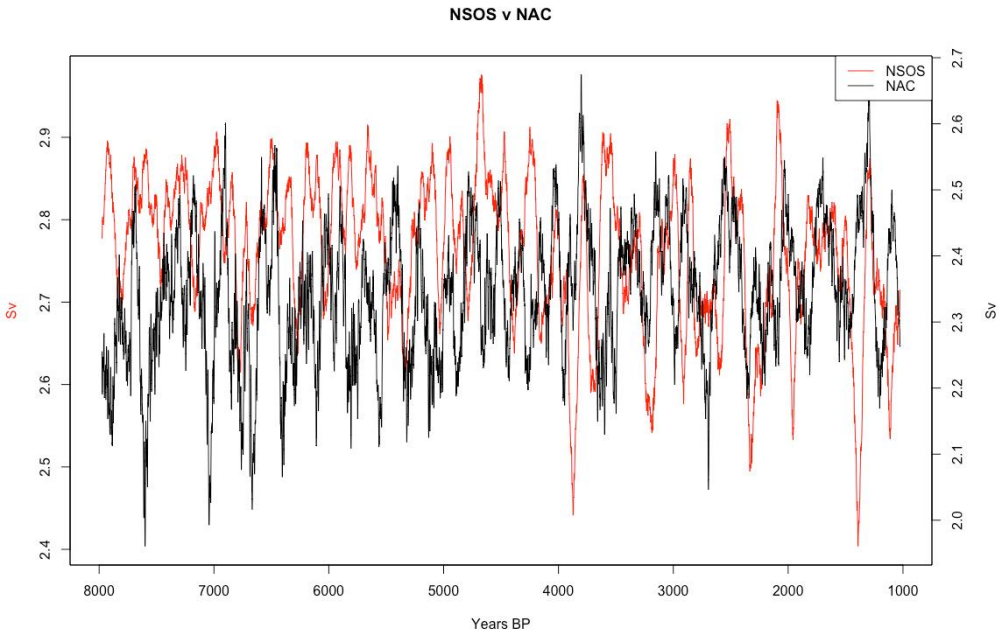

Fig.4.6. Time series (51-year running mean) of the simulated Nordic Seas overturning strength (NSOS) (red line) v North Atlantic Current (NAC) (black line).

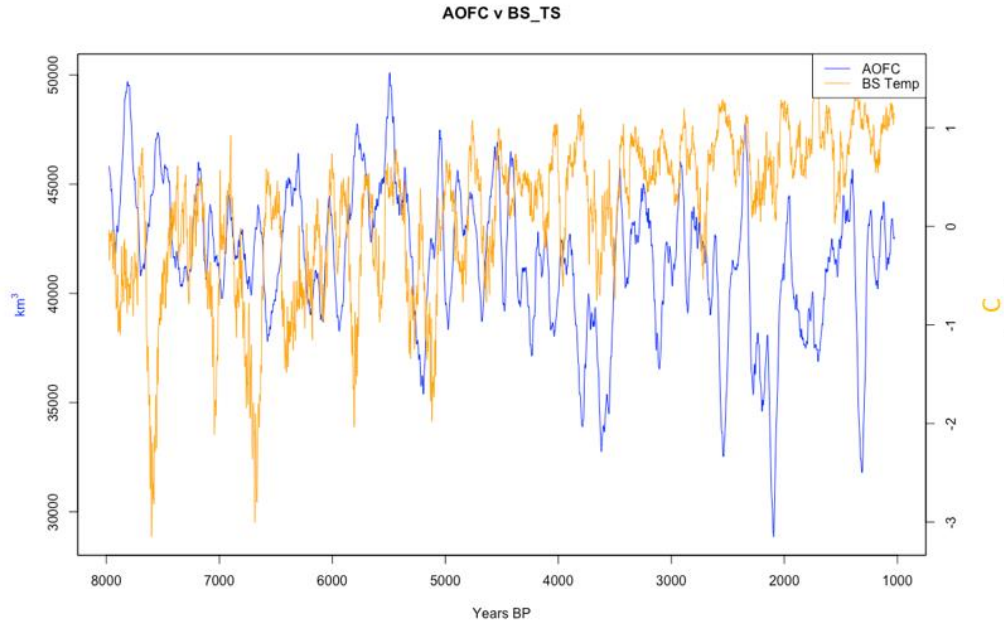

Fig.4.7. Time series (51-year running mean) of the simulated Arctic Ocean freshwater content (AOFC) (blue line) v Barents Sea surface temperature (orange line).

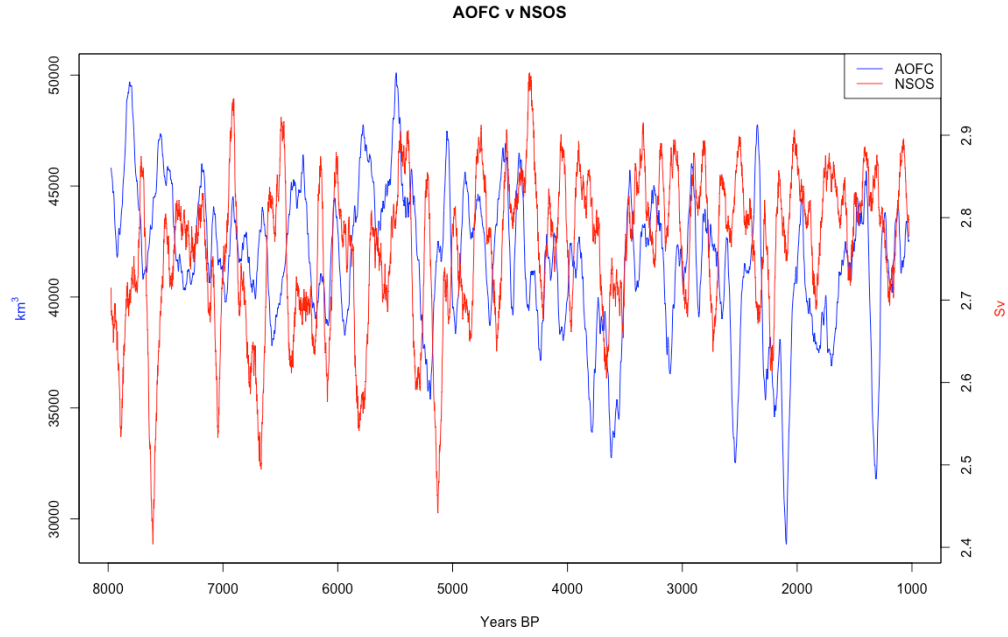

Fig.4.8. Time series (51-year running mean) of the simulated Arctic Ocean freshwater content (AOFC) (blue line) v Nordic Seas overturning strength (NSOS) (red line).

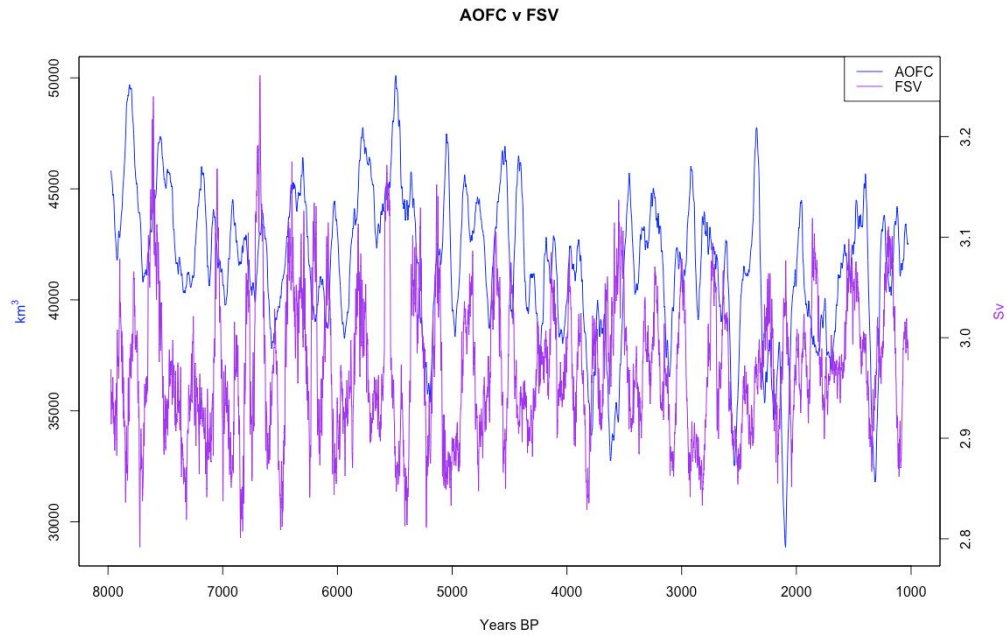

Fig.4.9. Time series (51-year running mean) of the simulated Arctic Ocean freshwater content (AOFC) (blue line) v the Fram Strait liquid volume export FS_V (purple line).

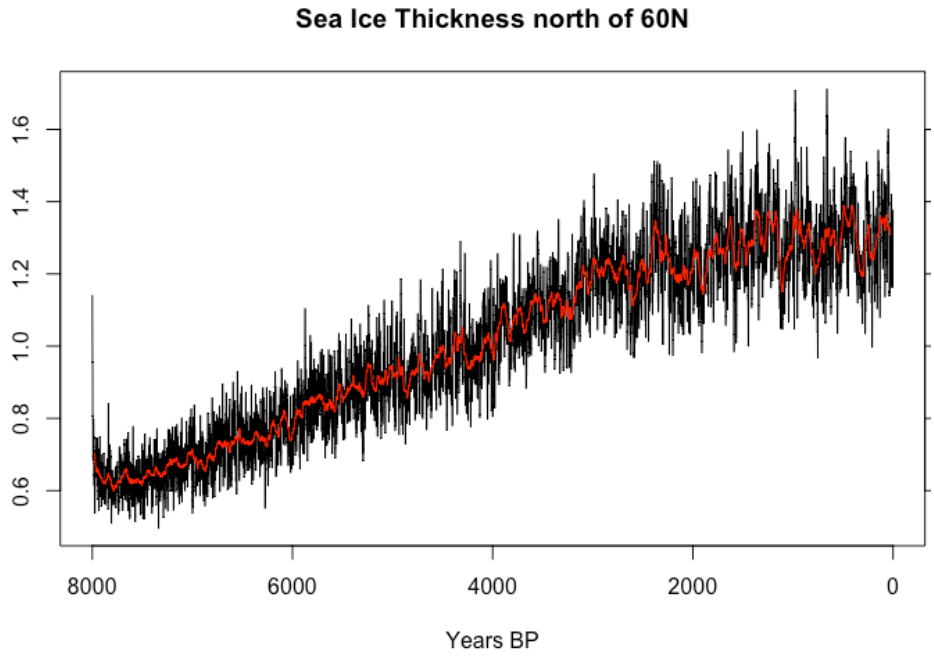

Fig.4.10a. Sea-ice thickness in the Arctic (defined north of 60°N) over the past 8000 years (black line) and filtered with a 51-year moving average (red line).

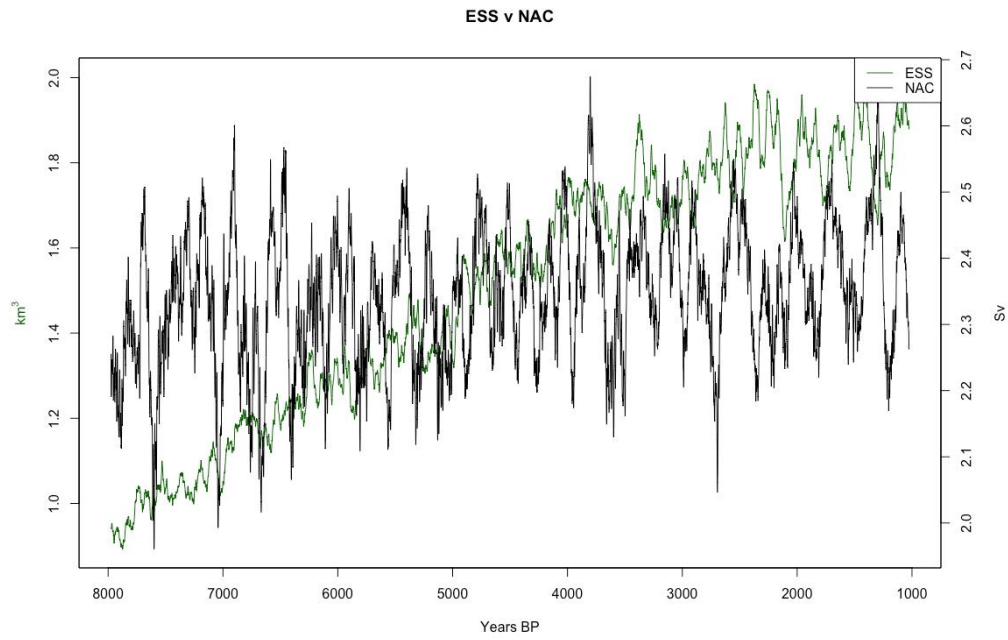

Fig.4.10b. Time series (51-year running mean) of the simulated East-Siberian Shelf sea-ice thickness (ESS) (green line) v North Atlantic Current NAC (black line).

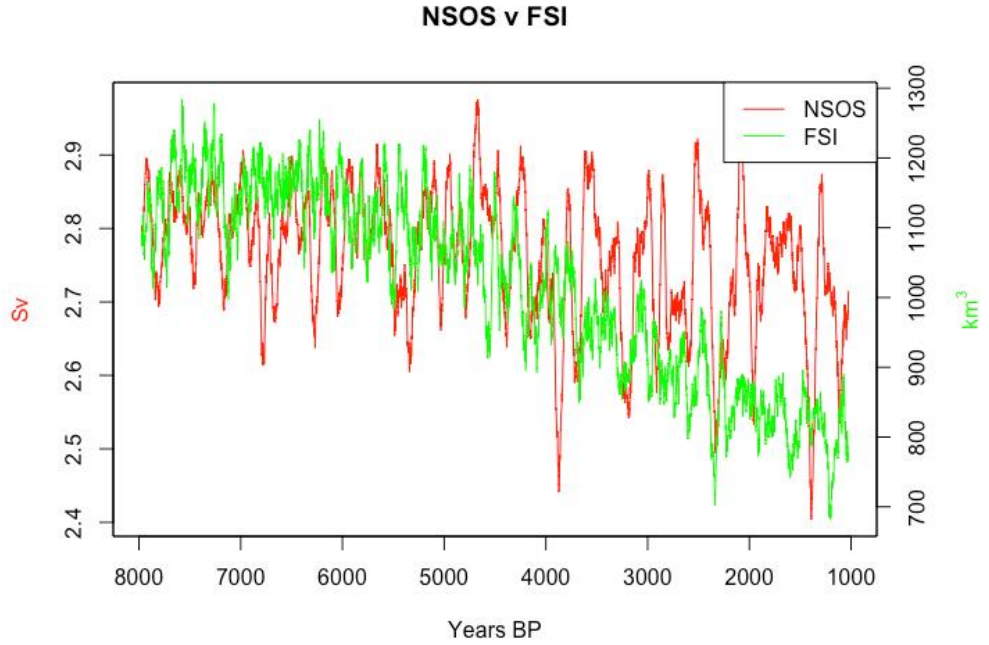

Fig.4.11. Time series (51-year running mean) of the simulated Nordic Seas overturning strength (NSOS) (red line) v the Fram Strait ice freshwater volume export FS_I (green line).

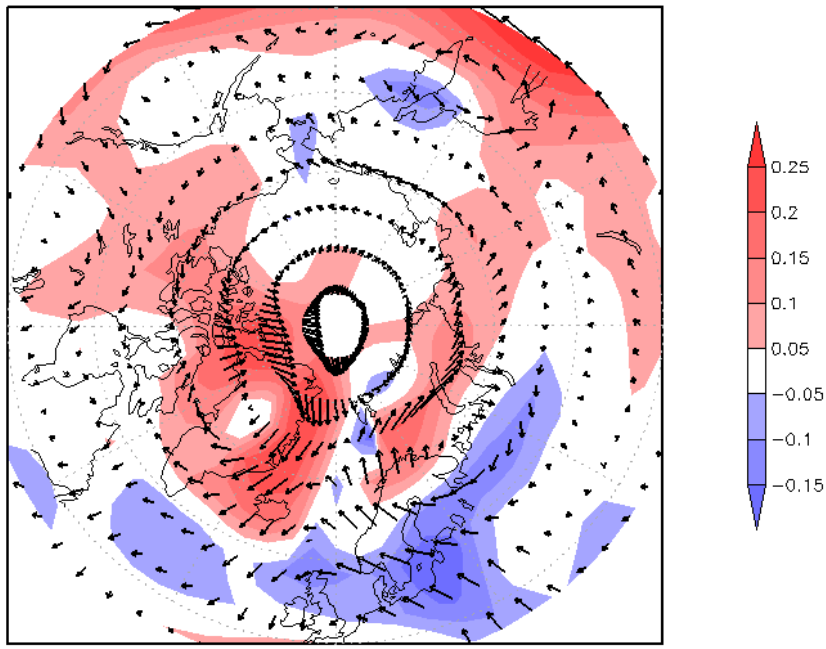

Fig.4.12. Composite anomaly plot of surface winds (vectors, see arrow in ms^{-1} for scale) of 118 MAX and 190 MIN years (max and min defined by + and – 2 standard deviations from the mean, respectively). Background colours relate to the magnitude of the wind between $AOFC_{MAX}$ and $AOFC_{MIN}$.

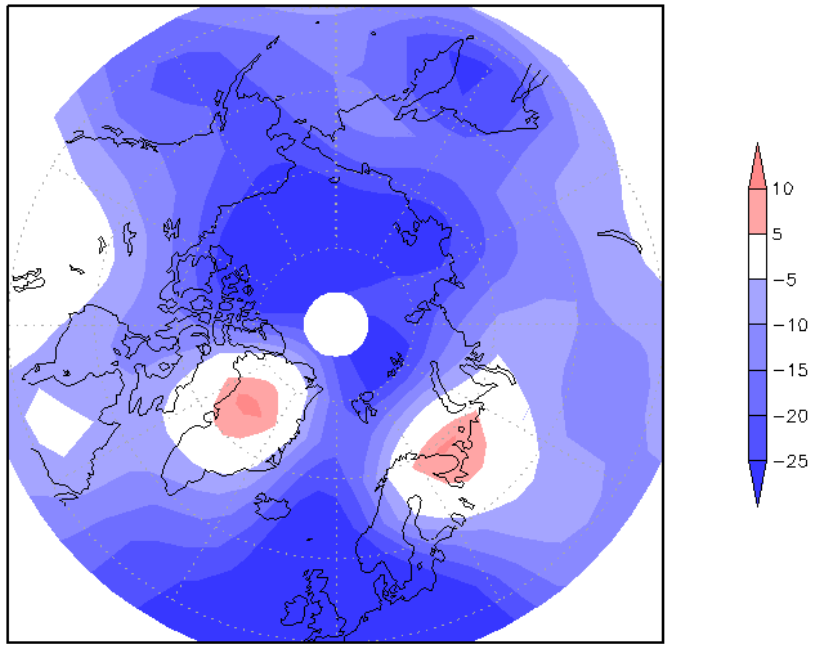

Fig.4.13. Composite anomaly plot of the 800hPa height (m) of 118 MAX and 190 MIN years (max and min defined by + and – 2 standard deviations from the mean, respectively).

In Chapter 3 of this thesis we discussed the control simulation where we explained that we expected the export of sea-ice from the Arctic Ocean via the Fram Strait to the Nordic Seas, would play an important role in supressing the Nordic Seas overturning strength during the freshening phase of the Arctic Ocean. However, whilst we did see large exports of sea-ice from the Arctic Ocean to the Nordic Seas, via the Fram Strait, these did not correlate with an expected response of the Nordic Seas overturning strength. Statistical analysis did not provide us with any further insights as the correlation was poor and not significant. However, in the transient Holocene simulation we see a different relationship between the Nordic Seas overturning strength and the Fram Strait ice freshwater volume export (Fig.4.11). Starting with Table 4.1, we can see that the Arctic Ocean freshwater content lags the Fram Strait ice freshwater volume export by 6 years and is inversely correlated (-0.6), suggesting that a decrease in ice export via the Fram Strait happens first, followed by an increase in the Arctic Ocean freshwater content. Eventually, the Arctic Ocean freshwater content reaches a maximum state, followed by increased winds through the Fram Strait (Fig.4.12), being driven by increased ridging over Greenland (Fig.4.13). This aids the export of ice through the Fram Strait, leading to an eventual reduction of the Arctic Ocean freshwater content via the feedback mechanism with the Nordic Seas overturning strength (at a lag of 199 years). It is a relatively slow mechanism and looking at Fig.4.11, it can been seen that in the Fram Strait ice freshwater volume export time series that for each 200-year block of progression through the simulation, the actual volumes of the Fram Strait ice freshwater volume export do not dramatically change, rather they are incrementally decreasing throughout the Holocene.

This observation provides us with a more plausible explanation for the final part of the mechanism, which we were unable to fully explain in the pre-industrial simulation. The increase in liquid freshwater export through the Fram Strait was previously used as an explanation for partly reducing the volume of the Arctic Ocean freshwater content, when a point was reached where the liquid freshwater export exceeded that of the freshening effect of reduced inflow of relatively saline waters associated with a weakening Nordic Seas overturning strength. However, it is clearer from this transient simulation that the sea-ice export from the Arctic Ocean to the Nordic Seas and the site of overturning, does plays an important role in driving multicentennial Arctic Ocean freshwater content variability.

Following this, when the Arctic Ocean freshwater content is reduced beyond a critical point, liquid export decreases. This leads to an increase in salinity in the Nordic Seas and a strengthening of the Nordic Seas overturning strength. As the Nordic Seas overturning strength increases, the volume of warm, saline waters transported to the Arctic Ocean, in the form of the North Atlantic Current via the Barents and Kara Seas increases. This reduces the Arctic Ocean freshwater content and the subsequent export of freshwater from the Arctic Ocean, to the Nordic Seas via the Fram Strait and thus helps keep the Nordic Seas overturning strength strong. Additionally, with an increase of warmer waters reaching the Arctic Ocean, temperatures begin to rise, sea-ice begins to melt and thin, and the freshwater stored in the form of sea-ice is remobilised. Thus, the

proportion of freshwater stored as sea-ice decreases, the amount stored as freshwater export via the Fram Strait begins to increase again, which acts to suppress the Nordic Seas Overturning Strength, completing the full cycle.

While we have a credible explanation for the mechanism driving of Arctic Ocean freshwater content variability through the Holocene, it is important to see how this compares to palaeoclimatic studies. However, palaeoclimatic records of Arctic Ocean freshwater content are not common. Despite this we have been able to find a study that allows some comparison between our results and those from the palaeorecord.

In assessing the variability of SST in the Norwegian Sea, particularly on the Vøring Plateau off the west coast of Norway in the later part of the Holocene, Miettinen *et al.* (2012) found a series of prominent periodicities. Reconstructing August Sea-surface temperatures (SST) using diatoms from a marine core they found a significant spectral peak at 249 years, similar to the cycle we find for our mechanism (220 years). Whilst we did not explicitly look at August SST in the Norwegian Sea, we did look at the SST in the Barents Sea. Given that the North Atlantic Current flows directly into the Barents Sea it is fair to assume that temperature changes in the Vøring Plateau are synonymous with those in the Barents Sea. In their paper, Miettinen *et al.* (2012) accredited the driver of this variability to the AMOC, driven by the Holocene insolation variability. However, our results show that SST variability in the North Atlantic Current could form part of the Arctic Ocean freshwater content variability mechanism described in our paper.

Of the modelling studies that have been conducted on this topic, they tend to focus on the change in freshwater variability between recent times and the 21st century. In such a study, Koenigk *et al.* (2007), whilst analysing the freshwater balance of the Arctic Ocean during the 21st century, found that during the 21st century the enhanced warming of the Arctic region led to an almost complete removal of sea-ice during summer, along with an increase of net precipitation and river runoff. They explain that this leads to an increase in freshwater storage in the Arctic Ocean, whilst the export of freshwater from the Arctic remains unchanged. However, they do see the export of freshwater via the Fram Strait become more dominated by a liquid export, as opposed to sea-ice, as the Arctic Ocean warms up and freshwater storage increases. These results of Koenigk *et al.* (2007) are somewhat comparable to the results presented in our paper as we have demonstrated that during an elevated Arctic Ocean freshwater content, the export of liquid freshwater via the Fram Strait increases, supressing convection in the Nordic Seas, a process also reported by Koenigk *et al.* (2007). The major takeaway from this observation is that the response of the Arctic Ocean freshwater content under different climatic forcings is similar and we would propose that it is possible that what is observed in the Koenigk *et al.* (2007) study could be partly attributable to an intrinsic variability, as demonstrated in this chapter and Chapter 3 of this thesis.

4.5. Conclusion

We have analysed the output of an 8000-year transient Holocene simulation of the LOVECLIM climate model and have demonstrated that within this exists a noticeable

multi-centennial pattern of variability of the Arctic Ocean freshwater content, with a periodicity of ~220 years. This pattern of variability was first observed in a control simulation, with no external forcings, in Chapter 3. However, the control simulation could not fully explain one specific part of the mechanism. This was the interaction of sea-ice export from the Arctic Ocean via the Fram strait, with the Nordic Seas overturning strength. It would be expected that such a relationship would exist, however this was not fully resolved by the control simulation. However, with this transient simulation we see a greater build-up of sea-ice in the Arctic Ocean in the form of the East-Siberian Shelf, which in turns leads to increased volumes of sea-ice export via the Fram Strait, and a greater interaction between this exported sea-ice and the Nordic Seas overturning strength.

The results of this paper and those of our previous paper show that in our model the Arctic Ocean freshwater content possess a low-frequency mode of variability, which is driven by the transport of heat and saline waters to the high-northern latitudes. These results reaffirm our findings from our previous paper, which highlights the need for low-frequency mechanisms to be incorporated into current discussions of climatic variability.

"We shall stick it out to the end, but we are getting weaker of course and the end cannot be far. It seems a pity, but I do not think I can write more. For God's sake, look after our people"

Robert Falcon Scott

Chapter 5: The impact of Sahara desertification on Arctic cooling during the Holocene

Published as: Davies FJ, Renssen H, Blaschek M, Muschitiello F (2015) The Impact of Sahara desertification on Arctic cooling during the Holocene. Clim. Past 11: 571-586. https://doi.org/10.5194/cp-11-571-2015

Abstract

Since the start of the Holocene, temperatures in the Arctic have steadily declined. This has been accredited to the orbitally forced decrease in summer insolation reconstructed over the same period. However, here we present climate modelling results from an Earth model of intermediate complexity (EMIC) that indicate that 17-40 % of the cooling in the Arctic, over the period 9-0 ka, was a direct result of the desertification that occurred in the Sahara after the termination of the African Humid Period. We have performed a suite of sensitivity experiments to analyse the impact of different combinations of forcings, including various vegetation covers in the Sahara. Our simulations suggest that over the course of the Holocene, a strong increase in surface albedo in the Sahara as a result of desertification led to a regional increase in surface pressure, a weakening of the trade winds, the westerlies and the polar easterlies, which in turn reduced the meridional heat transported by the atmosphere to the Arctic. We conclude that during interglacials, the climate of the Northern Hemisphere is sensitive to changes in Sahara vegetation type.

5.1 Introduction

The Holocene is characterized by an early thermal maximum (~ 11-6ka) in the Northern Hemisphere, followed by gradually declining global temperatures that persisted up until the recent period of anthropogenically induced warming. This cooling was most prevalent in the high northern latitudes with July temperatures, north of 60°N, decreasing by 3-4°C from 9 to 0 ka (Renssen *et al.*, 2005), which is attributable to the orbitally forced reduction in summer insolation (Renssen *et al.*, 2005, 2009) which, at 65°N, decreased by 42 Wm^{-2} over the same period (Berger, 1978). The early Holocene positive summer insolation anomaly (declining by 36 Wm^{-2} at 30°N from 9 to 0 ka) also had a strong impact on the vegetation in northern Africa through a strengthening of the summer monsoons, leading to enhanced precipitation and grassland vegetation in the Sahara region (Kutzbach and Street-Perrott, 1985). This phase is often referred to as the African Humid Period (AHP), which lasted until the mid-Holocene, although the exact timing of its demise and the subsequent rate at which it occurred is still a contentious issue (deMenocal *et al.*, 2000; Kröpelin *et al.*, 2008). Following the AHP, the Sahara, under the influence of the long-term decline in summer insolation, evolved into a desert environment.

The termination of the AHP and the associated vegetation–climate interactions have been studied in numerous climate model studies (Claussen *et al.*, 1999; Renssen *et al.*, 2003; Liu *et al.*, 2006; Notaro *et al.*, 2008; Timm *et al.*, 2010). However, these

simulations were mostly focused on the regional climate effects in northern Africa, implying that the impact of the Saharan desertification on the global climate has not yet been addressed in model studies. It is important to realise that the Sahara covers a large area (approximately 9.4×10^6 km^2), making it plausible that changes in its surface albedo, caused by the large-scale shift in vegetation during the Holocene, could have profound effects on global climate. For instance, previous studies have shown that drastic vegetation changes in the Amazon can influence winter precipitation in the North Atlantic and Europe, which are brought about by large-scale circulation changes in the mid- and high latitudes (Gedney and Valdes, 2000). Accordingly, in this study, we have designed a series of experiments to assess the first-order impact of long-term radiative forcing of the Sahara during the Holocene. This involved performing a large suite of equilibrium simulations using LOVECLIM, an Earth model of intermediate complexity (EMIC). Given the large number of simulations performed (29) and the long time integration involved in performing such an array of simulations (equivalent to 83 000 model years of simulation), we feel that this type of model is ideally suited to address such an issue. Our discussion focuses on how Sahara vegetation changes during the Holocene have contributed to cooling in the Arctic (defined herein as north of 66.5°N).

5.2 Model and experimental design

5.2.1 Model

We applied LOVECLIM, an Earth model of intermediate complexity (Goosse *et al.*, 2010), which is comprised of a coupled atmosphere, ocean, sea-ice and vegetation model. The atmospheric component (ECBilt) is a quasi-geostrophic model of the atmosphere with a horizontal T21 truncation and three vertical layers, 800, 500 and 200 hPa (Opsteegh *et al.*, 1998) and includes a full hydrological cycle. Clouds are prescribed based on the ISCCP D2 data set (1983 to 1995) from Rossow (1996), with the total upward and downward radiative fluxes computed as a function of this data set (Schaeffer *et al.*, 1998; Goosse *et al.*, 2010). Clouds and precipitation are decoupled from one another within the model, with the precipitation dependent on the total precipitable water content between the surface and 500 hPa, which is a prognostic variable within the model (Goosse *et al.*, 2010). This variable is transported horizontally using a fraction (60 %) of the sum of the geostrophic and ageostrophic winds at 800 hPa to account for the fact that humidity is generally higher closer to the surface, where wind speeds are lower. Above 500 hPa, it is assumed that the atmosphere is completely dry, and thus, all water above this level is converted to precipitable water. Precipitation also occurs below 500 hPa, if the total precipitable water passes a threshold. This threshold is defined by 0.83 times the vertically integrated saturated specific humidity, assuming constant relative humidity within the layer (Goosse *et al.*, 2010).

The oceanic component (CLIO) is a primitive-equation, free-surface general ocean circulation model (Deleersnijder and Campin, 1995; Deleersnijder *et al.*, 1997) coupled to a thermodynamic-dynamic sea-ice model (Fichefet and Morales Maqueda,

1997, 1999), and has a resolution of 3°x 3° latitude–longitude and realistic bathymetry. The vegetation component (VECODE) is a reduced-form dynamic global vegetation model and is capable of simulating the dynamics of two plant functional types, trees and grasses, as well as desert as a dummy type (Brovkin *et al.*, 2002). These vegetation types have an effect on the surface albedo, soil moisture content and net precipitation.

LOVECLIM simulates a modern climate that is in reasonable agreement with observations, including large-scale distributions of temperature and precipitation, and sea-ice cover in both hemispheres (Goosse *et al.*, 2010). It has a climate sensitivity to a doubling of the atmospheric CO_2 level of 1.9°C, which is in the lower end of the range reported for general circulation models (GCMs) (Flato *et al.*, 2013). It has successfully been applied to simulate various past climates, including the last millennium (Goosse *et al.*, 2005), the last glacial maximum (LGM) (Roche *et al.*, 2007), the Holocene (Renssen *et al.*, 2009), the 8.2 ka event (Wiersma and Renssen, 2006), and the last interglacial (Bakker *et al.*, 2013). The results of these simulations are consistent with those of comprehensive GCMs (Goosse *et al.*, 2010; Bakker *et al.*, 2013; Nikolova *et al.*, 2013).

5.2.2 Experimental design

In order to calculate the contribution of Sahara desertification to cooling in the Arctic during the Holocene, a series of experiments were designed. The experiments can be broken into two categories. Firstly, we performed a series of transient Holocene simulations (9-0 ka) that allowed us to capture the natural evolution of the Sahara within our model. Secondly, we applied the vegetation fractions of the Sahara at 9, 6 and 0 ka from the transient simulations in a series of equilibrium experiments. Further details of each suite of experiments are given below.

5.2.2.1 Defining the Sahara

An initial transient simulation from 9 to 0 ka was performed, forced with appropriate orbital parameter settings (Berger, 1978) and greenhouse gas concentrations (Loulergue *et al.*, 2008; Schilt *et al.*, 2010), whilst the solar and volcanic forcings were fixed at pre-industrial levels. This simulation is referred to as OG. In addition, another simulation, which included the same forcings as OG, plus additional Laurentide (LIS) and Greenland (GIS) Ice Sheet meltwater fluxes and topography changes, was performed. This simulation is referred to as OGGIS. The LIS meltwater fluxes were based on the reconstructions of Licciardi *et al.* (1999), and those for the GIS on Blaschek and Renssen (2013). The associated topographic and surface albedo changes of the LIS were based on reconstructions by Peltier (2004) and applied at 50-year time steps. However, GIS topographic changes were not accounted for because the changes are only minor at the spatial resolution of our model. For a more detailed description of the experimental setup of OGGIS, the reader is referred to Blaschek and Renssen (2013). In both OG and OGGIS, global vegetation changes were calculated interactively using VECODE.

5.2.2.2 Equilibrium simulations

The transient experiments OG and OGGIS provided simulated estimates of the evolution of the Sahara over the Holocene. Using these transient simulations, we could thus define the vegetation composition of the Sahara at 9, 6 and 0 ka under both OG and OGGIS forcings. Following this, a series of 18 equilibrium experiments were designed (see Appendix 5.A) to assess the impacts of the different forcings on the temperature change from 9 to 6, 9 to 0 and 6 to 0 ka (see Appendix 5.B). In these simulations, the relative percentages of Saharan vegetation cover at 9, 6 and 0 ka (see Appendix 5.C for OG vegetation fractions), taken from both the OG and OGGIS simulations, were combined with orbital and trace gas levels for 9, 6 and 0 ka, which followed the guidelines of PMIP3 (http://pmip3.lsce.ipsl.fr/). The name of each experiment reflects the forcings that were used. For example, 0k6kEQ_OG refers to the orbital and greenhouse gas forcings being set to 0 ka levels, vegetation was set to a 6 ka state, EQ indicates that this was an equilibrium simulation, and OG means that vegetation state was derived from the OG simulation. This nomenclature is used throughout the manuscript.

All equilibrium simulations were run for 2500 years, allowing the model, in particular the deep oceans, to reach a quasi-equilibrium state (Renssen *et al.*, 2006). The initial conditions for these simulations were derived from a control experiment with pre-industrial forcings. For the OGGIS equilibrium simulations, LIS and GIS topography were kept constant. However, LIS and GIS melt fluxes were not included, as this would have resulted in continuous freshening of the oceans during the 2500 years of model integration, implying that the simulated climate would not reach a quasi-equilibrium, in particular in the deep oceans. Since our analysis is focused on a comparison of the equilibrium responses to forcings (see Appendix 5.B), such analysis of LIS and GIS melt fluxes would not be particularly meaningful. Although we recognise this as a potential weakness of our 9 ka equilibrium simulations, it must be noted that with an earlier version of LOVECLIM, experiments performed including LIS melt fluxes showed that the impact of these on the Nordic Seas was a modest 0.5∘C cooling between 9 and 8 ka (Blaschek and Renssen, 2013). Therefore, we feel that omitting this potentially important source of freshwater forcing to the high northern latitudes will not adversely affect our results and we are confident that our series of sensitivity experiments are suitable in assessing the first-order impact of radiative forcings on the Holocene climate.

From the OG and OGGIS equilibrium experiments we were able to deduce the contribution of Sahara desertification to Arctic cooling during the Holocene (see Appendix 5.B). Data presented are averages over the last 500 years of each simulation. To investigate an "extreme" example of Sahara desertification between the mid- and late Holocene, we also performed six equilibrium simulations that had 100 % grass and desert in the Sahara at 9, 6 and 0 ka (see Appendix 5.D). In LOVECLIM, the albedo of grass and desert are 0.2 and 0.4, respectively. The Sahara was defined as 15°W-35°E and 11-33°N.

5.3 Results and discussion

We separate our results into several distinct sections. Firstly, we describe the results from our sensitivity experiments (Sect. 5.3.1). Following this we explain the mechanism that is responsible for the reduction in poleward heat transport during the Holocene (Sect. 5.3.2), and the role that sea-ice feedbacks play in the Arctic cooling we simulate (Sect. 5.3.3). We then introduce the results of additional sensitivity experiments (Sect. 5.3.4), which we performed to test the robustness of our initial findings. We follow this with a discussion of the uncertainties of our results (Sect. 5.3.5). To finish, we discuss these findings in the context of the limitations of our model and how these could be overcome in future work (Sect. 5.3.6)

5.3.1 Results

Our results for both the OG and OGGIS equilibrium experiments can be separated into two distinct phases, 9-6 and 6-0 ka (Fig.5.1a and b). In the OG experiment there is a total cooling in the Arctic from 9 to 0 ka of 2.9°C (Figs.5.1a and 5.2a), with 0.7°C occurring between 9 and 6 ka, and 2.1°C between 6 and 0 ka. Of this total cooling, 2.1°C is due to direct orbital and greenhouse gas forcing (Figs.5.1b and 5.2b), whilst 0.5°C (17 %) is due to Sahara desertification alone (Figs.5.1a and 5.2c). The overall decrease in Arctic mean annual temperatures in our OG experiments, from 9 to 0 ka, is consistent with those observed in a transient experiment performed with a previous version of LOVECLIM (Renssen *et al.*, 2005), in which a 1–3°C decrease in mean annual temperatures in the high northern latitudes was observed. In addition, our observed decrease from 6 to 0 ka, essentially the Holocene thermal maximum (HTM) to present day, of 2.1°C, is in line with the proxy-based temperature reconstructions from Greenland ice cores (Dahl-Jensen *et al.*, 1998), in which there is an observed decrease of 2.5°C between the mid-Holocene climate optimum and present day. Our results also lie within the range of proxy-based temperature reconstructions for 16 terrestrial sites from the western Arctic, where it has been shown that temperatures during the Holocene Thermal Maximum (HTM) were on average 1.6 ±0.8°C warmer than 20th century temperatures (Kaufman *et al.*, 2004), which is consistent with proxy-based temperature reconstructions for northern Eurasia (Renssen *et al.*, 2009; Sundqvist *et al.*, 2010).

In our OGGIS transient experiment, the 9 ka climate is relatively cold due to the cooling effect of the LIS topography and albedo, and the GIS albedo, which leads to a delayed thermal maximum over most of the Arctic domain. This delayed onset of the thermal maximum for the early to mid-Holocene has been observed in numerous proxy records (Kaufman *et al.*, 2004) and is consistent with previous experiments performed with LOVECLIM. In particular Renssen *et al.* (2009), who simulated a ~ 1°C increase in mean annual temperatures north of 60° between 9 and 6 ka in a transient experiment that included the same forcings as our 6 and 9 ka OGGIS equilibrium experiments. This delayed response of high-latitude warming is truly representative of our observation of a 1°C increase in mean annual temperature from 9 to 6 ka (Fig.5.1b). The simulated

temperature increase in OGGIS between 9 and 6 ka is also present in temperature reconstructions from lakes in northern Iceland, in which a temperature increase of ~0.75°C was observed (Axford *et al.*, 2007). Additionally, the change in Sahara vegetation had a cooling effect of 0.2°C between 9 and 6 ka and without this moderating effect, the warming would have even been higher (1.3°C).

The second phase, 6-0 ka, of the OGGIS equilibrium experiment was identical to the OG equilibrium experiment, with a total decrease in mean annual Arctic temperature of 2.1°C, with 0.4°C due to desertification in the Sahara and the remainder of the cooling due to the localised effects of insolation changes. As previously discussed, the decrease in mean annual temperatures from the mid- to late Holocene are representative of a proxy temperature reconstruction from Greenland ice cores (Dahl-Jensen *et al.*, 1998) and terrestrial records from the Arctic (Kaufman *et al.*, 2004; Renssen *et al.*, 2009; Sundqvist *et al.*, 2010).

For 9 to 0 ka, the cooling due to Saharan desertification is 0.5°C in OG, which is 17% of the total cooling of 2.9°C simulated with all forcings (Fig.5.1a). In the OGGIS experiment, the Saharan desertification suppressed the warming by 15% between 9 and 6 ka (i.e. by 1.0°C instead of 1.3°C), and from 6 to 0 ka, it was responsible for 19% of the observed cooling in the Arctic (-0.4°C vs. -2.1°C, Fig.5.1b).

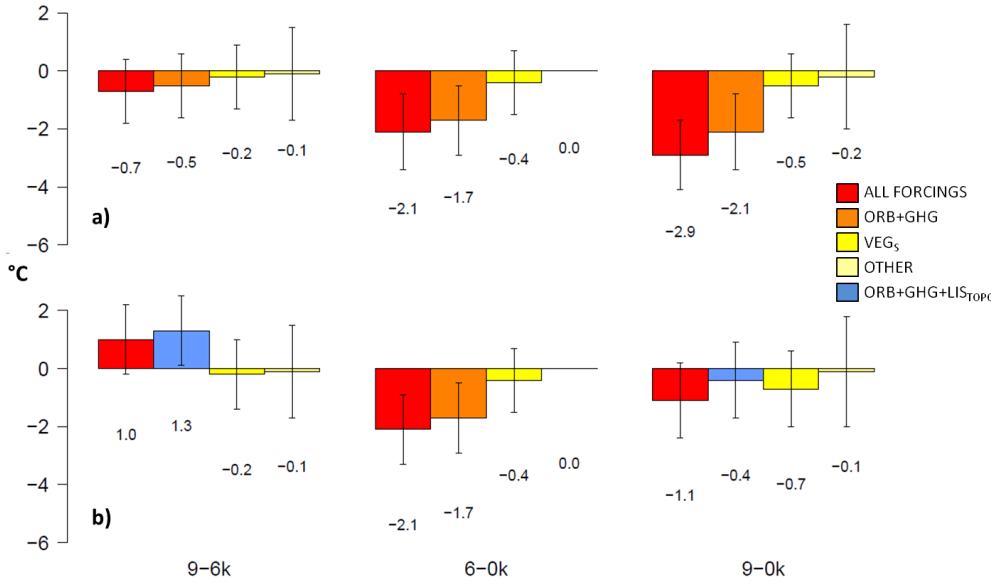

Fig.5.1. Simulated temperature change in the Arctic for a) OG and b) OGGIS equilibrium simulations, showing the relative contributions of different forcings; ORB+GHG (Orbital and Greenhouse gases), VEG_S (Vegetation changes in the Sahara), OTHER (other factors outside the Sahara region such as vegetation changes), ORB+GHG+LISTOPO (Orbital and Greenhouse Gases and Laurentide Icesheet Topography, which is only relevant for the period 9 to 6ka) and ALL (For OG this includes: GHG, ORB and prescribed Sahara vegetation; for OGGIS this includes: GHG, ORB, prescribed Sahara vegetation, LIS melt, GIS melt and LIS topography changes). Error bars represent $\pm 1\sigma$.

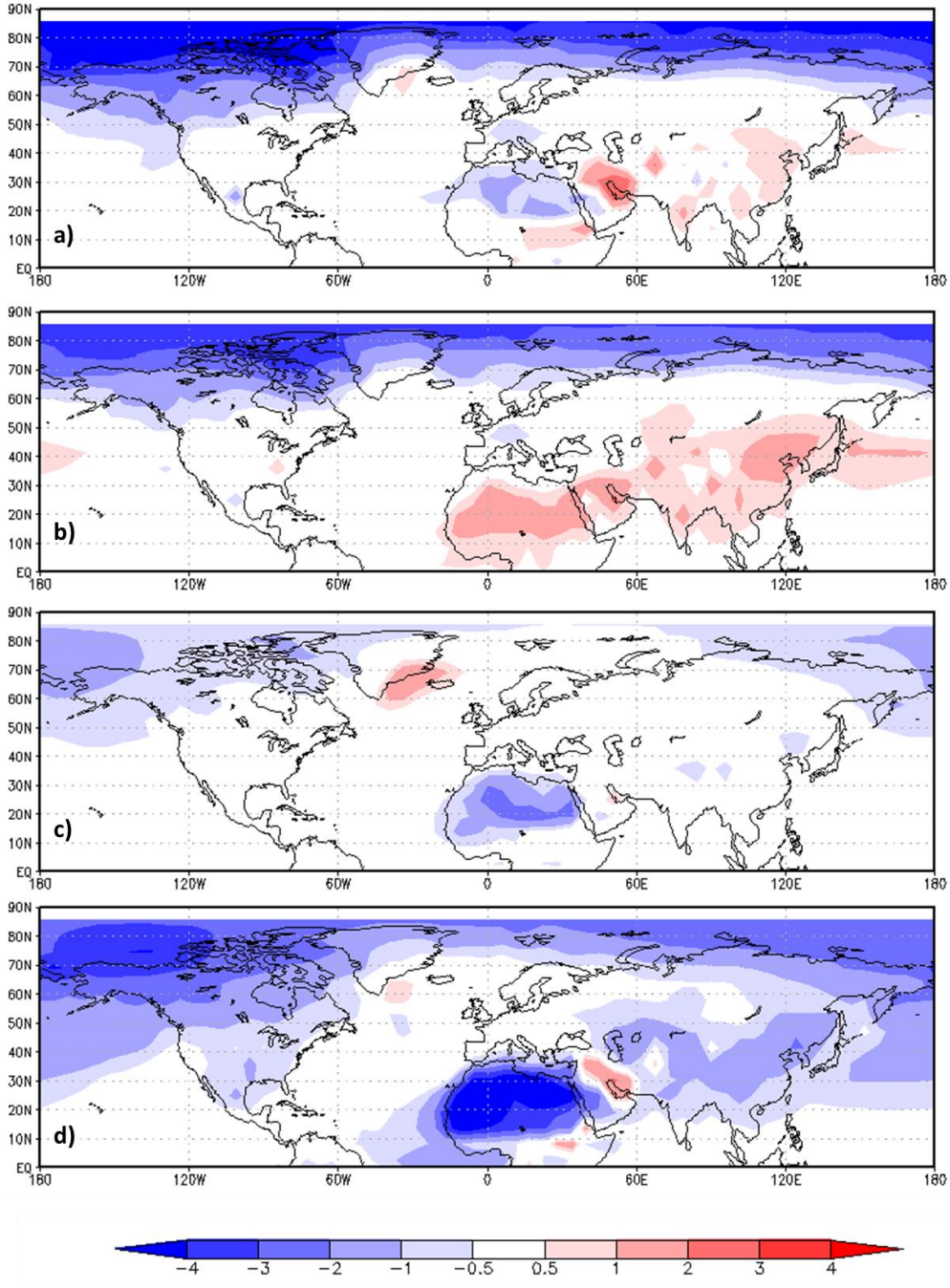

Fig.5.2. Mean annual surface temperature (°C) anomaly plots from the OG equilibrium simulation from 9 to 0ka showing the relative contributions of a) ALL (0-9ka); b) ORB+GHG (0-9ka); c) VEG (0-9ka); and d) 100% Desert Sahara - 100% Green Sahara (0ka) forcings upon global climate. Values are 500 year means.

5.3.2 Mechanisms connecting the Sahara to the Arctic

The model experiments indicate that part of the cooling in the Arctic over the Holocene is a direct consequence of Sahara desertification, which invokes a land–atmosphere teleconnection. Due to the prescribed desertification in the Sahara in our equilibrium simulations, over the course of the Holocene net albedo and radiative heat loss increases, leading to a decrease in surface temperatures and an increase in surface pressure in the Sahara.

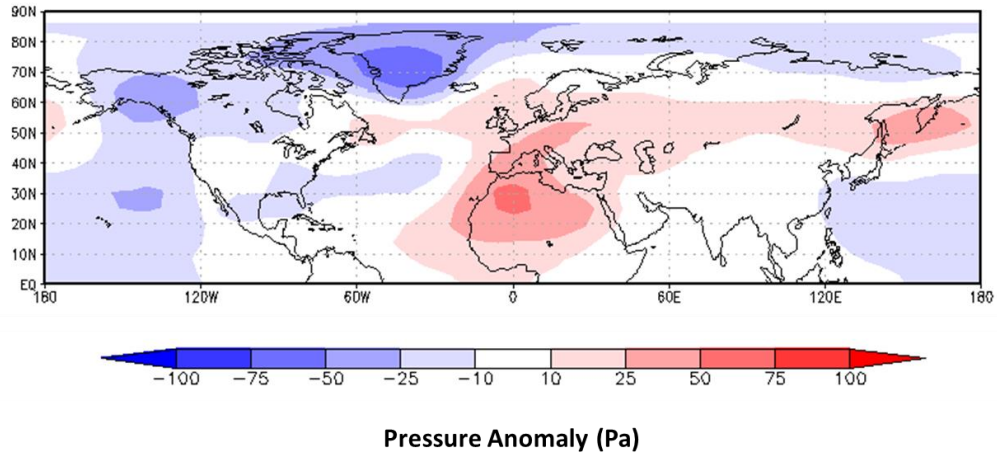

Fig.5.3. 9k0kEQ-9k9kEQ_OG 800hPa Geopotential Height, allowing the effects of changing vegetation in the Sahara, on pressure, to be visualised.

The decreasing temperatures in the Sahara cause an increase in the surface pressure (Fig.5.3) with an extension over the Tropical Atlantic, leading to an easterly zonal shift, plus an expansion, of the Azores high. Additionally, we observe a weakening of the low-latitude trade winds and a net overall decrease in the atmospheric meridional heat flux (Fig.5.4). In particular, we observe a weakening of the mid-latitude westerlies. This overall weakening of the winds and atmospheric heat transport over the Atlantic Ocean is consistent with a decrease in the meridional temperature gradient due the relatively strong cooling over the Sahara. As a result, the Icelandic Low stabilises, which in turns results in a weakening of the polar easterlies. The Bjerknes compensation theory suggests that weakened atmospheric heat transport would be compensated by an increase in oceanic heat transport (Bjerknes, 1964). This is indeed what we observe (Fig.5.4), however the increase in oceanic heat transport (0.058 PW at 7°N, before gradually reducing to 0 PW in the Arctic) is less than the decrease in total atmospheric heat transport (VQ + VT), resulting in an overall decrease of poleward heat transport. Mid-latitude storms are responsible for the majority of the heat transport from the equator to the Arctic (Peixoto and Oort, 1992; Zhang and Rossow, 1997). In our simulations, the weakening of the Northern Hemisphere winds are shown to be robust (Fig.5.4), in particular the westerlies, which results in a reduced meridional atmospheric heat transport from the low

latitudes to the Arctic (Fig.5.4), leading to widespread cooling north of 60°N.

In the OGGIS simulation, we see the same long-range land–atmosphere–ocean teleconnection present. However, the localised effects of the increase in albedo between 9 and 6 ka, due to the diminishing LIS and the localised effects of insolation changes, results in a warming over North America. This warming emanates eastwards over the North Atlantic and the rest of northern Europe and Eurasia, as well as penetrating the Arctic,

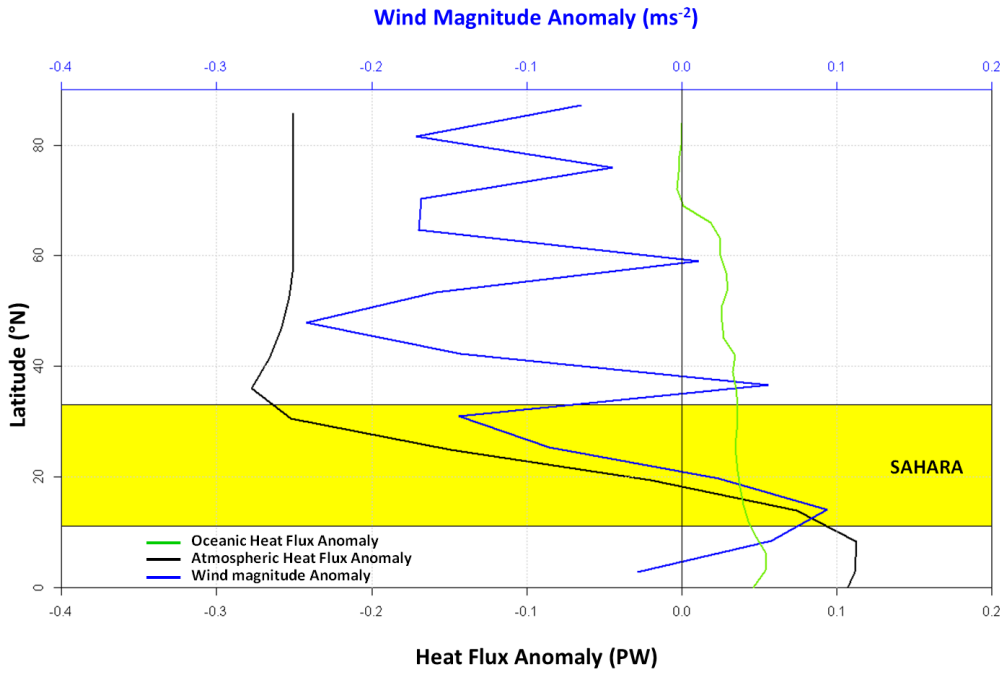

Fig.5.4. Depicts both the i) Mean annual oceanic heat flux anomaly (PW) (Green Line), ii) Mean annual atmospheric heat flux anomaly (PW) (Black Line) and iii) Mean annual wind magnitude anomaly (ms^{-2}) (Blue Line) over the North Atlantic (defined as 60°W to 15°E) (9k0kEQ_OG-9k9kEQ_OG). The latitudinal extent of the Sahara is highlighted for reference.

accounting for the observed warming between 9 and 6 ka in the OGGIS experiment.

5.3.3 Contribution of sea-ice feedbacks to Arctic cooling

Since the peak in the Holocene thermal maximum (~ 6 to 8 ka), the high northern latitudes cooled, sea-ice and snow cover increased, leading to an increase in surface albedo, which thus induced further cooling (Kerwin *et al.*, 1999; Crucifix *et al.*, 2002). In addition, Arctic cooling also resulted in thickening of the sea-ice cover during the Holocene, leading to a reduction in the ocean-to-atmosphere heat flux and relatively cooler conditions in the lower atmosphere through the ice-insulation feedback, especially in winter (Renssen *et al.*, 2005). It is important to see to what extent these important positive feedbacks of the climate system contributed to the Arctic cooling initiated by the Saharan desertification.

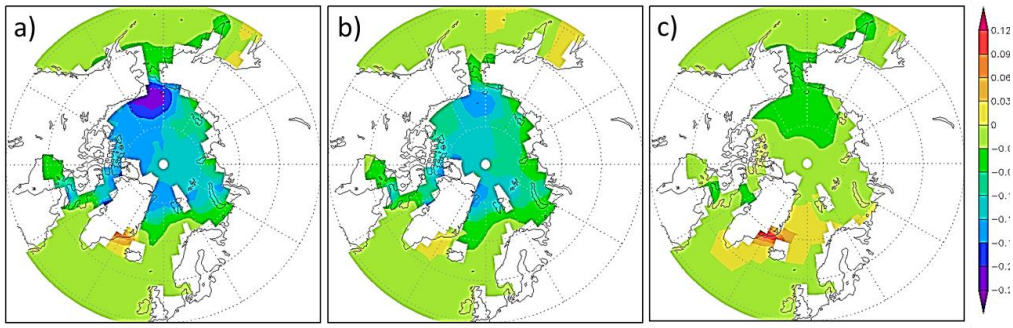

Fig.5.5. Mean annual sea-ice concentration (%) anomaly plots from the OG equilibrium simulation from 9 to 0ka showing the relative contributions of a) ALL (0-9ka); b) ORB+GHG (0-9ka); and c) VEG (0-9ka) forcings upon global climate. Values are 500 year means and range from 1 to 0 (1 = 100% sea-ice coverage).

Our results for the OG equilibrium simulations show that from 9 to 0 ka there is a reduction in sea-ice coverage of 25% in the Beaufort Sea, 15% across the rest of the Canadian Basin and 12 % across the majority of the eastern Arctic and its shelves (Fig.5.5a). However, this is a result of all of the forcings, orbital, greenhouse gases and vegetation changes in the Sahara. This indicates that LOVECLIM has captured this important feedback and is in line with previous results (Renssen *et al.*, 2005). Of this observed reduction, it can be seen that the majority is a direct result of the combination of changes in orbital and greenhouse gases (Fig.5.5b) and that a minor amount of sea-ice reduction (3%) can be accredited to the perturbed Sahara vegetation fractions within our experiments (Fig.5.5c). Additionally, we see a similar response in the sea-ice thickness (not shown). This clearly shows that the positive feedbacks associated with sea-ice play a modest role in the Arctic cooling that we accredited to the change in the vegetation in the Sahara (17%).

5.3.4 Sensitivity experiments

To evaluate the full potential of the impact of Saharan vegetation changes on the Arctic climate, we performed seven additional sensitivity experiments in which we prescribed either 100 % grassland or 100 % desert cover in the Sahara (see Appendix 5.D). Biome reconstructions of pollen and plant macrofossils show that during the mid-Holocene the Sahara was fully covered by grass and shrubs (Hoelzmann *et al.*, 1998; Jolly *et al.*, 1998). Hoelzmann *et al.* (1998) produced estimated percentages of various tree types across northern Africa and the Arabian Peninsula for 6 ka, showing steppe and savannah covering much of northern Africa (>90%). Claussen *et al.* (1999) were the first to replicate the results of Hoelzmann *et al.* (1998) and Jolly *et al.* (1998) in a climate model, successfully reproducing the drastic decrease in Sahara vegetation fraction over the Holocene from 90 to 0%.

However, in our OG simulation from 9 to 0 ka, the vegetation fraction decreases from 65 to 20%, clearly showing that whilst LOVECLIM is capable of simulating the

general pattern of vegetation change observed (Claussen *et al.*, 1999), it is unable to adequately capture the full amplitude of this highly unstable period that characterised the termination of the AHP.

Therefore, this suggests that the impact of Sahara vegetation on Arctic cooling could be greater than the 17% we estimated from our initial sensitivity experiments. To account for this, and to constrain our results, we simulated extreme, early (9 ka) and late (0 ka) Holocene environments. By "extreme" we imply that for 9 ka we replicated a 100% grass-vegetated environment, and for 0 ka we replicated a 100% desert environment within our model. This was done because if we had decided to follow the results of Jolly *et al.* (1998) and Claussen *et al.* (1999), that of a 90% vegetated Sahara region at 9 ka and a 0% vegetated Sahara region at 0 ka, we would have been left with several questions. Firstly, how would we allocate the 90% vegetation at 9 ka, given that we would have to make the decision of doing so per grid cell or over the entire Sahara domain? If over the Sahara domain, which regions do we leave arid? Compounding the difficulty of this, it must be noted that there is no proxy data available for the spatial extent of vegetation at 9 ka. Therefore, we opted for 100% vegetated cover at 9 ka. The results from these experiments enable us to place an upper limit of the potential impact of Sahara desertification has upon Arctic cooling over the Holocene.

The results show that from a 9 ka, 100% "green" Sahara to a 0 ka, 100% "desert" Sahara, temperatures decrease by 4.0°C (Fig.5.2d), of which 1.6°C (40 %) is attributable to the change in vegetation. However, given the extreme vegetation scenarios we prescribed at 0 and 9 ka, care must be taken when interpreting this result.

5.3.5 Uncertainty in our results

One important requirement for our results is that the Sahara region was warmer at 9 and 6 ka than at 0 ka, as suggested by our simulations. However, it is not possible to confirm or refute this on the basis of field-based evidence due to the absence of proxy-based temperature reconstructions for the Sahara region during the early and mid-Holocene. Although our LOVECLIM result is consistent with GCM simulations for the mid-Holocene (Braconnot *et al.*, 2007), it is important to critically address this aspect of our simulations, especially because the prescribed cloud cover in our model has likely significantly affected the surface energy balance over the Sahara.

In LOVECLIM, the total upward and downward shortwave fluxes are calculated as a function of the ISCCP D2 cloud cover data set consisting of modern-day observations. Whilst this is a reasonable first-order approximation for the modern-day Sahara, it is not so during periods when the Sahara was vegetated, i.e. 9 and 6 ka. This is because having a cloud cover that is essentially associated with a desert environment, as opposed to a vegetated environment, results in less clouds than there was in reality for 9 and 6 ka. Hence, the simulations at 9 and 6 ka ignore changes in cloud albedo. These changes in cloud albedo would approximately balance impacts from changes in surface albedo, which

we do include within our original equilibrium simulations.

For instance, if we assume that desert albedo is 0.4, and we have a 100% cloudless desert environment, then the downward solar radiation reaching the surface of the Sahara is 342 Wm^{-2} (Kiehl and Trenberth, 1997). Thus, the total solar radiation absorbed at the surface is 205 Wm^{-2} [(1-0.4)·342]. In a cloud covered, vegetated region, with surface albedo of 0.2, and assuming that 23 % of incoming solar radiation is reflected by clouds (Kiehl and Trenberth, 1997) then the downward solar radiation reaching the surface of the Sahara is 265 Wm^{-2} [342·(1-0.23)]. Therefore, the solar radiation absorbed at the surface is 211 Wm^{-2} [(1-0.2)·(342·0.77)]. Hence, in theory and as a first-order approximation, the surface of a cloudy vegetated region and that of a cloudless desert environment absorb approximately similar amounts of incoming solar radiation (211 and 205 Wm^{-2} respectively). As a result, temperature differences seen between these states would depend on differences between the latent and sensible heat fluxes, with less moisture available, lower latent heat flux and high sensible heat flux.

To test this we devised a series of sensitivity experiments that would allow for the addition of cloud cover over the Sahara at 9 and 6 ka. To achieve this we took the modern cloud cover that is prescribed in our model for the Amazon region and applied it directly to the Sahara in both the 9 and 6 ka sensitivity simulations. Hence, artificially induced cloud cover over the Sahara at these time periods is based on the modern day cloud cover for the Amazon. Given that the Amazon region consists of trees as opposed to a vegetated Sahara that more than likely consisted of grasses and shrubs during its vegetated period in the mid- and late Holocene, this prescribed cloud cover is probably an over estimation, but still serves the purpose of assessing the impact of cloud cover over a vegetated Sahara on surface temperature.

As can be seen (Fig.5.6), the Sahara was warmer during the mid-Holocene in both the simulation with the original modern day cloud data set at 6 ka (Fig.5.6a) and also in the simulation with the appropriate prescribed cloud cover for a vegetated Sahara at 6 ka (Fig.5.6b). The difference between these two simulations, in essence the impact of the difference between the two-cloud cover set ups we employed, is shown in Fig.6c. Here, it can be seen that with the modern-day cloud cover, the surface temperature in the Sahara is warmer by 0.7 to 1.3°C. This results in the Arctic being 0.3 to 0.7°C warmer due to the modern-day cloud data set over the Sahara.

As a final test of the sensitivity experiments, when we compare the temperature changes in the Arctic at 9 ka between simulations 9k9kEQ_OG and 9k9kEQ_OG_clouds, we see that the mean annual Arctic temperatures are -11.0±0.8°C and -11.1±0.8°C respectively (see Appendix 5.D). Therefore, based on these sensitivity experiments, we can say that a major premise of our original experiments, that the Sahara was warmer at 9 and 6 ka, compared to 0 ka holds, and thus, the land–atmosphere teleconnection between the Arctic and Sahara that we previously introduced is robust.

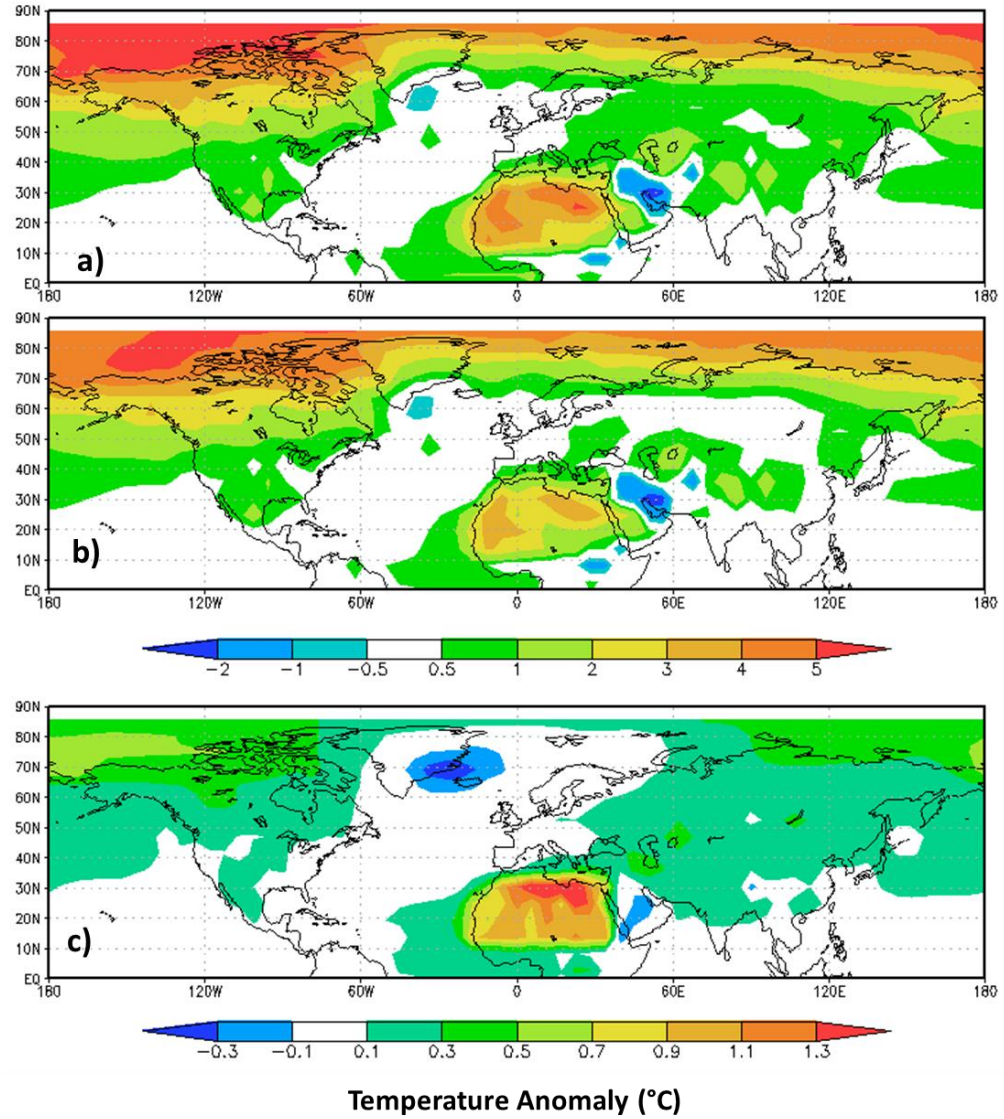

Fig.5.6. Temperature change between a) 6k Green Sahara – 0k Sahara (with modern day clouds prescribed in both experiments) (6k100gEQ-0k100dEQ); b) 6k Green Sahara (with 6k prescribed clouds) – 0k Sahara (with modern days clouds prescribed) (6k100gEQ_clouds-0k100dEQ); and c) Fig.6a – Fig.6b (equivalent to 6k Green Sahara with prescribed clouds – 6k Sahara with modern day clouds).

5.3.6 Limitations of LOVECLIM

The results presented here provide a first-order approach to understanding the impact of long-term radiative forcing of the Sahara over the course of the Holocene (9-0 ka). Whilst we have good confidence in the mechanisms driving the land–atmosphere teleconnection we observe over the Atlantic region, it is important to highlight the

limitations associated with our approach.

The land–atmosphere teleconnection we have outlined is initiated by a change in vegetation cover in the Sahara region and then carried through the atmosphere from the equatorial region to the Arctic. However, this draws close scrutiny of the atmospheric component of LOVECLIM. Given the relative simplicity of the ECBilt model compared to GCMs, it would be easy to dismiss our findings. However, as the model uses relatively simple physics, any findings in such a model should also be detectable in a more complex model. To highlight this, we shall compare the response of LOVECLIM in other studies to more complex models. Specifically, we shall highlight studies that have focused on interglacial climate only as this will allow us to show the response of LOVECLIM to different perturbations, over a variety of temporal and spatial extents.

The primary focus of our study is the cooling of the Arctic over the Holocene. Therefore, it would be apt for us to investigate how the temperature profile of LOVECLIM compares with more complex models. In this study and previous studies (Renssen *et al.*, 2005), it is shown that LOVECLIM shows a gradual cooling over the Holocene as a response to reduced summer insolation forcing and decreasing greenhouse gases. In a recent study (Liu *et al.*, 2014), the primary focus of which was trying to understand the apparent discrepancy between a reconstructed global temperature study (Marcott *et al.*, 2013) and models, it was shown that the three models employed in the study, LOVECLIM, CCSM3 and FAMOUS (the latter two being GCMs) all simulated a robust annual mean global warming (0.5°C) throughout the Holocene.

In a study of the last interglacial, Nikolova *et al.* (2013) provide a detailed analysis of a variety of climatic parameters, as simulated in both LOVECLIM and CCSM3. In these experiments they perturbed the climate for forcings equivalent to MIS-5e (127 ka). The results of these experiments show that the JJA surface temperature evolution during MIS-5e for both models is an exceptionally good match. This is especially true in the tropics over northern Africa, Greenland and North America. In the Arctic (defined as 60-90°N), the simulated warming is 3 and 2.2∘C for LOVECLIM and CCSM3, respectively, which is in agreement with another model–data comparison (Otto-Bliesner *et al.*, 2006). In addition, they show that the JJA precipitation between the two models to also be of a reasonable good fit, with both models simulating an intensification of both the African and Asian monsoons in line with proxy reconstructions. In addition, both models are consistent in replicating increased low-level wind speed and moisture transport over Africa during this period, as well a stronger upper-level (200hPa) tropical easterly jet over Africa (Nikolova *et al.*, 2013).

In a multimodel-data study (Bakker and Renssen, 2014), which included six GCMs and three EMICs, the data showed that when comparing the simulated period of maximum warmth during the last interglacial period against proxy-based temperature reconstructions, LOVECLIM, along with the two other EMICs in the study, all overestimated the maximum temperature the least, across all latitudes. This is probably on account of models with lower resolution displaying less internal variability, when compared to GCMs (Gregory *et al.*, 2005), leading to a more spatially coherent evolution

of the climate.

In another series of sensitivity experiments performed for the period MIS-13 (~ 500 ka), LOVECLIM was used to investigate the East Asian monsoon activity during this period (Yin *et al.*, 2008). The results of this study were conferred by Muri *et al.* (2013), who replicated these results with HadCM3, a fully coupled atmosphere–ocean general circulation model.

As we have outlined above when compared to GCMs, LOVECLIM has shown itself to be able to replicate similar results across a range of interglacial climates. Although just a selection are included here, it serves to demonstrate that despite its apparent shortcomings, LOVECLIM is an effective tool for climate investigations over a variety of spatial and temporal scales.

Another limitation in our study is due to the simplistic cloud parameterisation scheme that is employed within our model. As discussed in Sect. 5.3.4, we designed a series of sensitivity experiments to test this; although this is not a perfect solution, we were able to show that our original land–atmosphere teleconnection holds. However, without the evolution of clouds in response to changes in the climate system, particularly in response to surface temperature and sea-ice coverage changes, we are still missing potentially important feedbacks. However, this issue is not easily solved as it is a problem that persists through the entire spectrum of the modelling community, and it is widely accepted that this is a major source of uncertainty in climate model sensitivity experiments (Randall *et al.*, 2007).

Another potential source of error in our results lies in the vegetation fractions simulated in our transient simulations, which were then used to define the Sahara vegetation fractions in our equilibrium experiments. As previously noted (Sect. 5.3.3), the vegetation fraction in our model decreases from 65 to 20 % from 9 to 0 ka, as opposed to reconstructions and modelling studies which indicate an approximate 90–0 % decrease over the same period (Claussen *et al.*, 1999; Hoelzmann *et al.*, 1998; Jolly *et al.*, 1998).

As a result of this, our 9 ka simulations (with a 65% tree fraction at 9 ka, as opposed to a 90% tree fraction) have a higher surface albedo than proxy reconstructions and modelling studies indicate, and thus simulate a lower surface temperature at 9 ka. Additionally, if we consider our 0 ka simulations (with a 20% tree fraction, as opposed to a 0% tree fraction) results in a lower surface albedo, and thus a higher surface temperature at 0 ka.

As a result, the temperature gradient between the early and late Holocene in our experiments is not as steep as it possibly would be. Therefore, it would be interesting to see in future experiments, with a model that captures a more realistic temperature gradient between the early and late Holocene, how the polewards transported heat flux over the course of the Holocene is impacted.

To summarise, compared to comprehensive GCMs, LOVECLIM has several simplifications, of which the fixed cloud cover and the relatively simple vegetation scheme are likely to be the most important for this study. However, model inter-comparison

studies have shown that LOVECLIM produces similar interglacial climate responses to changes in forcings as GCMs, making it likely that our results will be confirmed in future studies with more comprehensive models.

5.4 Concluding remarks

In conclusion, our simulation experiments indicate that over the course of the Holocene, the observed cooling in the Arctic region is not only driven by local changes in insolation, but that the effects of desertification in the Sahara initiate a long-range land–atmosphere teleconnection. In our model experiments, this teleconnection accounts for between 17 and 40% of the observed Arctic cooling between 9 and 0 ka, and it is likely that the actual effect is nearer the upper end of this range. We also show through a series of sensitivity experiments that despite an apparent weakness of our model, with its prescribed modern-day cloud data set, our overall findings are conclusive and robust, withstanding the sensitivity experiments we performed. Therefore, our results indicate that high-latitude interglacial climate is sensitive to large-scale changes in Saharan vegetation cover.

Acknowledgements

F. J. Davies, H. Renssen, and M. Blaschek are funded by the "European Communities 7th Framework Programme FP7/2013, Marie Curie Actions, under grant agreement no. 238111: CASEITN". F. Muschitiello is funded by the Bolin Centre for Climate Research. All support is greatly appreciated.

Appendix 5.A

Table 5.A1

OG				ARCTIC TEMP (°C)	
ORB+GHG	VEG	TYPE	NAME	temp	s.d. (±)
0k	0k	EQ	**0k0kEQ_OG**	-13.9	1.0
0k	6k	EQ	**0k6kEQ_OG**	-13.5	1.0
0k	9k	EQ	**0k9kEQ_OG**	-13.1	1.0
6k	0k	EQ	**6k0kEQ_OG**	-12.2	0.8
6k	6k	EQ	**6k6kEQ_OG**	-11.8	0.8
6k	9k	EQ	**6k9kEQ_OG**	-11.5	0.8
9k	0k	EQ	**9k0kEQ_OG**	-11.6	0.8
9k	6k	EQ	**9k6kEQ_OG**	-11.2	0.8
9k	9k	EQ	**9k9kEQ_OG**	-11.0	0.8
9k	9k	EQ	**9k9kEQ_OG_clouds**	-11.1	0.8

Table 5.A2

OGGIS				ARCTIC TEMP (°C)	
ORB+GHG	VEG	TYPE	NAME	temp	s.d. (±)
0k	0k	EQ	**0k0kEQ_OGGIS**	-13.9	0.9
0k	6k	EQ	**0k6kEQ_OGGIS**	-13.5	0.9
0k	9k	EQ	**0k9kEQ_OGGIS**	-13.2	1.0
6k	0k	EQ	**6k0kEQ_OGGIS**	-12.2	0.8
6k	6k	EQ	**6k6kEQ_OGGIS**	-11.8	0.8
6k	9k	EQ	**6k9kEQ_OGGIS**	-11.5	0.8
9k	0k	EQ	**9k0kEQ_OGGIS**	-13.5	0.9
9k	6k	EQ	**9k6kEQ_OGGIS**	-13.0	0.9
9k	9k	EQ	**9k9kEQ_OGGIS**	-12.8	0.9

Appendix 5.B

Equations to calculate the relative contributions of ORBG + GHG and vegetation to the cooling in the Arctic, for OGGIS, OG and 100 % (extreme) runs.

OGGIS:

9 to 6 ka

9k9kEQ_OGGIS–6k6kEQ_OGGIS =Δ ∘C due to ALL forcings[a]
9k9kEQ_OGGIS–9k6kEQ_OGGIS =Δ ∘C due to VEGETATION forcing
9k9kEQ_OGGIS–6k9kEQ_OGGIS =Δ ∘C due to ORB & GHG forcings

6 to 0 ka

6k6kEQ_OGGIS–0k0kEQ_OGGIS =Δ ∘C due to ALL forcings[a]
6k6kEQ_OGGIS–6k0kEQ_OGGIS =Δ ∘C due to VEGETATION forcing
6k6kEQ_OGGIS–0k6kEQ_OGGIS =Δ ∘C due to ORB & GHG forcings

9 to 0 ka

9k9kEQ_OGGIS–0k0kEQ_OGGIS =Δ ∘C due to ALL forcings[a]
9k9kEQ_OGGIS–9k0kEQ_OGGIS =Δ ∘C due to VEGETATION forcing
9k9kEQ_OGGIS–0k9kEQ_OGGIS =Δ ∘C due to ORB & GHG forcings

OG:

9 to 6 ka

9k9kEQ_OG–6k6kEQ_OG =Δ ∘C due to ALL forcings[b]
9k9kEQ_OG–9k6kEQ_OG =Δ ∘C due to VEGETATION forcing
9k9kEQ_OG–6k9kEQ_OG =Δ ∘C due to ORB & GHG forcings

6 to 0 ka

6k6kEQ_OG–0k0kEQ_OG =Δ ∘C due to ALL forcings[b]
6k6kEQ_OG–6k0kEQ_OG =Δ ∘C due to VEGETATION forcing
6k6kEQ_OG–0k6kEQ_OG =Δ ∘C due to ORB & GHG forcings

9 to 0 ka

9k9kEQ_OG–0k0kEQ_OG =Δ ∘C due to ALL forcings[b]
9k9kEQ_OG–9k0kEQ_OG =Δ ∘C due to VEGETATION forcing
9k9kEQ_OG–0k9kEQ_OG =Δ ∘C due to ORB & GHG forcings

100 %

6 to 0 ka

6k100gEQ_OG–0k100dEQ_OG =Δ ∘C due to ALL forcings[b]

6k100gEQ_OG–6k100dEQ_OG =Δ ∘C due to VEGETATION forcing
6k100gEQ_OG–0k100gEQ_OG =Δ ∘C due to ORB & GHG forcings

9 to 0 ka

9k100gEQ_OG– 0k100dEQ_OG =Δ ∘C due to ALL forcings[b]
9k100gEQ_OG–9k100dEQ_OG =Δ ∘C due to VEGETATION forcing
9k100gEQ_OG–0k100gEQ_OG =Δ ∘C due to ORB & GHG forcings

[a] All forcings = GHG, ORB, prescribed Sahara vegetation, LIS and GIS topography.
[b] All forcings = GHG, ORB and prescribed Sahara vegetation.

Appendix 5.C

Vegetation fractions (%) of trees and grass (desert =100 - grass- trees) at 0, 6 and 9 ka, as derived from the OG transient simulation (Blaschek and Renssen, 2013). Albedo of grass, trees and desert are 0.2, 0.13 and 0.4 respectively.

Figure 5.C1

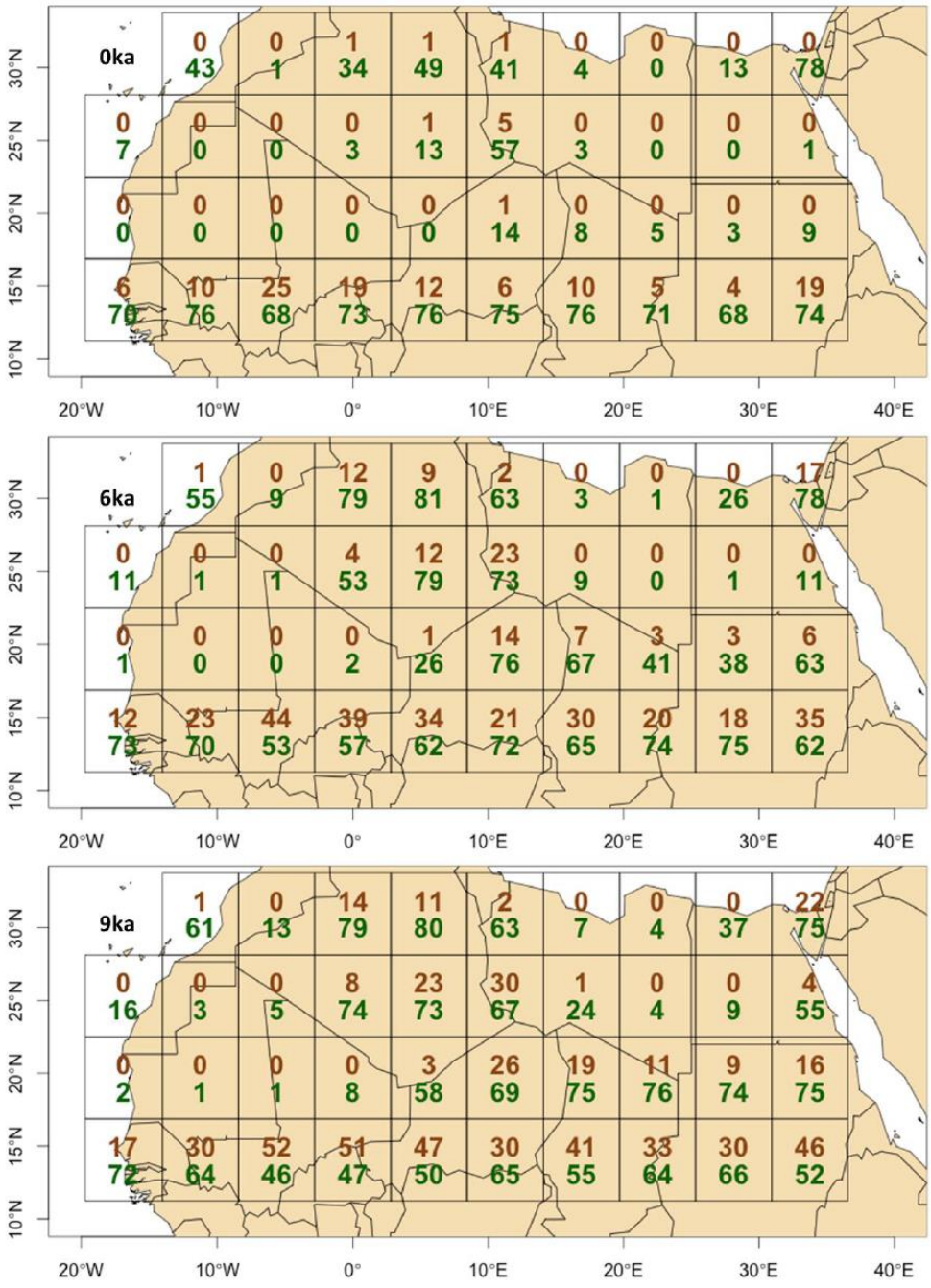
0ka
0 0 1 1 1 0 0 0 0
43 1 34 49 41 4 0 13 78
0 0 0 0 1 5 0 0 0 0
7 0 0 3 13 57 3 0 0 1
0 0 0 0 0 1 0 0 0 0
0 0 0 0 0 14 8 5 3 9
6 10 25 19 12 6 10 5 4 19
76 76 68 73 76 75 76 71 68 74
6ka
1 0 12 9 2 0 0 0 17
55 9 79 81 63 3 1 26 78
0 0 0 4 12 23 0 0 0 0
11 1 1 53 79 73 9 0 1 11
0 0 0 0 1 14 7 3 3 6
1 0 0 2 26 76 67 41 38 63
12 23 44 39 34 21 30 20 18 35
73 70 53 57 62 72 65 74 75 62
9ka
1 0 14 11 2 0 0 0 22
61 13 79 80 63 7 4 37 75
0 0 0 8 23 30 1 0 0 4
16 3 5 74 73 67 24 4 9 55
0 0 0 0 3 26 19 11 9 16
2 1 1 8 58 69 75 76 74 75
17 30 52 51 47 30 41 33 30 46
72 64 46 47 50 65 55 64 66 52
30°N
25°N
20°N
15°N
10°N
20°W
10°W
0°
10°E
20°E
30°E
40°E

Appendix 5.D

SIMULATION				ARCTIC TEMP (°C)	
ORB+GHG	VEG	TYPE	NAME	temp	s.d (±)
9k	100% Grass	EQ	**9k100gEQ**	-10.5	0.8
9k	100% Desert	EQ	**9k100dEQ**	-12.1	0.8
6k	100% Grass	EQ	**6k100gEQ_clouds**	-11.3	0.8
6k	100% Grass	EQ	**6k100gEQ**	-10.9	0.8
6k	100% Desert	EQ	**6k100dEQ**	-12.7	0.8
0k	100% Grass	EQ	**0k100gEQ**	-12.5	0.9
0k	100% Desert	EQ	**0k100dEQ**	-14.5	0.9

"Alas! Alas! Life is full of disappointments; as one reaches one ridge there is always another and a higher one beyond which blocks the view"

Fridtjof Nansen

Chapter 6: Synthesis, Conclusions, and Recommendations

6.1 Introduction

The aim of the research presented in this thesis is to discuss the Arctic Ocean freshwater cycle in the context of the Holocene and the 21st century. Firstly, this is achieved through looking at the comparison between climate model simulations of the mid-Holocene climate optimum (~6ka) and the 21st century. The study of past warm periods is often assumed to be useful to gain a better understanding of future climate change projections, however it is important to go beyond the mere comparison of temperatures and explore other atmospheric and oceanic components that have the potential to vary. This is what we seek to do in Chapter 2.

Following this, in Chapter 3 and 4 we then explore the atmospheric and oceanic mechanisms driving the intrinsic variability of the Arctic Ocean freshwater cycle in the LOVECLIM model during the Holocene on multicentennial timescales. The reason why it is important to look at these timescales is because they allow us to put the current freshening of the Arctic in a broader, more complete context of climate variability. With a better understanding of the intrinsic climate variability of the climate system, we will have a greater ability to interpret climate variability and its causes in past and future climates. I feel that these chapters highlight the need for such studies.

Finally, Chapter 5, challenges the notion that the cooling on the Arctic observed during the Holocene was primarily driven by the reduction in summer insolation forcing. Instead, I focused on the teleconnection between vegetation changes in the Sahara and Arctic cooling. Studies typically look at how the climate impacted vegetation change, but in Chapter 5 we approached it from the opposite angle and asked ourselves how do vegetation changes impact climate. Chapter 5 highlights the need to sometimes look for other drivers of the climate.

In the following section, I shall summarise the main research questions and conclusions from within this thesis and finish with some final perspectives on this research and potential research avenues this thesis could lead to.

6.2 The Arctic freshwater hydrological cycle during two warm periods

The initial focus of our research was the analysis of the various components that comprise the Arctic freshwater hydrological cycle, precipitation, evaporation, river-runoff, ocean fluxes and sea-ice, and to investigate how these components vary between two relatively warm periods, the 21st century and the mid-Holocene thermal maximum (~6kyr BP). These two periods were chosen because proxy-based reconstructions show that the warming during the mid-Holocene thermal maximum is similar in magnitude to the warming shown for the 21st century in climate modelling simulations. However, temperature is only one component of the Arctic climate system, thus it is relevant to examine how the components of the Arctic freshwater hydrological cycle responded to the increase in temperatures during these warm periods. An additional factor to consider is that the forcings during these warm periods are different, so "*Is it correct to use the mid-Holocene thermal maximum as a reference for the 21st century?*"

Our results showed that up until 2010, the simulated annual surface temperature in the Arctic was within the bounds of natural variability that was exhibited during the mid-Holocene thermal maximum, albeit at the extreme end of that range. However, after 2010 surface temperatures surpassed those exhibited during the mid-Holocene. Thus, we can say that after 2010 using the mid-Holocene thermal maximum as an analogue for the 21st Century is not appropriate. When comparing the various components of the Arctic freshwater hydrological cycle up to 2010, we observed that the Fram Strait liquid export (+18%), and river-runoff (+4%) were all greater than observed during the mid-Holocene. As a result, the Arctic Ocean was fresher, and this led to a suppression of the Nordic Seas overturning strength (by 18%). In addition, up to 2010 sea-ice volume was greater than during the mid-Holocene (+15%).

As discussed in Chapter 2 at length, a key question of this chapter is "Is it correct to use the mid-Holocene thermal maximum as a reference for the 21st century", with respect to the Arctic we conclude that after 2010 it is not a good analogue and after 2010, the response of the Arctic Ocean hydrological cycle, as seen in its constituent parts, to anthropogenic warming, is likely to be one that sees it transition to a state that exceeds the levels seen during the mid-Holocene.

6.3 An intrinsic mechanism of Arctic Ocean freshwater content multicentennial variability

An observation of our results from Chapter 2 was the periodic nature of the Arctic Ocean freshwater content variability and we sought to investigate this further in Chapter 3. Therefore, we performed a 10,000-year preindustrial control simulation and we were able to identify a multicentennial periodicity of ~165-years. We then investigated the mechanisms driving this intrinsic variability.

We found that the mechanism was driven by the variability of the Nordic Seas overturning strength. This altered between relatively 'strong' and 'weak' states, which in turn influenced the heat and saline content transported to the Arctic Ocean within the North Atlantic current, via the Barents and Kara Seas. The Arctic Ocean freshwater content increases when the Nordic Seas overturning circulation is suppressed, essentially reducing what is a net-saline flow into the Arctic Ocean via the North Atlantic Current. However, during this period, we see a relatively small outflow of freshwater via the Fram Strait, and eventually we begin to see the increased freshwater content of the Arctic lead to an increase in freshwater stored as sea-ice in the Arctic Ocean. Eventually, the reduction of freshwater entering the Nordic Seas from the Arctic Ocean, via the Fram Strait leads to an increase in saline waters in the Nordic Seas which act to strengthen the overturning circulation and thus increase the flow of heat and saline waters to the Arctic Ocean, and a reversal of the cycle is observed. These results presented in this thesis show that the freshwater content of the Arctic Ocean, potentially, has an intrinsic variability that operates on multicentennial timescales and is driven by the low-frequency variability of the transportation of heat and saline waters polewards. Recent studies (Giles *et al.*, 2012; Mauritzen, 2012; Haine *et al.*, 2015) have focused on shorter timescales and have

attributed freshening of the Arctic Ocean to anthropogenic climate change, however this could possibly be a too simplistic and convenient answer, potentially ignoring low-frequency intrinsic variability.

6.4 An intrinsic mechanism of Arctic Ocean freshwater content multicentennial variability during the Holocene

In Chapter 4 we built upon the work of Chapter 3 as we wanted to test our mechanism within a more 'real-world' simulation i.e., one driven by transient forcings over the past 8000-years. So, in essence, we repeated the experiment, but with the forcings for GHG's and orbital parameters matching those of the past 8000 years.

The pre-industrial forcings are CO_2 = 280ppm, CH_4 = 760ppb, whereas the transient forcings see CO_2 increase from 260 to 280ppm (8ka to 0ka) and CH_4 go from 650ppb to 550ppb between 8ka to 5.5ka, followed by an increase to 800ppb, please see Fig.4.4 of this thesis for a visual depiction of these changes.

In this study we found that the mechanism does hold within to the transient simulation, but the periodicity increased from ~165 years to ~220 years. In addition, in the previous chapter one aspect that we could not explain was the lack of impact sea-ice export via the Fram Strait to the Nordic Seas, the site of overturning, had on the mechanism. In Chapter 3, we found no significant correlation or impact at all. However, within the transient simulation we found that sea-ice export via the Fram Strait does play a significant role in the mechanism. This is because throughout the transient simulation the sea-ice thickness across the Arctic increases, particular in the East-Siberian shelf region, which was not observed within the previous chapter, instead sea-ice volumes remained constant. Instead in the transient simulation, we observed that this increase in sea-ice within the Arctic, led to an increase in sea-ice exported via the Fram Strait to the Nordic Seas, the site of overturning and had more of an impact on our mechanism.

6.5 The role of the Sahara in Arctic climate change over the Holocene

For the final part of the thesis, Chapter 5, we presented a study that challenged the notion that the main driver of decreasing Arctic temperatures over the course of the Holocene was orbital parameters and the associated reduction of summer insolation. Instead, we looked at how a teleconnection from the Sahara, driven by the vegetation changes in the Sahara over the course of the Holocene, impacted climate in the Arctic and contributed to the cooling observed in proxy records.

Over the course of the Holocene, as the Sahara undergoes vegetation loss and continued desertification, net albedo, radiative heat loses, surface temperatures and surface pressure increase in the Sahara region. Surface pressure increases lead to an easterly shift and expansion of the Azores high. In addition, the low-latitude trade winds weaken and there is a decrease in the atmospheric meridional heat flux, and a weakening of the mid-latitude westerlies. This weakening of the winds and atmospheric heat transport over the Atlantic Ocean reduces the meridional temperature gradient, which causes the Icelandic low to stabilise and weaken the polar easterlies. Overall, atmospheric poleward heat

transport is reduced, but is not compensated by an increased oceanic heat transport, and thus we see cooling in the Arctic, due to the desertification in the Sahara.

As a result, we were able to show that 17-40 % of the cooling in the Arctic, over the period 9-0 ka, was a direct result of the desertification that occurred in the Sahara after the termination of the African Humid Period. The results of this paper were further explored by Muschitiello *et al.*, (2015) who were able to confirm the results we have presented here.

This cooling is likely to impact the Arctic hydrological system and the mechanism of intrinsic variability discussed in Chapter 3 and 4 of this thesis. Although this was not explored within this thesis, we can also hypothesis as to the what the likely implications would have been. The experiments in Chapters 3 and 4 used fixed modern-day vegetation forcings, thus the additional cooling that occurs due to the inclusion of a dynamic Saharan vegetation would have likely resulted in addition cooling in the Arctic during these simulations and allowed for greater sea-ice formation in the Arctic Ocean. This would have allowed for greater sea-ice export via the Fram Strait and potentially providing a stronger signal of the Fram Strait ice export component of the mechanism of intrinsic variability. However, further experimentation would be encouraged in future work.

6.6 Perspectives

Putting the contents of this thesis into perspective is not a straightforward task, however one will strive to do so. Firstly, all the work presented here has been done with the use of a climate model. Just one model. Therefore, it is open to criticism about the model's suitability to be used in such studies. Throughout the chapters we have sought to alleviate these concerns with explanations and examples of other studies using the same model. Given the depth at which these are covered in the chapters a lengthy argument here is not necessary. However, despite the limitations of the model we hope that the work presented here has sparked the imagination of the reader and has asked them to challenge some previously held ideas and opened them up to some new ones. The work did this with myself, and has left me with the following thoughts that I would like to share with you:

1) The work presented here, particularly Chapters 3 and 4, show there are intrinsic modes of variability within the climate system that we do not fully understand at this point in time, particularly at the multicentennial timescale, as is discussed by Crucifix *et al.*, (2017). Our results also add to previous work that has identified low-frequency intrinsic climate variability within the high-northern latitudes, including the Atlantic Meridional Oscillation (65 to 70 years) (Schlesinger and Ramankutty, 1994); the Arctic Oscillation (1500 years) (Darby *et al.*, 2012); the North Atlantic Oscillation (170 and 300 years) (Olsen *et al.*, 2012); the heat transported by the Atlantic Meridional Overturning Circulation (300 to 400 years) (Park and Latif, 2008); and sea-ice cover in the Kara Sea (400 and 950 years) (Hörner *et al.*, 2017), centennial to millennial scale variability during the Holocene, including changes in sea-level (Kopp *et al.*, 2017), the AMOC (Ayache *et al.*, 2018) and sea surface temperatures in the North Atlantic (Sicre *et al.*, 2008).

Therefore, studies like the ones presented in Chapters 3 and 4 are necessary to allow us to further disentangle the causes of climate variability that we observe in proxy records and modelling studies. This only adds more clarity to furthering our understanding of how the future climate is going to evolve.

2) The output from any climate model comes attached with a degree of uncertainty attached to it. A significant source of such model uncertainty arises from the parameter sets within the model that are used. Many of these values are not perfect and therefore the outcome of the model can be questioned. A way to tackle this issue would be to create an ensemble of different versions of a model, all with different parameter sets. A similar study has been performed using LOVECLIM (Loutre *et al.*, 2011), which applied 27 different parameter sets to assess the response of a range of climate variables for the present day climate. These were a combination of nine climate parameter datasets and three carbon cycle datasets. Of course, it would not be possible to blindly apply these parameter sets to our study, but it provides an example of how to approach such work. In addition, we could also apply the experimental design for different interglacial periods (Otto-Bliesner *et al.*, 2017) and the mid-Pliocene Warm Period (Haywood *et al.*, 2016). This would allow us to see if similar climatic variability exists under different 'warm climatic conditions' and would improve the robustness of our analysis. In addition, we could compare these results to proxy reconstructions.

3) Another useful extension of this thesis would be to undertake the study of the intrinsic mode of Arctic Ocean freshwater content variability with a suite of higher complexity climate models, allowing for an ensemble assessment to be made. The ideal guidelines in which to conduct these experiments would be to follow the experimental design outlined by the PMIP4 series of Palaeoclimate modelling experiments (Kageyama *et al.*, 2016), which have allowed for multimodel studies of pre-determined climate periods. The periods that would of interest in advancing the work presented in this thesis are the mid-Holocene (6ka BP) experiment (Otto-Bliesner *et al.*, 2017) and the last millennium experiment (Jungclaus *et al.*, 2017).

4) During the last deglaciation, during the period 16.5-7ka BP, as land-based icesheets retreated, the meltwater released from these caused sea-levels to rise by ~120m (Lambeck *et al.*, 2014; Siddall *et al.*, 2003). This caused many exposed sea-shelves to become flooded. This is particularly relevant for the Arctic Ocean which saw the East-Siberian Shelf become inundated around 7.5ka BP, with its current bathymetry reached around 5ka BP. This area has been identified as an important one for sea-ice production within the Arctic (Bauch *et al.*, 2001), with the theory being that as these shelves become flooded the volume of sea-ice produced increases which subsequently leads to an increase in sea-ice export via the Fram Strait through to the Nordic Seas. However as discussed by Blaschek and Renssen (2013) this is not entirely the case. In their study they simulated, using LOVECLIM, the changing bathymetry in the Arctic Ocean for the early Holocene and the late Holocene and

calculated the change in sea-ice production in the East-Siberian Seas and export through the Fram Strait. They did observe an increase in sea-ice production in the East-Siberian Seas as they flooded, but they did not observe the expected increase in sea-ice export via the Fram Strait. Therefore, when conducting any future studies into the Arctic Ocean freshwater cycle through the Holocene, it would be important to include the changing bathymetry of the Arctic Ocean.

5) In Chapter 5 we explored the role that Sahara desertification had on the observed cooling during the Holocene. Given the focus of our research on the Arctic Ocean freshwater content in Chapters 2, 3 and 4, a logical next step would be to look at how the Arctic Ocean freshwater cycle was impacted by the Sahara desertification. Muschitiello *et al.*, (2015), also conducted a study similar to ours presented in Chapter 5. In their study they concluded that changes brought about in the Arctic, due to the mid-Holocene Sahara desertification were due to a change from a positive to a negative Arctic Oscillation phase-like conditions, brought about by a weakening of the mid-latitude westerlies, which we also discussed. If the AO is to play a crucial role in the mid-Holocene cooling in the Arctic, then this would likely alter the wind and flow patterns of freshwater through the Arctic and potentially the Fram Strait as we discussed in Chapters 3 and 4. Therefore, repeating our experiments of Chapter 5, but with a renewed focus on the Arctic Ocean freshwater response to the mid-Holocene Sahara desertification would be very pertinent.

References

Aagaard K, Carmack EC (1989) The role of sea ice and other fresh water in the Arctic circulation. J Geophys Res 94: 14485-14498

Aagaard K, Coachman LK, Carmack EC (1981) On the halocline of the Arctic Ocean. Deep-Sea Res 28(6): 529-545. doi.org/10.1016/0198-0149(81)90115-1

Arzel O, Fichefet T, Goosse H, Dufresne, JL (2008) Causes and impacts of changes in the Arctic freshwater budget during the twentieth and twenty-first centuries in an AOGCM. Clim Dyn 30:37-58. doi: 10.1007/s00382-007-0258-5

Axford Y, Miller GH, Geirsdóttir Á, Langdon PG (2007) Holocene temperature history of northern Iceland inferred from subfossil midges. Quat Sci Rev 26: 3344-3358

Ayache M, Swindegouw D, Mary Y, Eynaud F, Colin C (2016) Multi-centennial variability of the AMOC over the Holocene: A new reconstruction based on multiple proxy-derived SST records, Glob Planet Change 170: 172-189. doi.org/10.1016/j.gloplacha.2018.08.016

Bakker P, Renssen H (2014) Last interglacial model–data mismatch of thermal maximum temperatures partially explained. Clim Past 10: 1633–1644, 10.5194/cp-10-1633-2014

Bakker P, Stone EJ, Charbit S, Gröger M, Krebs-Kanzow U, Ritz SP, Varma V, Khon V, Lunt DJ, Mikolajewicz U, Prange M, Renssen H, Schneider B, Schulz M (2013) Last interglacial temperature evolution - a model inter-comparison. Clim Past 9: 605–61, 10.5194/cp-9-605-2013

Bauch H, Mueller-Lupp T, Taldenkova E, Spielhagen R, Kassens H, Grootes P, Thiede J, Heinemeier J, Petryashov V (2001) Chronology of the Holocene transgression at the North Siberian margin. Global Planet Change 31: 125-139

Bennike O (2000) Palaeoecological studies of Holocene lake sediments from West Greenland. Palaeogeor, Palaeoclim, Palaeoecol 155: 285-304

Berger AL (1978) Long-term variations of daily insolation and Quaternary climatic changes. J Atmos Sci 35: 2362-2367

Birks CJA, Koç N (2002) A high-resolution diatom record of late-Quaternary sea-surface temperatures and oceanographic conditions from the Eastern Norwegian Sea. Boreas 31: 323-344

Bjerknes J (1964) Atlantic air-sea interaction. Adv Geophys 10: 1-82

Blaschek M, Renssen H (2013) The Holocene thermal maximum in the Nordic Seas: the impact of Greenland Ice Sheet melt and other forcings in a coupled atmosphere-sea-ice–ocean model. Clim Past 9: 1629-1643, 10.5194/cp-9-1629-2013

Blindheim J (1989) Cascading of Barents Sea bottom water into the Norwegian Sea. Rapports et Proce`s-verbaux des Re´unions du Conseil International par l'Exploration de la Mer 188: 49-58.

Bond G, Showers W, Cheseby M, Lotti R, Almasi P, de Menocal P, Priore P, Cullen H, Hajdas I, Bonani G (1997) A Pervasive Millennial-Scale Cycle in North Atlantic Holocene and Glacial Climates. Science 278(5341): 1257

Box GEP, Pierce DA (2012) Distribution of Residual Autocorrelations in Autoregressive-Integrated Moving Average Time Series Models, J. Am. Stat. Assoc 65(332): 1509-1526. doi:10.1080/01621459.1970.10481180

Braconnot P, Otto-Bliesner B, Harrison S, Joussaume S, Peterchmitt JY, Abe-Ouchi A, Crucifix M, Driesschaert E, Fichefet T, Hewitt CD, Kageyama M, Kitoh A, Loutre M, Marti O, Merkel U, Ramstein G, Valdes P, Weber SL, Yu Y, Zhao Y (2007) Results of PMIP2 coupled simulations of the Mid-Holocene and Last Glacial Maximum part 2: feedbacks with emphasis on the location of the ITCZ and mid- and high latitudes heat budget. Clim Past 3: 279-296

Broecker WS (2010) The Great Ocean Conveyor: Discovering the Trigger for Abrupt Climate Change. Princeton University Press

Brovkin V, Bendtsen J, Claussen M, Ganopolski A, Kubatzki C, Petoukhov V, Andreev A (2002) Carbon cycle, vegetation and climate dynamics in the Holocene: experiments with the CLIMBER-2 model. Glob Biogeochem Cycles 16(4): 1139. doi:10.1029/2001GB001662

Bügelmayer M, Roche DM, Renssen H (2015) How do icebergs affect the Greenland ice sheet under pre-industrial conditions? – a model study with a fully coupled ice-sheet–climate model, Cryosphere 9: 821-835. https://doi.org/10.5194/tc-9-821-2015

Calvo E, Grimalt J, Jansen E (2002) High resolution U^{K}_{37} sea surface temperature reconstruction in the Norwegian Sea during the Holocene. Quat Sci Rev 21: 1385-1394

Caseldine C, Geirsdóttir Á, Langdon P (2003) Efstadalsvatn-A multi-proxy study of a Holocene lacustrine sequence from NW Iceland. J of Paleolim 30: 55-73

Caseldine C, Langdon P, Holmes N (2006) Early Holocene climate variability and the timing and extent of the Holocene Thermal Maximum (HTM) in Northern Iceland. Quat Sci Rev 25: 2314-2331

Chen JL, Wilson CR, Tapley BD (2006) Satellite gravity measurements confirm accelerated melting of Greenland Ice Sheet. Science 313: 1958-1960

Christensen JH, Hewitson B, Busuioc A, Chen A, Gao X, Held I, Jones R, Kolli RK, Kwon WT, Laprise R, Magaña Rueda V, Mearns L, Menéndez CG, Räisänen J, Rinke A, Sarr A, Whetton P (2007) Regional Climate Projections. In: Solomon S, Qin D, Manning M, Chen Z, Marquis M, Averyt KB, Tignor M, Miller HL (ed) Climate Change 2007: The Physical Science Basis. Contribution of Working Group I to the Fourth Assessment Report of the Intergovernmental Panel on Climate Change, Cambridge University Press, Cambridge, United Kingdom and New York, NY, USA, pp 848-940

Christiansen HH, Bennike O, Böcher J, Elberling B, Humlum O, Jakobsen BH (2002) Holocene environmental reconstruction from deltaic deposits in Northeast Greenland. J Quat Sci 17: 145-160

Claussen M, Kubatzki C, Brovkin V, Ganopolski A, Hoelzmann P, Pachur H-J (1999) Simulation of an abrupt change in Saharan vegetation in the mid-Holocene. Geophys Res Lett 26: 2037-2040

Comiso JC, Parkinson CL, Gersten R, Stock L (2008) Accelerated decline in the Arctic sea ice cover. Geophys Res Lett 35: L01703. doi: 10.1029/2007GL031972

Crowley TJ, Zielinski G, Vinther B, Udisti R, Kreutz K, Cole-Dai J, Castellano E (2008) Volcanism and the Little Ice Age. PAGES News 16: 22-23

Crucifix M, Loutre MF, Tulkens P, Fichefet T, Berger A (2002) Climate evolution during the Holocene: a study with an Earth system model of intermediate complexity. Clim Dynam 19: 43-60

Curry J (2017) Nature Unbound III: Holocene climate variability https://judithcurry.com/2017/04/30/nature-unbound-iii-holocene-climate-variability-part-a/Accessed 23 June 2020

Dahl-Jensen D, Mosegaard K, Gundestrup N, Clow GD, Johnsen SJ, Hansen AW, Balling N (1998) Past Temperatures Directly from the Greenland Ice Sheet. Science 282: 268-271

Darby DA, Ortiz JD, Grosch CE, Lund SP (2012) 1,500-year cycle in the Arctic Oscillation identified in Holocene Arctic sea-ice drift. Nat Geosci 5: 897-900. doi:10.1038/ngeo1629

Davis MB, Spear RW, Shane LCK (1980) Holocene climate of New England. Quat Res 14: 240-250

Davies FJ, Renssen H, Blaschek M, Muschitiello F (2015) The Impact of Sahara desertification on Arctic cooling during the Holocene. Clim Past 11: 571-586. https://doi.org/10.5194/cp-11-571-2015

Davies FJ, Renssen H, Goosse H (2014) The Arctic freshwater cycle during a naturally and an anthropogenically induced warm climate. Clim Dyn 42: 2099-2112. doi.10.1007/s00382-013-1849-y

Delaygue G, Bard E (2009) Solar forcing based on Be-10 in Antarctica ice over the past millennium and beyond. EGU 2009 General Assembly. #EGU2009-6943

Deleersnijder E, Campin JM, (1995) On the computation of the barotropic mode of a free-surface world ocean model. Ann Geophys 13: 675-688

Deleersnijder E, Beckers JM, Campin JM, El Mohajir M, Fichefet T, Luyten P (1997) Some mathematical problems associated with the development and use of marine models. In: Diaz JI (Ed) The mathematics of model for climatology and environment, NATO ASI Series. Springer-Verlag, pp 39-86

de Menocal P, Ortiz J, Guilderson T, Adkins J, Sarnthein M, Baker L, Yarusinsky M (2000) Abrupt onset and termination of the African Humid Period: rapid climate responses to gradual insolation forcing. Quat Sci Rev 19: 347-361

Déry SJ, Hernández-Henríquez MA, Burford JE, Wood EF (2009) Observational evidence of an intensifying hydrological cycle in Northern Canada. Geophys Res Lett 36: L13402. doi:10.1029/2009GL038852

Déry SJ, Wood EF (2005) Decreasing river discharge in Northern Canada. Geophys Res Lett 32: L10401. doi: 10.1029/2005GL022845

Dickey DA, Fuller WA (2012) Distribution of the Estimators for Autoregressive Time Series with a Unit Root, J AM Stat Assoc 74(366a): 427-431. doi: 10.1080/01621459.1979.10482531

Dickson RR, Blindheim J (1984) On the abnormal hydrographic conditions in the European Arctic during the 1970s. ICES Rapports et Procès-Verbaux des Réunions 185: 201-213

Dickson RR, Rudels B, Dye S, Karcher M, Meincke J, Yashayaev I (2007) Current estimates of freshwater fluxes through Arctic and Subarctic Seas. Prog Oceanogr 73: 210-230

Döscher R, Vihma T, Maksimovich E (2014) Recent advances in understanding the Arctic climate system state and change from a sea ice perspective: a review, Atmos Chem Phys 14: 13751-13600. doi: 10.5194/acp-14-13571-2014

Driesschaert E, Fichefet T, Goosse H, Huybrechts P, Janssens I, Mouchet A, Munhoven G, Brovkin V, Weber SL (2007) Modelling the influence of Greenland Ice Sheet melting on the atlantic meridional overturning circulation during the next millennia. Geophys Res Lett 34: L10707. doi:10.1029/2007GL029516

Duplessy JC, Ivanova E, Murdmaa I, Paterne M, Labeyrie L (2001) Holocene paleoceanography of the northern Barents Sea and variations of the northward heat transport by the Atlantic Ocean. Boreas 30: 2-16

Dyke AS, Prest V K (1987) Late Wisconsinan and Holocene History of the Laurentide Ice Sheet. Géographie physique et Quaternaire 41 (2): 237-263

Eddy JA (1979) The Maunder Minimum. Science 192(4245): 1189-1202

Fichefet T, Morales Maqueda MA (1997) Sensitivity of a global sea ice model to the treatment of ice thermodynamics and dynamics. J Geophys Res 102: 12609-12646

Fichefet T, Morales Maqueda MA (1999) Modelling the influence of snow accumulation and snow-ice formation on the seasonal cycle of the Antarctic sea-ice cover. Clim Dyn 15: 251-268

Flato G, Marotzke J, Abiodun B, Braconnot P, Chou SC, Collins W, Cox P, Driouech F, Emori S, Eyring V, Forest C, Gleckler P, Guilyardi E, Jakob C, Kattsov V, Reason C, Rummukainen M (2013) Evaluation of Climate models, in: Climate Change 2013: The Physical Science Basis. Contribution of Working Group I to the Fifth

Assessment Report of the Intergovernmental Panel on Climate Change, edited by: Stocker TF, Qin D, Plattner G-K, Tignor M, Allen SK, Boschung J, Nauels A, Xia Y, Bex V, Midgley P M, Cambridge University Press, Cambridge, United Kingdom and New York, NY, USA

Gedney N, Valdes P J (2000) The effect of Amazonian deforestation on the northern hemisphere circulation and climate. Geophys Res Lett 27: 3053-3056

Gent PR, McWilliams JC (1990) Isopycnal mixing in ocean circulation models. J Phys Oceanogr 20: 150-155

Giles KA, Laxon SW, Ridout AL, Wingham DJ, Bacon S (2012) Western Arctic ocean freshwater storage increased by wind-driven spin-up of the Beaufort gyre. Nat Geosci doi:10.1038/NGE01379

Goosse H, Fichefet T (1999) Importance of ice-ocean interactions for the global ocean circulation: a model study. J Geophys Res 104: 23337-23355

Goosse H, Brovkin V, Fichefet T, Haarsma R, Huybrechts P, Jongma J, Mouchet A, Selten F, Barriat P-Y, Campin J-M, Deleersnijder E, Driesschaert E, Goelzer H, Janssens I, Loutre M-F, Morales Maqueda MA, Opsteegh T, Mathieu P-P, Munhoven G, Pettersson, EJ, Renssen H, Roche DM, Schaeffer M, Tartinville B, Timmermann A, Weber SL (2010) Description of the earth system model of intermediate complexity LOVECLIM version 1.2. Geosci Model Dev 3: 603-633. doi: 10.5194/gmd-3-603-2010

Goosse H, Campin JM, Fichefet T, Deleersnijder E (1997) Sensitivity of a global ice-ocean model to the Bering strait throughflow. Clim Dyn 13: 349-358

Goosse H, Crowley TJ, Zorita E, Ammann CM, Renssen H, Driesschaert E (2005) Modelling the climate of the last millennium: What causes the differences between simulations?, Geophys Res Lett 32: L06710, 10.1029/2005GL022368

Gregory JM, Dixon KW, Stouffer RJ, Weaver AJ, Driesschaert E, Eby M, Fichefet T, Hasumi H, Hu A, Jungclaus JH, Kamenkovich IV, Levermann A, Montoya M, Murakami S, Nawrath S, Oka A, Sokolov AP, Thorpe RB (2005) A model intercomparison of changes in the atlantic thermohaline circulation in response to increasing atmospheric CO2 concentration. Geophys Res Lett 32: L12703. doi:10.1029/2005GL023209

Haak H, Jungclaus J, Mikolajewicz U, Latif M (2003) Formation and propagation of great salinity anomalies. Geophys Res Lett 30 (9): 1473. https://doi.org/10/1029.2003GL017065

Haarsma RJ, Selten FM, Opsteegh JD, Lenderink G, Liu Q (1996) A coupled atmosphere ocean sea-ice model for climate predictability studies. KNMI, De Bilt, The Netherlands, 31

Haine TWN, Curry B, Gerdes R, Hansen E, Karcher M, Lee C, Rudels B, Spreen G, Steur L, Kial D, Stewart KD, Woodgate R (2015) Arctic freshwater export: Status, mechanisms, and prospects. Glob Planet Change 125: 13-35

Häkkinen S, Proshutinsky A (2004) Freshwater content variability in the Arctic Ocean. J Geophys Res 109: C03051. doi:10.1029/2003JC001940

Hansen G, Stone D (2016) Assessing the observed impact of anthropogenic climate change. Nature Climate Change 6(5): 532-537, doi:10.1038/nclimate2896

Hass C, Eicken H (2001) Interannual variability of summer sea ice thickness in the Siberian and central Arctic under different atmospheric circulation regimes. J Geophys Res 106: 4449-4462

Hátún H, Sandø AB, Drange H, Hansen B, Valdimarsson H (2005) Influence of the Atlantic Subpolar Gyre on the Thermohaline Circulation. Science 309(5742): 1841-1844. doi:10.1126/science.1114777

Hays JD, Imbrie J, Shackleton NJ (1976) Variations in the Earth's Orbit: Pacemaker of the Ice Ages. Science 194(4270): 1121-1132

Haywood AM, Dowsett HJ, Dolan AM, Rowley D, Abe-Ouchi A, Otto-Bliesner B, Chandler MA, Hunter SJ, Lunt DJ, Pound M, Salzmann U (2016) The Pliocene Model Intercomparison Project (PlioMIP) Phase 2: scientific objectives and experimental design. Clim Past 12: 663-675, https://doi.org/10.5194/cp-12-663-2016

Hoelzmann P, Jolly D, Harrison SP, Laarif F, Bonnefille R, Pachur H-J (1998) Mid-Holocene land-surface conditions in northern Africa and the Arabian Peninsula: A data set for the analysis of biogeophysical feedbacks in the climate system. Global Biogeochem Cycles 12: 35-51

Holland MM, Finnis J, Barrett AP, Serreze MC (2007) Projected changes in Arctic Ocean freshwater budgets. J Geophys Res 112: G04S55. Doi10.1029/2006JG000354

Holland MM, Finnis J, Serreze MC (2006) Simulated Arctic Ocean freshwater budgets in the twentieth and twenty-first centuries. J Clim 19: 6221-6242

Hörner T, Stein R, Fahl K (2017) Evidence for Holocene centennial variability in sea ice cover based on IP25 biomarker reconstructed in the southern Kara Sea (Arctic Ocean) Geo-Mar Lett 37(5): 515-526. doi: 10.1007/s00367-017-0501-y

Hu A, Meehl GA, Han W, Yin J (2009) Transient response of the MOC and climate to potential melting of the Greenland Ice Sheet in the 21st century. Geophys Res Lett 36: L10707. doi:10.1029/2009GL037998

Hu FS, Ito E, Brubaker LB, Anderson PM (1998) Ostracode geochemical record of Holocene climatic change and implications for vegetational response in the Northwestern Alaska range. Quat Res 49: 86-95

Ice and Climate (2019) Climate during the Holocene: https://www.iceandclimate.nbi.ku.dk/research/climatechange/glacial_interglacial/climate_holocene/. Accessed 25th October 2020

IPCC (2001) Climate Change 2001: The Scientific Basis. Contribution of Working Group I to the Third Assessment Report of the Intergovernmental Panel on Climate Change [Houghton JT, Ding Y, Griggs DJ, Noguer M, van der Linden PJ, Dai X, Maskell K, Johnson CA] Cambridge University Press, Cambridge, United Kingdom and New York, NY, USA, 881pp

IPCC (2014) Climate Change 2014: Synthesis Report. Contribution of Working Groups I, II and III to the Fifth Assessment Report of the Intergovernmental Panel on Climate Change [Core Writing Team, Pachauri RK and Meyer LA]. IPCC, Geneva, Switzerland, 151 pp

Jansen E, Overpeck J, Briffa KR, Duplessy JC, Joos F, Masson-Delmotte V, Olago D, Otto-Bliesner B, Peltier WR, Rahmstorf S, Ramesh R, Raynaud D, Rind D, Solomina O, Villalba R, Zhang D (2007) Palaeoclimate. In: Climate Change 2007: The Physical Science Basis. Contribution of Working Group I to the Fourth Assessment Report of the Intergovernmental Panel on Climate Change [Solomon S, Qin D, Manning M, Chen Z, Marquis M, Averyt KB, Tignor M, Miller HL]. Cambridge University Press, Cambridge, United Kingdom and New York, NY, USA

Jolly D, Prentice IC, Bonnefille R, Ballouche A, Bengo M, Brenac P, Buchet G, Burney D, Cazet JP, Cheddadi R, Edorh T, Elenga H, Elmoutaki S, Guiot J, Laarif F,

Lamb H, Lezine AM, Maley J, Mbenza M, Peyron O, Reille M, Reynaud-Farrera I, Riollet G, Ritchie JC, Roche E, Scott L, Ssemmanda I, Straka H, Umer M, Van Campo E, Vilimumbalo S, Vincens A, Waller M (1998) Biome reconstruction from pollen and plant macrofossil data for Africa and the Arabian peninsula at 0 and 6000 years. J Biogeogr 25: 1007-1027

Jorgenson MT, Racine CH, Walters JC, Osterkamp TE (2001) Permafrost degradation and ecological changes associated with a warming climate in central Alaska. Clim Change 48: 551-579

Jungclaus JH, Bard E, Baroni M, Braconnot P, Cao J, Chini LP, Egorova T, Evans M, González-Rouco JF, Goosse H, Hurtt GC, Joos F, Kaplan JO, Khodri M, Klein Goldewijk K, Krivova N, LeGrande AN, Lorenz SJ, Luterbacher J, Man W, Maycock AC, Meinshausen M, Moberg A, Muscheler R, Nehrbass-Ahles C, Otto-Bliesner BI, Phipps SJ, Pongratz J, Rozanov E, Schmidt GA, Schmidt H, Schmutz W, Schurer A, Shapiro AI, Sigl M, Smerdon JE, Solanki SK, Timmreck C, Toohey M, Usoskin IG, Wagner S, Wu CJ, Yeo KL, Zanchettin D, Zhang Q, Zorita E (2017) The PMIP4 contribution to CMIP6 – Part 3: The last millennium, scientific objective, and experimental design for the PMIP4 *past1000* simulations, Geosci Model Dev 10: 4005-4033, https://doi.org/10.5194/gmd-10-4005-2017

Jungclaus JH, Haak H, Esch M, Roeckner E, Marotzke J (2006) Will Greenland melting halt the thermohaline circulation? (2006) Geophys Res Lett 33: L17708. doi:10.1029/2006GL026815

Kageyama M, Braconnot P, Harrison SP, Haywood AM, Jungclaus JH, Otto-Bliesner BL, Peterschmitt JY, Abe-Ouchi A, Albani S, Bartlein PJ, Brierley C, Crucifix M, Dolan A, Fernandez-Donado L, Fischer H, Hopcroft PO, Ivanovic RF, Lambert F, Lunt DJ, Mahowald NM, Peltier WR, Phipps SJ, Roche DM, Schmidt GA, Tarasov L, Valdes PJ, Zhang Q, Zhou T (2018) The PMIP4 contribution to CMIP6 – Part 1: Overview and over-arching analysis plan. Geosci Model Dev 11: 1033-1057. doi.org/10.5194/gmd-11-1033-2018

Kaplan MR, Wolfe AP, Miller GH (2002) Holocene environmental variability in southern Greenland inferred from lake sediments. Quat Res 58: 149-159

Karcher M, Gerdes R, Kauker F, Köberle C, Yashayaev I (2005) Arctic Ocean change heralds North Atlantic freshening. Geophys Res Lett. 32: L21606. doi:10.1029/2005GL023861

Kattsov VM, Walsh JE (2000) Twentieth-century trends of Arctic precipitation from observational data and a climate model simulation. J Clim 13: 1362-1370

Kaufman DS, Ager TA, Anderson NJ, Anderson PM, Andrews JT, Bartlein PJ, Brubaker LB, Coats, LL, Cwynar LC, Duvall ML, Dyke AS, Edwards ME, Eisner WR, Gajewski K, Geirsdottir A, Hu FS, Jennings AE, Kaplan MR, Kerwin MW, Lozhkin AV, MacDonald GM, Miller GH, Mock CJ, Oswald WW, Otto-Bliesner BL, Porinchu DF, Rühland K, Smol JP, Steig EJ, Wolfe, BB (2004) Holocene thermal maximum in the western Arctic (0-180°W). Quat Sci Rev 23: 529-560

Kerwin MW, Overpeck JT, Webb RS, Anderson KH (2004) Pollen-based summer temperature reconstructions for the eastern Canadian boreal forest, subarctic, and Arctic. Quat Sci Rev 23: 1901-1924

Kerwin MW, Overpeck JT, Webb RS, Rind DH, Healy RJ (1999) The role of oceanic forcing in mid-Holocene Northern Hemisphere climatic change. Paleoceanography 14: 200-210

Kiehl JT, Trenberth KE (1997) Earth's Annual Global Mean Energy Budget. B Am Meteorol Soc 78: 197-208

Kirtman B, Power SB, Adedoyin JA, Boer GJ, Bojariu R, Camilloni I, Doblas-Reyes FJ, Fiore AM, Kimoto M, Meehl GA, Prather M, Sarr A, Schär C, Sutton R, van Oldenborgh GJ, Vecchi G, Wang HJ (2013) Near-term Climate Change: Projections and Predictability. In: Climate Change 2013: The Physical Science Basis. Contribution of Working Group I to the Fifth Assessment Report of the Intergovernmental Panel on Climate Change [Stocker TF, Qin D, Plattner G-K, Tignor M, Allen SK, Boschung J, Nauels A, Xia Y, Bex V, Midgley PM]. Cambridge University Press, Cambridge, United Kingdom and New York, NY, USA

Kobashi T, Severinghaus JP, Brook EJ, Barnola J-M, Grachev AM (2007) Precise timing and characterization of abrupt climate change 8200 years ago from air trapped in polar ice. Quat Sci Rev 26(9-10): 1212-1222

Koç N, Jansen E (1992) A high-resolution diatom record of the last deglaciation from the SE Norwegian Sea: Documentation of rapid climate changes. Paleoceanogr 7: 499-520

Koenigk T, Mikolajewicz U, Helmuth H, Jungclaus J (2007) Arctic freshwater export in the 20th and 21st centuries. J. Geophys. Res 12: G04S41. doi:10.1029/2006JG000274

Koerner RM, Fisher DA (1990) A record of Holocene summer climate from a Canadian high-Arctic ice core. Nature 343: 630-631

Kopp RE, Dutton A, Carlson AW (2017) Centennial-to millennial-scale sea-level change during the Holocene and Last Interglacial periods. PAGES 25(3): 148-149

Korhola A, Weckström J, Holmström L, Erästö P (2000) A quantitative Holocene climatic record from diatoms in Northern Fennoscandia. Quat Res 54: 284-294

Kostadinov TS, Gilb R (2014) Earth Orbit v2.1: a 3-D visualization and analysis model of Earth's orbit, Milankovitch cycles and insolation, Geosci Model Dev 7: 1051-1068. doi.org/10.5194/gmd-7-1051-2014

Krabill W, Hanna E, Huybrechts P, Abdalati W, Cappelen J, Csatho B, Fredrick E, Manizade S, Martin C, Sonntag J, Swift R, Thomas R, Yungel J (2004) Greenland Ice Sheet: Increased coastal thinning. Geophys Res Lett 31: L24402. doi: 10.1029/2004GL021533

Kröpelin S, Verschuren D, Lézine AM, Eggermont H, Cocquyt C, Francus P, Cazet J-P, Fagot M, Rumes B, Russell JM, Darius F, Conley DJ, Schuster M, von Suchodoletz H, Engstrom DR (2008) Climate-driven ecosystem succession in the Sahara: The past 6000 years. Science 320: 765-768

Kutzbach JE, Street-Perrott FA (1985) Milankovitch forcing of fluctuations in the level of tropical lakes from 18 to 0kyr BP. Nature 317: 130-134

Kwiatkowski D, Phillips PCB, Schmidt P, Shin Y (1992) Testing the null hypothesis of stationarity against the alternative of a unit root, J Econom 54(1-3): 159-178. doi:10.1016/0304-4076(92)90104-Y

Kwok R, Rothrock DA (2009) Decline in Arctic sea ice thickness from submarine and ICEsat records: 1958-2008. Geophys Res Lett 36: L15501. doi:10.1029/2009GL039035

Kwong JYT, Gan TY (1994) Northward migration of permafrost along the Mackenzie highway and climatic warming. Clim Change 26: 399-419

Lambeck K, Rouby H, Purcell A, Sun Y, Sambridge M (2014) Se level and global ice volumes from the Last Glacial Maximum to the Holocene. PNAS 111(43): 15296-15303

Levac E, De Vernal A, Blake W. Jr (2001) Sea-surface conditions in northernmost Baffin Bay during the Holocene: Palynological evidence. J Quat Sci 16: 353-363

Licciardi JM, Teller JT, Clark PU (1999) Freshwater routing by the Laurentide Ice Sheet during the last deglaciation, in: Mechanisms of Global Climate Change at Millennial Time Scales, edited by: Clark PU, Webb RS, Keigwin LD. American Geophysical Union, Washington, DC, Geophysical Monograph 112, 177-201

Lindsay R, Schweiger A (2015) Arctic sea ice thickness loss determined using subsurface, aircraft, and satellite observations, Cryosphere 9: 269-283, doi: 10.5194/tc-9-269-2015

Liu Z, Wang Y, Gallimore R, Notaro M, Prentice IC (2006) On the cause of abrupt vegetation collapse in North Africa during the Holocene: climate variability vs. vegetation feedback. Geophys Res Lett 33: L22709, 10.1029/2006GL028062

Liu Z, Zhu J, Rosenthal Y, Zhang X, Otto-Bliesner BL, Timmerman A, Smith RS, Lohmann G, Zheng W, Timm OE (2014) The Holocene temperature conundrum. Proc Natl Acad Sci U.S.A. 11: E3501-E3505, 10.1073/pnas.1407229111

Ljungqvist KC (2011) The spatio-temporal pattern of the mid-Holocene Thermal Maximum. Geografie 116: 91-110

Loulergue L, Schilt A, Spahni R, Masson-Delmotte V, Blunier T, Lemieux B, Barnola JM, Raynaud D, Stockern TF, Chappellaz J (2008) Orbital and millennial-scale features of atmospheric CH4 over the past 800,000 years. Nature 453: 383-386

Loutre MF, Mouchet A, Fichefet T, Goosse H, Goelzer H, Huybrechts P (2011) Evaluating climate model performance with various parameter sets using observations over the recent past. Clim Past 7: 511-526. doi:10.5194/cp-7-511-2011

Luthcke SB, Zwally HJ, Abdalati W, Rowlands DD, Day RD, Nerem RS, Lemoine FG, McCarthy JJ, Chinn DS (2006) Recent Greenland ice mass loss by drainage system from satellite gravity observations. Science 314: 1286-1289

Ljung GM, Box GEP (1978) On a measure of lack of fit in time series models. Biometrika 65(2): 297-303. doi.org/10.1093/biomet/65.2.297

Ma Q, Tipping RH (1998) The distribution of density matrices over potential-energy surfaces: Application to the calculation of the far-wing line shapes for CO_2. J. Chem Phys 108: 3386-3399. doi:10.1063/1.475774

MacDonald GM (2010) Some Holocene palaeoclimatic and palaeoenvironmental perspectives on Arctic/subarctic climate warming and the IPCC 4th assessment report. J Quat Sci 25: 39-47

MacDonald GM, Edwards TWD, Moser KA, Pienitz R, Smol JP (1993) Rapid response of treeline vegetation and lakes to past climate warming. Nature 361: 243-246

MacDonald GM, Velichko AA, Kremenetski CV, Borisova OK, Goleva AA, Andreev AA, Cwynar LC, Riding RT, Forman SL, Edwards TWD, Aravena R, Hammarlund D, Szeicz JM, Gattaulin VN (2000) Holocene treeline history and climate change across northern Eurasia. Quat Res 53: 302-311

Madec G, Imbard M (1996) A global ocean mesh to overcome the North Pole singularity. Clim Dyn 12: 381-388

Manabe S, Stouffer RJ (1980) Sensitivity of a global climate model to an Increase of CO2 concentration in the atmosphere. J Geophys Res 85: 5529-5554

Mann ME, Zhang Z, Rutherford S, Bradley R, Hughes MK, Shindell D, Ammann C, Faluvegi G, Ni F (2009) Global Signatures and Dynamical Origins of the Little Ice Age and Medieval Climate Anomaly. Science 326:1256-1260

Marchal O, Cacho I, Stocker TF, Grimalt JO, Cavo E, Martrat B, Shackleton N, Vautravers M, Cortijo E, Van Kreveld S, Anderson C, Koç N, Chapman M, Sbaffi L, Duplessy JC, Sarnthein M, Turon JL, Duprat J, Jansen E (2002) Apparent long-term cooling of the sea surface in the northeast Atlantic and Mediterranean during the Holocene. Quat Sci Rev 21: 455-483

Marcott SA, Shakun JD, Clark PU, Mix AC (2013) A reconstruction of regional and global temperature for the past 11,300 years. Science 339: 1198-1201

Matero ISO, Gregoire LJ, Ivanovic RF, Tindall JC, Haywood A (2017) The 8.2ka cooling event caused by the Laurentide ice saddle collapse. Earth Planet Sci Lett 473: 205-214

Mauritzen C (2012) Arctic freshwater. Nat Geosci 5: 162-164 doi.org/10.1038/ngeo1409

McGuffie K, Henderson-Sellers A (2014) The Climate Modelling Primer 4th Edition, London, Wiley-Blackwell

McPhee MG, Proshutinsky A, Morison JH, Steele M, Alkire, MB (2009) Rapid change in freshwater content of the Arctic Ocean Geophys Res Lett 36: L10602. doi:10.1029/2009GL037525

Meredith M, Heywood K, Dennis P, Goldson L, White R, Fahrbach E, Schauer U, Østerhus S (2001) Freshwater fluxes through the western Fram Strait. Geophys Res Lett 28(8): 1615-1618

Miettinen A, Divine D, Koç N, Godtliebsen F, Hall IR (2015) Multicentennial Variability of the Sea Surface Temperature Gradient across the Subpolar North Atlantic over the Last 2.8 kyr. J Clim 25: 4205-4219. doi.org/10.1175/JCLI-D-11-00581.1

Milankovitch M (1941) Kanon der Erdbestrahlungen und seine Anwendung auf das Eiszeiten Problem, Roy Serbian Acad Spec Pub 133

Miller JR, Russell GL (2000) Projected impact of climate change on the freshwater and salt budgets of the Arctic Ocean by a global climate model. Geophys Res Lett 27: 1183-1186

Monnin E, Indermühle A, Dällenbach A, Flückiger J, Stauffer B, Stocker T, Raynaud D, Barnola J (2001) Atmospheric CO_2 Concentrations over the Last Glacial Termination. Science 291:112-4. doi:10.1126/science.291.5501.112

Muri H, Berger A, Yin Q, Karami MP, Barriat P-Y (2013) The climate of the MIS-13 interglacial according to HadCM3. J Climate 26: 9696–9712. doi:10.1175/JCL1-D-12-00520.1

Muschitiello F, Zhang Q, Sundqvist HS, Davies FJ, Renssen H (2015) Arctic climate response to the termination of the African Humid Period Quat Sci Rev 125: 91-97. doi.org/10.1016/j.quascirev.2015.08.012

Nakicenovic N, Swart R (2000) IPCC Special report on emission scenarios. Cambridge University Press, UK

Nikolova I, Yin Q, Berger A, Singh UK, Karami MP (2013) The last interglacial (Eemian) climate simulated by LOVECLIM and CCSM3. Clim Past 9: 1789-1806, 10.5194/cp-9-1789-2013

NOAA National Centers for Environmental Information (2020) State of the Climate: Global Climate Report for Annual 2019 https://www.ncdc.noaa.gov/sotc/global/201913. Accessed August 23, 2020

Notaro M, Wang Y, Liu Z, Gallimore R, Levis S (2008) Combined statistical and dynamical assessment of simulated vegetation-rainfall interactions in North Africa during the mid-Holocene. Glob Change Biol 14: 347-368

Olsen J, Anderson NJ, Knudsen MF (2012) Variability of the North Atlantic Oscillation over the past 5,200 years. Nat Geosci 5: 808-812. doi:10.1038/ngeo1589

Opsteegh JD, Haarsma RJ, Selten FM, Kattenberg A (1998) ECBilt: a dynamic alternative to mixed boundary conditions in ocean models. Tellus A 50: 348-367

Otto-Bliesner BL, Braconnot P, Harrison SP, Lunt DJ, Abe-Ouchi A, Albani S, Bartlein PJ, Capron E, Carlson AE, Dutton A, Fischer H, Goelzer H, Govin A, Haywood A, Joos F, LeGrande AN, Lipscomb WH, Lohmann G, Mahowald N, Nehrbass-Ahles C, Pausata FSR, Peterschmitt JY, Phipps SJ, Renssen H, Zhang Q (2017) The PMIP4 contribution to CMIP6 - Part 2: Two interglacials, scientific objective and experimental design for Holocene and Last Interglacial simulations, Geosci Model Dev 10: 3979-4003. doi.org/10.5194/gmd-10-3979-2017

Otto-Bliesner BL, Marshall SJ, Overpeck JT, Miller GH, Hu A (2006) CAPE Last Interglacial Project Members: Simulating Arctic climate warmth and icefield retreat in the last interglacial. Science 311: 1751-1753

Overland JE, Dethloff K, Francis JA, Hall RJ, Hanna E, Kim SJ, Screen JA, Shepherd TG, Vihma T (2016) Nonlinear response of mid-latitude weather to the changing Arctic. Nat Clim Change 6: 992-999. doi:10.1038/nclimate3121

Overland JE, Wang M, Walsh JE, Stroeve JC (2013) Future Arctic climate changes: Adaptation and mitigation time scales. Earths Future 2: 68-74. doi:10.1002/2013EF000162

Paleoclimate Modelling Intercomparison Project Phase III (2014) http://pmip3.lsce.ipsl.fr. Accessed June 2013

Park W, Latif M (2008) Multidecadal and Multicentennial variability of the meridional overturning circulation. Geo Phys Lett 35: L22703. doi:10.1029/2008GL035779

Peixoto JP, Oort AH (1992) Physics of Climate, American Institute of Physics, New York,

520 pp

Peltier W (2004) Global glacial isostasy and the surface of the Ice-age Earth: the ICE-5G (VM2) model and grace. Annu Rev Earth Pl Sc 32: 111-149. 10.1146/annurev.earth.32.082503.144359

Peterson BJ, Holmes RM, McClelland JW, Vörösmarty CJ, Lammers RB, Shiklomanov AI, Shiklomanov IA, Rahmstorf S (2002) Increasing river discharge to the Arctic Ocean. Science 298: 2171-2173

Pisaric MFJ, Holt C, Szeicz JM, Karst T, Smol JP (2003) Holocene treeline dynamics in the mountains of northeastern British Columbia, Canada, inferred from fossil pollen and stomata. Holocene 13: 161-173

Pithan F, Mauritsen T (2014) Arctic amplification dominated by temperature feedbacks in contemporary climate models. Nat Geosci 7: 181-184

Polyakov IV, Alexeev VA, Belchansky GI, Dmitrenko IA, Ivanov VV, Kirillov SA, Korablev AA, Steele M, Timokhov LA, Yashayaev I (2008) Arctic Ocean freshwater changes over the past 100 years and their causes. J Climate 21: 364-384

Prinsenberg SJ, Hamilton J (2005) Monitoring the volume, freshwater and heat fluxes passing through Lancaster Sound in the Canadian Arctic Archipelago. Atmos-Ocean 43(1): 1-22.

Prowse TD (2016) The Arctic freshwater synthesis, Eos 97. doi.org/10.1029/2018EO057207. Accessed 10th February 2020

Puetz SJ, Prokoph A, Borchardt G (2016) Evaluating alternatives to the Milankovitch theory. J Stat Plan Inference 170: 158-165. doi.org/10.1016/j.jspi.2015.10.006

Rabe B, Karcher M, Schauer U, Toole JM, Krishfield RA, Pisarev S, Kauker F, Gerdes R, Kikuchi T (2011) An assessment of Arctic Ocean freshwater content changes from the 1990s to the 2006-2008 period. Deep-Sea Res I 58: 173-185

RACE Project (2015) Regional Atlantic Circulation and Global Change. https://race-synthese.de/the-atlantic-meridional-overturning-circulation. Accessed 20 October 2020

Randall DA, Wood RA, Bony S, Colman R, Fichefet T, Fyfe J, Kattsov V, Pitman A, Shukla J, Noda A, Srinivasan J, Stouffer R J, Sumi A, Taylor KE (2007) Climate

models and their evaluation. In: Climate Change 2007: The Physical Science Basis, in: Contribution of Working Group I to the Fourth Assessment Report of the Intergovernmental Panel on Climate Change, edited by: Solomon S, Qin D, Manning M, Chen Z, Marquis M, Averyt K B, Tignor M, Miller HL, Cambridge University Press, Cambridge, United Kingdom and New York, NY, USA, 2007

Renssen H, Brovkin V, Fichefet T, Goosse H (2003) Holocene climate instability during the termination of the African Humid Period. Geophys Res Lett 30: 1184, 10.1029/2002GL016636

Renssen H, Goosse H, Fichefet T, Brovkin V, Driesschaert E, Wolk F (2005) Simulating the Holocene climate evolution at northern high latitudes using a coupled atmosphere-sea ice-ocean-vegetation model. Clim Dynam 24: 23-43

Renssen H, Driesschaert E, Loutre MF, Fichefet T (2006) On the importance of initial conditions for simulations of the Mid-Holocene climate. Clim Past 2: 91-97, doi:10.5194/cp-2-91-2006

Renssen H, Seppä H, Crosta X, Goosse H, Roche DM (2012) Global characterization of the Holocene Thermal Maximum. Quat Sci Rev 48: 7-19. doi:10.1016/j.quascirev.2012.05.022

Renssen H, Seppä H, Heiri O, Roche DM, Goosse H, Fichefet T (2009) The spatial and temporal complexity of the Holocene thermal maximum. Nat Geosc 2: 411-414. doi:10.1038/NGE0513

Rignot E, Kanagaratnam P (2006) Changes in the velocity structure of the Greenland Ice Sheet. Science 311: 986-990. doi:10.1126/science.1121381

Ritchie JC, Cwynar LC, Spear RW (1983) Evidence from north-west Canada for an early Holocene Milankovitch thermal maximum. Nature 305: 126-128

Roach AT, Aagaard K, Pease CH, Salo SA, Weingartner T, Pavlov V, Kulakov M (1995) Direct measurements of transport and water properties through Bering Strait. J Geophys Res 100: 18443-18457

Roche DM (2013) $\delta^{18}O$ water isotope in the iLOVECLIM model (version 1.0) - Part 1: Implementation and verification, Geosci Model Dev 6: 1481-1491. doi.org/10.5194/gmd-6-1481-2013

Roche DM, Dokken TM, Goosse H, Renssen H, Weber SL (2007) Climate of the Last Glacial Maximum: sensitivity studies and model-data comparison with the

LOVECLIM coupled model. Clim Past 3: 205-224. doi:10.5194/cp-3-205-2007

Rossow WB, Walker AW, Beuschel DE, Roiter MD (1996) International satellite cloud climatology project (ISCCP) documentation of new cloud datasets. WMO/TD-No 737, World Meteorological Organisation

Sarnthein M, van Kreveld S, Erlenkeuser H, Grootes PM, Kucera M, Pflaumann U, Schulz M (2003) Centennial-to-millennial-scale periodicities of Holocene climate and sediment injections off the western Barents shelf, 75°N. Boreas 32: 447-461

Schaeffer M, Selten F, van Dorland R (1998) Linking Image and ECBilt, National Institute for public health and the environment (RIVM). Report no 4815008008, Bilthoven, The Netherlands

Schauer U, Beszczynska-Möller A, Walczowski W, Fahrbach E, Piechura J, Hansen E (2008), Variation of measured heat flow through the Fram Strait between 1997 and 2006, In: Dicksopn RR (ed) Arctic-Subarctic Ocean Fluxes. Springer, New York, pp 65-85

Schilt A, Baumgartner M, Blunier T, Schwander J, Spahni R, Fischer H, Stocker TF (2010) Glacial-interglacial and millennial-scale variations in the atmospheric nitrous oxide concentration during the last 800,000 years. Quat Sci Rev 29: 182-192

Schlesinger ME, Ramankutty N (1994) An Oscillation in the global climate system of period 65-70 years. Nature 367: 723-726. doi:10.1038/367723a0

Schlichtholz P, Houssais M-H (1999) An investigation of the dynamics of the East Greenland current in Fram Strait based on a simple analytical model. J Phys Oceanogr 29: 2240-2265

Serreze MC, Walsh JE, Chapin FS III, Osterkamp T, Dyurgerov M, Romanovsky V, Oechel WC, Morison J, Zhang T, Barry RG (2000) Observational evidence of recent change in the northern high-latitude environment. Clim Change 46: 159-207

Serreze MC, Bromwich DH, Clark MP, Etringer AJ, Zhang T, Lammers R (2003) Large-scale hydro-climatology of the terrestrial Arctic drainage system. J Geophys Res 108: doi:10.1029/2001JD000919

Serreze MC, Barrett A, Slater AG, Woodgate RA, Aagaard K, Lammers RB, Steele M, Moritz R, Meredith M, Lee CM (2006) The large-scale freshwater cycle of the Arctic. J Geophys Res. doi:10.1029/2005JC003424

Serreze MC, Barry R (2011) Processes and impacts of Arctic amplification: A research synthesis. Glob Planet Change 77: 85-96. 10.1016/j.gloplacha.2011.03.004

Shiklomanov IA (2000) Appraisal and assessment of world water resources. Water Int 25: 11-32

Shiklomanov AI, Lammers RB (2009), Record Russian river discharge in 2007 and the limits of analysis. Environ Res Lett 4: 1-9. doi:10.1088/1748-9326/4/4/045015

Sicre MA, Jacob J, Ezat U, Rousse S, Kissel C, Yiou P, Eiríksson J, Knudsen KL, Jansen E, Turon JL (2008) Decadal variability of sea surface temperatures off North Iceland over the last 2000 years. Earth Planet Sci Lett 268: 137-142

Siddall M, Rohling EJ, Almogi-Labin A, Hemleben CH, Meischner D, Schmelzer I, Smeed DA (2003) Sea-level fluctuations during the last glacial cycle. Nature 423: 853-858

Singarayer JS, Valdes PJ (2010) High-latitude Climate sensitivity to ice-sheet forcing over the last 120 kyr. Quat Sci Rev 29: 43-55

Smedsrud LH, Halvorsen MH, Stroeve JC, Zhang R, Kloster K (2017) Fram Strait sea ice export variability and September Arctic sea ice extent over the last 80 years. Cryosphere 11: 65-79. doi.org/10.5194/tc-11-65-2017

Smeed DA, McCarthy GD, Cunningham SA, Frajka-Williams E, Rayner D, Johns WE, Meinen CS, Baringer MO, Moat BI, Duchez A, Bryden HL (2014) Observed decline of the Atlantic meridional overturning circulation 2004-2012, Ocean Sci 10: 29-38. doi:10.5194/os-10-29-2014

Smith RI (2002) Diatom-based Holocene paleoenvironmental records from continental sites on northeastern Ellesmere Island, High Arctic, Canada. J Paleolim 27: 9-28

Stocker TF, Qin D, Plattner GK, Alexander LV, Allen SK, Bindoff NL, Bréon FM, Church JA, Cubasch U, Emori S, Forster P, Friedlingstein P, Gillett N, Gregory JM, Hartmann DL, Jansen E, Kirtman B, Knutti R, Krishna Kumar K, Lemke P, Marotzke J, Masson-Delmotte V, Meehl GA, Mokhov II, Piao S, Ramaswamy V, Randall D, Rhein M, Rojas M, Sabine C, Shindell D, Talley LD, Vaughan DG, Xie SP (2013) Technical Summary. In: Climate Change 2013: The Physical Science Basis. Contribution of Working Group I to the Fifth Assessment Report of the Intergovernmental Panel on Climate Change [Stocker TF, Qin D, Plattner

GK, Tignor M, Allen SK, Boschung J, Nauels A, Xia Y, Bex V, Midgley PM (eds.)]. Cambridge University Press, Cambridge, United Kingdom and New York, NY, USA

Stroeve JC, Serreze MC, Holland MM, Kay JE, Malanik J, Barrett AP (2012) The Arctic's rapidly shrinking sea ice cover: a research synthesis. Clim Change 110: 1005. doi:10.1007/s10584-011-0101-1

Stroeve J, Holland MM, Meier W, Scambos T, Serreze M (2007) Arctic sea-ice decline: Faster than forecast. Geophys Res Lett 34: L09501. doi:10.1029/2007GL029703

Stroeven AP, Hättestrand C, Kleman J, Heyman J, Fabel D, Fredin O, Goodfellow BW, Harbor JM, Jansen JD, Olsen L, Caffee MW, Fink D, Lundqvist J, Rosqvist GC, Strömberg B, Jansson KN (2016) Deglaciation of Fennoscandia, Quat Sci Rev 147: 91-121

Sundqvist HS, Zhang Q, Moberg A, Holmgren K, Körnich H, Nilsson J, Brattström G (2010) Climate change between the mid and late Holocene in northern high latitudes – Part 1: Survey of temperature and precipitation proxy data. Clim Past 6: 591-608. doi:10.5194/cp-6-591-2010

Szeicz JM, MacDonald GM, Duk-Rodin A (1995) Late quaternary vegetation history of the central Mackenzie Mountains, Northwest Territories, Canada. Palaeogeogr, Palaeoclim, Palaeoecol 113: 351-371. doi.org/10.1016/0031-0182(95)00070-3

Timm O, Kohler P, Timmermann A, Menviel L (2010) Mechanisms for the Onset of the African Humid Period and Sahara Greening 14.5-11 ka BP. J Climate 23: 2612–2633

Toulany B, Garrett C (1984) Geostrophic control of fluctuating barotropic flow through straits. J Phys Oceanogr 14:649-655.

Vellinga M, Wood RA (2002) Global climatic impacts of a collapse of the Atlantic Thermohaline Circulation. Clim Change 54: 251-267

Vinje T, Nordlund N, Kvambekk Å (2004) Monitoring ice thickness in Fram Strait. J Geophy Res 103(C5): 10437-10449

Vinther BM, Buchardt SL, Clausen HB, Dahl-Jensen D, Johnsen SJ, Fisher DA, Koerner RM, Raynaud D, Lipenkov V, Anderson KK, Blunier T, Rasmussen SO,

Steffensen JP, Svensson AM (2009) Holocene thinning of the Greenland ice sheet. Nature 461: 385-388

Wagner B, Melles M (2002) Holocene environmental history of western Ymer Ø, East Greenland, inferred from lake sediments. Quat Intern 89: 165-176

Wang Y-M, Lean JL, Sheeley NR Jr (2005) Modeling the sun's magnetic field and irradiance since 1713. Astrophys J 625: 522-538. doi:10.1086/429689

Wanner H, Beer J, Bütikofer J, Crowley TJ, Cubasch U, Flückiger J, Goosse H, Grosjean M, Joos F, Kaplan JO, Küttel M, Müller SA, Prentice IC, Solomina O, Stocker TF, Tarasov P, Wagner M, Widmann M (2008) Mid- to Late Holocene climate change: an overview. Quat Sci Rev 27, 1791-1828

Wiersma AP, Renssen H (2006) Model-data comparison for the 8.2ka BP event: Confirmation of a forcing mechanism by catastrophic drainage of Laurentide Lakes. Quat Sci Rev 25: 63-88

World Meteorological Organisation (2007) The Role of Climatological Normals in a Changing Climate. WCDMP-No. 61, WMO-TD/No. 1377, World Meteorological Organization

Woodgate RA Aagaard K (2005) Revising the Bering Strait freshwater flux into the Arctic Ocean. Geophys Res Lett 32 L02602. doi:10.1029/2004GL021747

Yin Q, Berger A, Driesschaert E, Goosse H, Loutre MF, Crucifix M (2008) The Eurasian ice sheet reinforces the East Asian summer monsoon during the interglacial 500 000 years ago. Clim Past 4: 79-90 doi:10.5194/cp-4-79-2008

Zhang T, Frauenfeld OW, Serreze MC, Etringer A, Oelke C, McCreight J, Barry RG, Gilichinsky D, Yang D, Ye H, Ling F, Chudinova S (2005) Spatial and temporal variability in active layer thickness over the Russian Arctic drainage basin. J Geophys Res 110: D16101. doi:10.1029/2004JD005642

Zhang Y-C, Rossow WB (1997) Estimating meridional energy transports by the atmospheric and oceanic general circulations using boundary fluxes. J Climate 10: 2358-2373

Zhang X, He J, Zhang J, Polyakov I, Gerdes R, Inoue J, Wu P (2012) Enhanced poleward moisture transport and amplified northern high-latitude wetting trend. Nat Clim Change 2(8): 1-5. doi:10.1038/nclimate1631